FINAL REPORT

FHWA-WY-10/07F

State of Wyoming
Department of Transportation

U.S. Department of Transportation
Federal Highway Administration

BRIDGE DECK EVALUATION USING NONDESTRUCTIVE TEST METHODS

By:

Tyler W. Robison, E.I.T.
Jennifer E. Tanner, Ph.D.
Department of Civil and Architectural Engineering
University of Wyoming
1000 East University Avenue, Dept. 3295
Laramie, WY 82071

March 2012

Notice

This document is disseminated under the sponsorship of the U.S. Department of Transportation in the interest of information exchange. The U.S. Government assumes no liability for the use of the information contained in this document.

The contents of this report reflect the views of the author(s) who are responsible for the facts and accuracy of the data presented herein. The contents do not necessarily reflect the official views or policies of the Wyoming Department of Transportation or the Federal Highway Administration. This report does not constitute a standard, specification, or regulation.

The United States Government and the State of Wyoming do not endorse products or manufacturers. Trademarks or manufacturers' names appear in this report only because they are considered essential to the objectives of the document.

Quality Assurance Statement

The Federal Highway Administration (FHWA) provides high-quality information to serve Government, industry, and the public in a manner that promotes public understanding. Standards and policies are used to ensure and maximize the quality, objectivity, utility, and integrity of its information. FHWA periodically reviews quality issues and adjusts its programs and processes to ensure continuous quality improvement.

Technical Report Documentation Page

Report No. FHWA-WY-10/07F	Government Accession No.	Recipients Catalog No.
Title and Subtitle: Bridge Deck Evaluation using Non-destructive Test Methods		Report Date June 2011 Performing Organization Code
Author(s) Tyler Robison, Jennifer Tanner		Performing Organization Report No.
Performing Organization Name and Address Department of Civil and Architectural Engineering University of Wyoming, Dept 3295 Laramie, WY 82071-3295		Work Unit No. RS04(209) Job No. RS04209 Contact or Grant No.
Sponsoring Agency Name and Address Wyoming Department of Transportation 5300 Bishop Blvd. Cheyenne, WY 82009-3340 WYDOT Research Center (307) 777-4182		Type of Report and Period Covered Final Report Jan 2009 June 2011 Sponsoring Agency Code

Supplementary Notes

Abstract:

The state of Wyoming has 13.1 million sq. ft of road bridges (FHWA 2009), and evaluations have become an important part of the Wyoming Department of Transportation's (WYDOT) management of bridge repairs. Nondestructive testing (NDE) methods developed in the past 20 years may provide an efficient, standardized, and accurate method for evaluating bridge deck conditions. This report presents the results of an exploratory study performed on three bridge decks in Wyoming: the First Street Bridge in Casper, the Douglas I-25 Bridge, and the Remount Bridge on I-80. The goal is to develop a practical solution that WYDOT can implement. In particular, the solution should capitalize on safety, efficiency and accuracy. The author evaluated each bridge using standard WYDOT practices for chain dragging and half-cell potentials, along with newer technologies of impact echo, thermal imaging, and ground penetrating radar (GPR), which provides a comprehensive assessment of the NDE evaluation techniques. Cores removed from the bridges were compared to the results from the evaluation methods. Damage locations indicated by impact echo, thermal imaging, and GPR generally correlated well and factors are presented in this report. This research suggests that a combination of impact echo with GPR testing provides the most accurate predictions of delamination, debonding, and active corrosion on bridge decks.

Key Words	Distribution Statement		
Wyoming, Bridge Deck, Non-destructive, Chain drag, Thermal Imaging, Impact Echo	Unlimited		
Security Classif. (of this report) Unclassified	Security Classif. (of this page) Unclassified	No. of Pages 212	Price

Form DOT F 1700.7 (8-72) Reproduction of form and completed page is authorized.

SI* (Modern Metric) Conversion Factors

Approximate Conversions from SI Units

Symbol	When You Know	Multiply By	To Find	Symbol
Length				
mm	millimeters	0.039	inches	in
m	meters	3.28	feet	ft
m	meters	1.09	yards	yd
km	kilometers	0.621	miles	mi
Area				
mm^2	square millimeters	0.0016	square inches	in^2
m^2	square meters	10.764	square feet	ft^2
m^2	square meters	1.195	square yards	yd^2
ha	hectares	2.47	acres	ac
km^2	square kilometers	0.386	square miles	mi^2
Volume				
ml	milliliters	0.034	fluid ounces	fl oz
l	liters	0.264	gallons	gal
m^3	cubic meters	35.71	cubic feet	ft^3
m^3	cubic meters	1.307	cubic yards	yd^3
Mass				
g	grams	0.035	ounces	oz
kg	kilograms	2.202	pounds	lb
Mg	megagrams	1.103	short tons (2000 lbs)	T

Approximate Conversions to SI Units

Symbol	When You Know	Multiply By	To Find	Symbol
Length				
in	inches	25.4	millimeters	mm
ft	feet	0.305	meters	m
yd	yards	0.914	meters	m
mi	miles	1.61	kilometers	km
Area				
in^2	square inches	645.2	square millimeters	mm^2
ft^2	square feet	0.093	square meters	m^2
yd^2	square yards	0.836	square meters	m^2
ac	acres	0.405	hectares	ha
mi^2	square miles	2.59	square kilometers	km^2
Volume				
fl oz	fluid ounces	29.57	milliliters	ml
gal	gallons	3.785	liters	l
ft^3	cubic feet	0.028	cubic meters	m^3
yd^3	cubic yards	0.765	cubic meters	m^3
Mass				
oz	ounces	28.35	grams	g
lb	pounds	0.454	kilograms	kg
T	short tons (2000 lbs)	0.907	megagrams	Mg

Temperature (exact)				
°C	Centigrade temperature	1.8 C + 32	Fahrenheit temperature	°F
Illumination				
lx	lux	0.0929	foot-candles	fc
cd/m^2	candela/m^2	0.2919	foot-Lamberts	fl
Force and Pressure or Stress				
N	newtons	0.225	poundforce	lbf
kPa	kilopascals	0.145	pound-force per square inch	psi

Temperature (exact)				
°F	Fahrenheit temperature	5(F-32)/9 or (F-32)/1.8	Celsius temperature	°C
Illumination				
fc	foot-candles	10.76	lux	lx
fl	foot-Lamberts	3.426	candela/m^2	cd/m^2
Force and Pressure or Stress				
lbf	pound-force	4.45	newtons	N
psi	pound-force per square inch	6.89	kilopascals	kPa

Acknowledgements

Appreciation is extended to the following individuals and groups for their invaluable help and support that made this project possible: Bob Rothwell, Rick Harvey, Gregg Frederick, and Keith Fulton of the Wyoming Department of Transportation for their technical and financial support; Chuck Cisco, Chris Romo, L.J. Maillet, Mike Reyes, Floyd Alcon, Ravid Ingram, Wayne Benedict, and Mark Papke of the Wyoming Department of Transportation for their continued patience, hard work and field expertise. The crews were always safe in their capable hands. Angela Jones and Scott Wolfer are thanked for participating in all of the bridge deck evaluations and supporting the research team throughout the duration of this project.

Executive Summary

This research project provides a comprehensive assessment of NDE evaluation techniques, which is a direct comparison of chain drag, half-cell potential, impact echo, thermal imaging and GPR methods. This analysis, rarely completed in field studies, is applied to three different types of bridge decks. The goal is to consider alternative yet practical solutions that WYDOT can implement. Chain dragging methods are frequently criticized for being subjective and inaccurate. As a result, bridge repair schedules based on this method may be inaccurate resulting in more costly repairs for WYDOT.

Three bridges with different surface compositions were evaluated: bare concrete deck (First Street Bridge, Casper), latex modified concrete overlay (Douglas), and asphalt overlay (Remount). Traditional WYDOT methods were completed by Chuck Cisco and the WYDOT bridge deck evaluation crew. Next, the University of Wyoming research team used impact echo, thermal imaging, and GPR methods to evaluate the three bridge decks and compare results to those obtained by WYDOT's traditional evaluation methods of chain dragging and half-cell potentials. Each of the test methods is discussed in the following paragraphs.

Description of each testing method

WYDOT performed chain dragging and half-cell potential evaluations on all three bridges. Chain dragging evaluations were set up on a 5 ft by 5 ft grid. The entire deck is then dragged by the evaluator. Whenever a dull or hollow sound was heard, the area was outlined as damaged by marking this section with paint. At the end of the test the marked areas were transferred to electronic format.

Half-cell data was collected according to ASTM C 876 and standard WYDOT practices. The sponge on the half-cell was wetted when needed to give a clearer voltage. Readings were taken at specific locations provided by WYDOT's computer software. Once the readings were taken, the data was entered into their software to produce voltage maps. Half-cell data was collected from the Casper and Douglas bridges. On the Remount Bridge, half-cell data could not be gathered because an epoxy coating on the rebar masked the signal.

To gather data for the impact echo test, a digital sounding device was used to measure the depth of concrete decks (Olson Instruments Concrete Thickness Gauge CTG™). This device uses a solenoid that strikes the surface and a receiver that converts the reading to

concrete depth via a Fast Fourier Transform. The impact echo tests also utilized a 3 ft by 3 ft grid provided the resolution recommended by previous research (Gucunski et al. 2008b). The thickness gauge was calibrated to provide accurate thickness readings. A location was selected on the deck in which the depth of the concrete was known to set the wave velocity. From there, data was collected methodically, with every test point's number and location recorded to later produce a graphical representation. Data was transferred to a laptop in the field. Olson Engineering's rolling impact echo bridge scanner was also used to test all three bridges as part of their development program for the apparatus.

Infrared cameras were rented for thermal imaging and the camera used for the Casper Bridge and the Douglas Bridge with the overlay was a FLIR T250 fitted with 45° lens that was used to increase the area the camera could cover in one photograph. The camera used for the Remount Bridge, with and without the overlay, and the Douglas Bridge, without the overlay, was a FLIR B200, and the same wide angle lens was used in these two surveys. A boom and cart were used to raise the camera and orient it perpendicular to the bridge deck surfaces. The same 3 ft by 3 ft grid that was used for the impact echo tests was used for thermal imaging. Metallic gold paint was used to clearly locate the marks using the thermal camera. A laptop was connected to the infrared camera to collect and store the images. Once the camera was in the air and oriented perpendicular to the deck, it could be centered over the point and saved as the location on the deck. The images were later stitched together using photo editing software. When the deck is heating up, damaged areas will be at a higher temperature than those of sound areas. This typically occurs a few hours after sunrise with clear skies. In the evening when the deck cools off, damaged areas will cool faster and will appear darker than sound areas. This is due to air's low conductance of heat compared to concrete, which allows the air to heat and cool more rapidly than concrete.

Olson Engineering of Wheat Ridge, Colorado conducted ground penetrating radar evaluations. They used both a ground-coupled system and a truck-mounted system to provide a thorough evaluation. The ground-coupled system was mounted on a cart similar to a jogging stroller. The antenna can also be used without a cart. The truck-mounted system was used on a pickup truck. Both systems used a GSSI interface. Dr. Chris Barnes of Dalhousie University in Nova Scotia performed the signal analysis and produced the damage maps. Normalized rebar reflection amplitudes were later corrected for the influence of varying bar depth using proprietary thresholds. This improved accuracy in predicting location and extent of

delaminations and active corrosion. Olson Engineering reported difficulty in obtaining clear data with the vehicle mounted system for both the Casper and Douglas bridges. As a result, another GPR air-coupled system was used on the Douglas Bridge when the overlay was present. Resource International, Inc. (Rii) from Ohio performed this test. This system was able to travel at 30 mi/h without impeding traffic.

Damage maps were created to visualize the results for each evaluation. All data was recorded and plotted using computational and computer-aided design (CAD) software. These plots were standardized by using Microsoft Publisher to outline areas of concern and were color-coded for this thesis: chain dragging maps are grey; half-cell potential maps are purple; impact echo maps are red; thermal imaging maps are blue; GPR delaminations are green; and GPR corrosion maps are purple. Each damage map was compared pair-wise to see how the locations of damage correlated to one another. An example for 9 data points is shown in Chapter 4. Each map was evaluated using the 3 ft by 3 ft grid and values were assigned to each grid intersection: a value of zero indicates no damage was predicted and a value of one indicates damage was predicted by this method. The process was repeated for the other methods under consideration. The numerical ratings for both methods were then added together at each grid intersection. If both methods predicted no damage a value of zero was assigned to this grid point. If one method predicted damage and the other method did not, a value of one was assigned, and a value of two was assigned if both methods predicted damage. Values of 0 and 2 were equally weighted to calculate a percent correlation which is an indication of how many times the two methods aligned. Perfect agreement between two methods would result in a score of 100 percent. Results of pair-wise correlations are shown in Appendix A.

Cores were removed from each bridge to give a visual confirmation of the damage to the bridge deck in locations that had a range of methods indicating areas of concern. Areas that did not indicate damage were also taken to give a control core to compare with the others when possible. The overlay was present when the cores from the Douglas Bridge were removed whereas the coring on Casper and Remount bridges occurred on the bare concrete decks. The most useful data from cores was the observation of concrete condition during extraction. Compression testing did not provide information on delaminations because this test simply pushed the two distinct pieces of concrete together.

Recommendations and conclusions for WYDOT

One goal of this research project was to recommend a system-wide program for WYDOT that would save time while increasing safety, efficiency, and accuracy. A local level analysis, or bridge by bridge evaluation, is the most common form of bridge investigation for WYDOT. The system that would best meet these three goals combined is a vehicle mounted system such as the one used by Rii. This system improves the safety of an evaluation because the WYDOT crew remains in a vehicle with a following truck alerting other travelers to move around the inspection vehicle. The time required to perform scans would also be minimized if multiple evaluations could occur at a single given time. Any vehicle mounted system would need to overcome the issue of recording where each data collection point began and ended and estimating the positioning of the van based on the striping of the road. In the case of a rolling impact echo scanner such as that used by Olson Engineering, the accuracy would be improved due to the finer grid that could be obtained. It should be noted that the accuracy of GPR systems is decreased when the system is not in direct contact with the bridge deck surface. The cost of the Rii GPR system is estimated at 30 dollars per linear foot of a traditional 2-lane bridge. At this time a rolling impact echo scanner is not available. The authors recommend that WYDOT wait for systems to become commercially available and affordable before making a system-wide decision.

Impact echo, thermal imaging, and GPR methods are discussed below citing their merits and concerns for daily use. At the current time, these three systems only minimally improve the safety or efficiency of the bridge deck evaluation process because they require personnel on the bridge at all times, but they do increase accuracy by removing the bias that can occur with chain dragging.

The impact echo method can easily be implemented into a bridge deck analysis. For immediate results using the impact echo method, which is one advantage of chain dragging, individual grid points could be marked immediately on the deck instead of waiting to analyzing the data in the office. The initial cost of a typical Concrete Thickness Gauge from Olson Engineering and training would be approximately 8,500 dollars. In terms of field expense, the smaller the grid, the more expensive and time-consuming the investigation. On the other hand, Olson Engineering's rolling bridge deck scanning system has 18 times more data points than the University of Wyoming's manual data collection system. The results correlated well. Olson's rolling bridge deck impact echo scanner, still in the developmental stage, may be a

quicker and more accurate solution for this method. The cost of this system is unknown because it is not yet commercially available.

Thermal imaging is not recommended for bridge investigations in Wyoming. The time to perform this test is much longer than the other methods, and it requires additional analysis to interpret the temperatures shown on the picture. The thermal camera is dependent on clear weather and eliminating surrounding obstructions. Neither of these two criteria is guaranteed for any particular testing date or bridge deck. The test is also subjective in that colors obtained may be dependent on the particular temperature. This issue could be resolved but the above criteria may still limit use of thermal imaging. The asphalt overlay on Remount seemed to compound this issue. There are solutions that will automatically scan the deck, but that technology starts at 90,000 dollars.

The ground penetrating radar systems provide a detailed analysis of the bridge decks. Corrosion in the deck can be quantified which can remove the necessity for collecting half-cell potentials. The GSSI BridgeScan System is recommended. The base price for this system is 30,000 dollars and training is available for the users of the system. Another advantage of the GPR method is that depth of a defect can be observed because it provides a cross-section of the data. The next step would be to eliminate the resolution difference between a vehicle mounted system and a direct-contact system. For example, if a vehicle mounted system provided the same level of accuracy, this would be the preferred method of evaluating bridge decks.

The research team recommends a combination of impact echo scanning and GPR for more accurate bridge deck evaluations. It may be useful to wait for these systems to become commercially available or work together to develop a vehicle mounted system that improves safety while providing the same level of accuracy.

Table of Contents

List of Figures

List of Tables

Chapter 1 Introduction

Bridge deck evaluations have become an integral part of the Wyoming Department of Transportation's (WYDOT) management of bridge repairs and reconstruction. Currently, evaluation crews are sent out to perform tests on the bridges using chain dragging, half-cell potentials, and chloride sampling. Chain dragging can indicate the presence of delaminations, whereas half-cell potentials indicate levels of corrosion in steel reinforcement. Chain dragging, which can be affected by outside variables such as traffic and wind noise, identifies only those delaminations that are in progressive stages (Gucunski et al. 2005). Chain dragging and half-cell potentials are discussed in greater detail in Section 3.1 and 3.2. Chloride sampling, which determines the amount of chloride in the concrete (lb./yd^3), was not part of this study.

WYDOT currently uses data from these tests to put repair schedules out to bid. The current practice is to evaluate bridges every two years. The state of Wyoming has 13.1 million sq. ft of bridges, and the entire United States has more than 3.7 billion sq. ft of bridges (FHWA 2009).

Because nondestructive evaluation (NDE) is minimally invasive and bridges can remain in service while being tested, it is the preferred method of evaluating bridges. After an extensive literature review, three types of NDE were chosen for this project: impact echo scanning, thermal imaging, and ground penetrating radar (GPR). These NDE methods are discussed in detail in Sections 3.3 through 3.5. The purpose of this research is to investigate the effectiveness of these three types of NDE in the hope that it may enhance WYDOT's bridge deck evaluation efforts.

Chapter 2 Objectives

This research project provides a detailed assessment of NDE evaluation techniques, which is a direct comparison of chain drag, half-cell potential, impact echo, thermal imaging and GPR methods. This comprehensive analysis, rarely completed in field studies, is applied to three different types of bridge decks. The goal is to recommend a practical solution that WYDOT can implement. A solution is crucial in promoting the department's desire to be leaders in bridge deck evaluation. In particular, the solution should capitalize on safety, efficiency and accuracy.

The research can be broken down into the following objectives:

- Evaluate three bridges with different surface compositions: bare concrete deck, latex modified concrete overlay, and asphalt overlay. Traditional WYDOT methods will be used.
- Use impact echo, thermal imaging, and GPR methods to evaluate the three bridge decks and compare results to those obtained by WYDOT's traditional evaluation methods of chain dragging and half-cell potentials.
- Extract cores from the bridge decks where possible and attempt to compare these cores to all evaluation methods.
- Reevaluate the bridges that had overlays after the bridge decks after the overlays were milled off.
- Provide advantages and disadvantages of alternate procedures for bridge deck evaluations.

Chapter 3 Literature Review and Background

This section presents a review of the literature pertaining to the development and use of NDE methods with an emphasis on the examination of concrete bridge decks. It also describes the NDE methods used in this research and provides results of previous investigations using these methods.

WYDOT currently uses a combination of chain dragging, half-cell potential evaluations, and chloride sampling for their bridge deck inspections. Chain dragging is used to measure delaminations and areas of concern in the concrete decks whereas half-cell potentials investigate for potential corrosion in the steel reinforcement. Chloride sampling was not part of this study.

3.1 Chain Dragging

Chain dragging utilizes a row of chains attached to a handle which is moved back and forth across a bridge deck. Common configurations consist of four or five segments of 1 in. chain links approximately 18 in. long (ASTM D 4580). The operator drags the chains over the entire bridge deck, listening for dull tones that indicate hollow sections. When the process is completed, the operator records the delamination locations on a map of the bridge deck. Due to varying levels of operator experience and hearing acuity, several investigators report that determining areas of damage with this test is a subjective process (Graybeal et al. 2001; Gucunski et al. 2005; Parillo and Roberts 2006; Huston et al. 2007a).

Henderson et al. (1999) connected the chain drag apparatus to a microphone in an attempt to standardize and automate the evaluation. A cart was customized to hold the chains and microphone equipment. Because preliminary testing on defect frequencies provided values outside the suggested range from the most up-to-date version of the standard at the time of publication, these researchers suggest using an automated impactor to penetrate areas of the deck deeper than those accessible by dragging chains. This concept is similar to the impact echo technique used in this research (Section 3.3).

3.2 Half-cell Potential Evaluation

To determine if the bridge deck's reinforcing steel is corroding, WYDOT uses a half-cell to measure voltage potentials. An electrical circuit is used to measure the half-cell potential as shown in Figure 1. One of the voltmeter leads is connected to the reinforcing steel in a predrilled hole, while the other lead is connected to the copper-copper sulfate half-cell. A sponge on the half-cell end provides electrical continuity. The sponge is wetted with a contact

solution to standardize the potential drop (ASTM C 876). The half-cell, which produces an electrical field, is then moved about the deck, and voltages are read and recorded.

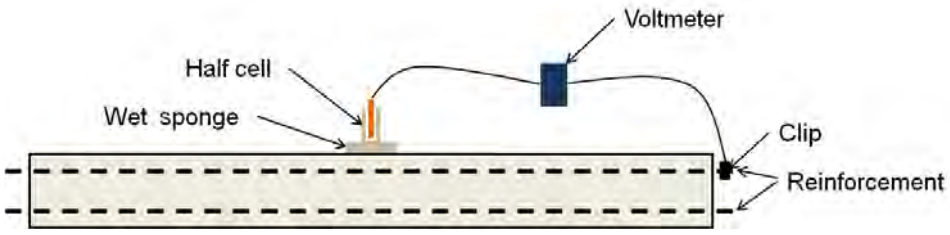

Figure 1: Half-cell potential circuit.

The results are presented as an equipotential contour map with a maximum contour interval of 0.10 V. Data interpretation is based on the guidelines shown in Table 1 (ASTM C 876).

Table 1: Probability of corrosion in the reinforcing steel (ASTM C 876).

Potential	Probability
Potentials are more positive than -0.20 V.	90% probability that no corrosion is occurring.
Potentials are between -0.20 V to -0.35 V.	Corrosion activity is uncertain.
Potentials are more negative than -0.35 V.	90% probability that corrosion is occurring.

3.3 Impact Echo Scanning

Since its development at Cornell University, numerous articles have been published about the history and background of impact echo scanning (Sansalone and Carino 1988; Sansalone 1997). In addition, a textbook has been published and serves as the primary reference for the test method (Sansalone and Streett 1997). Impact echo scanning is used to locate cracks, delaminations, voids, honeycombing, and debonding in concrete and is covered by ASTM C 1383 (Jaeger et al. 1996; Tinkey and Olson 2008). The majority of impact echo tests are currently being carried out on bridges to find delaminations and voids in post tensioning grouted ducts, and to determine deck thicknesses.

Impact echo scanning utilizes the propagation of sound waves through concrete and masonry to measure thickness and identify internal flaws. Sound waves propagating through the structure reflect back when they encounter a transition zone such as an internal flaw or external surface. The relationship between the thickness of the concrete with air interfaces on both sides and the frequency of the sound wave is shown below (Sansalone and Streett 1997):

Equation 3-1

$$f = \frac{C_p}{2T}$$

where

f = the frequency of the waveform (hz),
C_p = the velocity of the wave (ft/s), and
T = thickness of test area (ft).

A typical wave velocity for 3,000 to 4,000 psi concrete is 12,000 ft/s. A denser concrete will have a higher wave velocity. The sound wave is transformed from the time domain to the frequency domain where a peak forms indicating the general thickness of the concrete (Figure 2). In the event of a delamination or a void, two peaks will occur showing the delamination thickness as well as an increased thickness showing the path the sound waves traveled around the void (Figure 3 and Figure 4). However, some researchers note that when a delamination or void is encountered, the apparent thickness shift in the frequency makes it difficult to determine the depth of the void (Abraham and Cote 2002; Tinkey and Olson 2008).

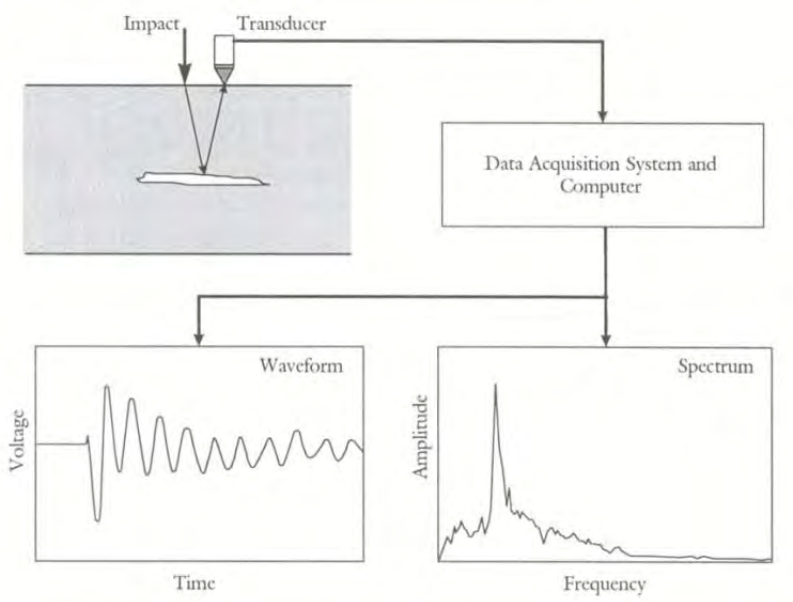

Figure 2: Basic impact echo process (Sansalone and Streett 1997).

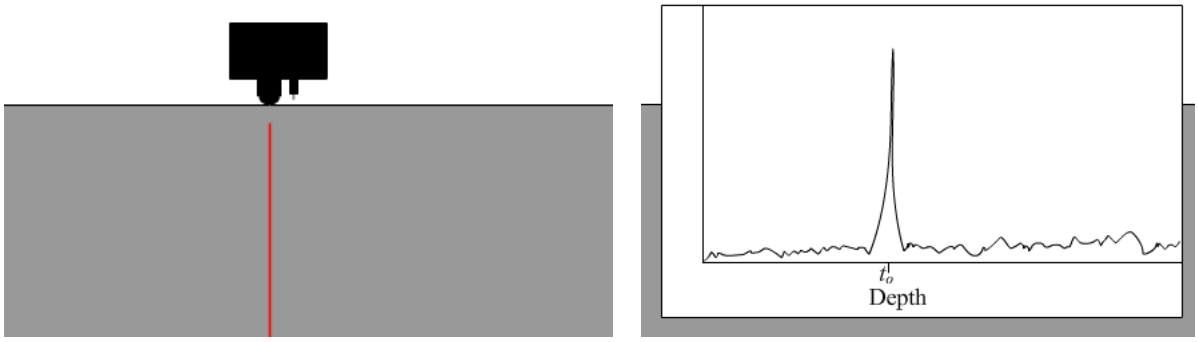

Figure 3: Example of sound wave path and corresponding frequency plot in sound concrete (Coombs 2007).

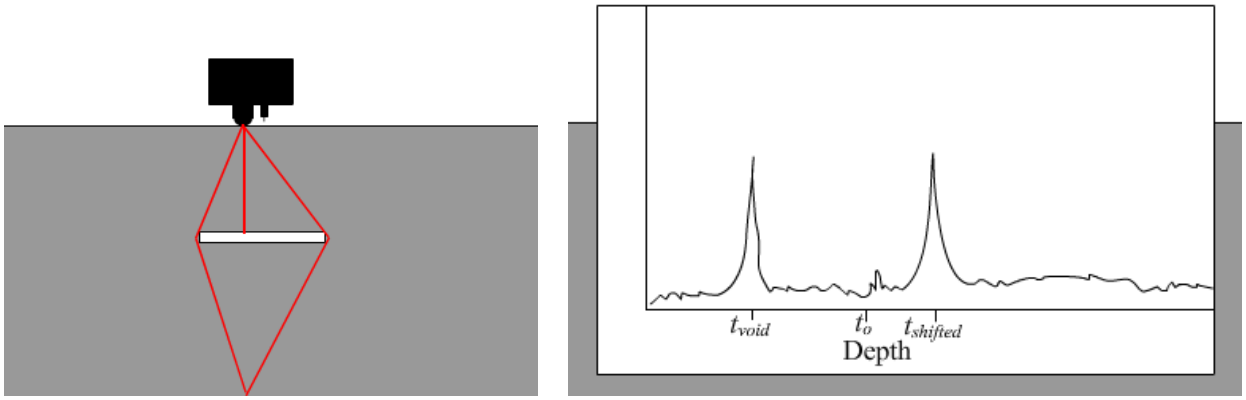

Figure 4: Example of wave path and corresponding frequency plot in concrete with internal flaw or delamination (Coombs 2007).

Olson Engineering is developing a vehicle-mounted scanner consisting of a set of wheels with six impact echo devices spread around the perimeter to increase the speed of data acquisition. Figure 5 shows a prototype of the scanner (Tinkey and Olson 2010).

Figure 5: Olson Engineering's Impact Echo Bridge Scanner.

3.3.1 Bridge Decks

Many investigations of bridge deck evaluations using impact echo have been completed. One group completed evaluations on existing bridge decks, resulting in numerous publications (Gucunski et al. 2005; Gucunski et al. 2006; Gucunski et al. 2008a, b). This research team considered methods to present the data using 3D visualization techniques, and impact echo testing was deemed successful in monitoring and evaluating bridge decks (Gucunski et al. 2008b). They also recommended a complementary evaluation with ground penetrating radar to make a more complete evaluation.

Henriksen (1995) presented results of three case studies regarding the use of impact echo to evaluate both poor and slightly damaged concrete structures. The author described the impact echo method as a powerful tool as long as the user is experienced in performing and analyzing the tests. The author also claimed that the impact echo method can detect areas of alkali-aggregate reaction. In addition, the investigator studied the economics of bridge repair and recommended that testing costs should not exceed 1-5% of repair costs.

Tawhed and Gassman (2002) transported sections of a bridge deck to a laboratory to complete studies on them. This bridge deck was over 45 years old. Impact echo methods were successful in determining relative quality of concrete, localized failures, and cracks in the slab.

Impact echo tests can also be used to evaluate the condition of a bridge deck overlay such as asphalt, latex modified concrete, or silica fume. Asphalt overlay is a softer material

than concrete, which causes a change in the material wave speeds (Sansalone and Streett 1997). Sansalone and Streett performed a case study in which they were able to account for differences in wave velocities and correctly identify the interface of the overlay and concrete and locate delaminations between the layers (1997).

3.3.2 Summary of Impact Echo Capabilities

The capabilities and limitations of impact echo are summarized in Table 2 (Abudayyeh et al. 2004; Yehia et al. 2007). Section 3.6 provides tables of previous tests and important findings and comments from each.

Table 2: Summary of impact echo (Abudayyeh et al. 2004; Yehia et al. 2007).

Uses	Advantages	Limitations
• Detecting voids, cracks, delaminations, unconsolidated concrete, and debonding. • Determining thickness.	• Requires one surface of the tested material to be exposed, independent of the geometry of the structure. • Less susceptible to steel reinforcement. • High accuracy.	• Size of detected flaws is highly dependent on the impact duration. • Less reliable in the presence of asphalt overlays. • Interpretation of the results is difficult.

3.4 Thermal Image Scanning

Thermal imaging is another common technique used for NDE to evaluate the condition of a wide spectrum of materials. Infrared radiation makes up part of the electromagnetic spectrum and falls between visible light and radio waves with wave lengths ranging from 0.75 μm to 1 mm. All objects above zero degrees Kelvin emit infrared energy with emission be proportional to the temperature to the 4^{th} power. Thermal imaging uses infrared radiation that is felt in the form of heat. A thermal imaging camera is able to detect temperature variations between sound and damaged concrete (Clark et al. 2002). To achieve a good thermal image, a temperature difference is required and can be achieved through solar radiation or a forced temperature change to one side of a structure.

Radiation is the transfer of energy between different bodies of matter. In the case of bridge decks, energy is transferred from the sun to the bridge deck, and then from the bridge deck to the surrounding environment. This transfer of heat is governed by the Stefan-Boltzmann law (Cengel and Boles 2006), which is expressed as:

Equation 3-2

$$\dot{Q} = \varepsilon \sigma A T_s^4$$

where

$\dot{Q}$ = the rate of emission of energy (Watts),
ε = the emissivity of the surface (dimensionless, a fraction of a perfectly radiant body depending
on the material,
σ = Stefan-Boltzmann constant, 5.67 x 10^{-8} Watts/(m^2K^4),
A = the surface area of the object (m^2), and
T_s = absolute temperature of the surface (K).

The thermal camera converts this radiation to an image where differences in energy emission are definable by contrasting colors.

3.4.1 Bridge Decks

Thermal imaging investigations of bridge decks have been completed using both lab and field testing. Seven studies successfully used thermal imaging of concrete structures, of which most involved bridge decks (Knorr et al. 1983; Kunz and Eales 1985; Manning and Holt 1986; Halabe et al. 2003; Shroff 2005; Yehia et al. 2007; Abdel-Qader et al. 2008).

Previous studies conducted using thermal imaging and ASTM D 4788 Standard Test Method for Detecting Delaminations in Bridge Decks Using Infrared Thermography resulted in the following conclusions:

- Infrared technology cannot always differentiate between a delamination and a debonding of the overlay (Kunz and Eales 1985).
- During periods of heating, delaminated concrete heats more rapidly than sound concrete. The reverse occurs during periods of cooling. These areas will be visible in the thermal images and delaminations can be located (Manning and Holt 1986).
- Oil drippings, tire marks, and other markings can show up on the camera (Knorr et al. 1983). These authors recommended testing between 8:00 a.m. and 2:00 p.m.
- Do not test when the wind is above 30 mph or when the temperature is below 32 F (ASTM D 4788).
- It does not give information about the depth or extents of defects (Knorr et al. 1983; Yehia et al. 2007).

- Three hours of direct sunlight are necessary for the deck to emit enough heat for the camera to recognize a temperature difference (ASTM D 4788).

Juranty (1995) claims that thermal imaging on a bridge deck with asphalt overlay will denote areas of concern, but that debonding of the asphalt from the deck will be confused with delaminations in the deck. When this researcher combined thermal imaging results with GPR and visual inspection, the predicted areas of damages were found to be within 4% of actual deterioration.

3.4.2 Summary of Thermal Imaging Capabilities

A summary of the capabilities of thermal imaging is presented in Table 3 (Abudayyeh et al. 2004; Yehia et al. 2007). Section 3.6 provides tables of previous tests and important findings and comments from each.

Table 3: Summary of thermal imaging (Abudayyeh et al. 2004; Yehia et al. 2007).

Uses	Advantages	Limitations
• Detection of thermal differences, delaminations, cracks, and voids.	• Portable. • Simple, easy interpretation. • Minimum traffic interference (if mounted on a vehicle for continuous recording).	• No information about depth of defects. • Dependant on environmental conditions. • Can interfere with traffic if single still images are taken.

Knorr et al. (1983) discussed the cost effectiveness of thermal imaging. The initial costs were very high and thermography was not recommended for smaller systems with few bridges. They did, however, mention that developing a van-mounted system to automate the test would increase the cost effectiveness of the system.

3.5 Ground Penetrating Radar

Ground penetrating radar was originally used to search for buried objects and to map subterranean geology (Davidson and Chase 1998). Built on electromagnetic theory, GPR results from more than two centuries of work. Maxwell's equations of electromagnetic fields and constitutive relationships allow the quantitative analysis of GPR signals (Annan 2009).

Ground penetrating radar systems are made up of a control unit (computer) and an antenna (Figure 6). The GPR method involves moving an antenna across a test surface while periodically pulsing electromagnetic waves from the antenna and measuring the return strength. The internal makeup of the system being investigated can then be mapped. The pulses are sent out from the GPR computer driving the antenna at a frequency range centered on the design center frequency of the antenna. Huston et al. (2002) recommends using a 2 GHz antenna as the minimum frequency to collect data. Geophysical Survey Systems, Inc. (GSSI) provides recommendations for radar frequencies for specific jobs (Table 4).

Table 4: Recommended radar frequencies (GSSI 2006).

Depth Range	Antenna Frequency	Appropriate Application
0-1.5 ft	1600 MHz	Structural Concrete, Roadways, Bridge Decks
0-3 ft	900 MHz	Concrete, Shallow Soils, Archaeology
0-12 ft	400 MHz	Shallow Geology, Utilities, Archaeology
0-25 ft	200 MHz	Geology, Environmental, Utility, Archaeology
0-90 ft	100 MHz	Geologic Profiling
Greater than 90 ft	80, 40, 32, 20, 16 MHz	Geologic Profiling

The higher the frequency, the more detailed the results will be. However, the depth the unit can reach is inversely proportional to the frequency. The data from a GPR test is the reflected response from the wave pulses sent into the deck in which the weakened energy response affects the waveform and will tell whether or not there is a change in material (Barnes and Trottier 2002).

GPR systems can locate reinforcements as well as detect voids, cracks, delaminations, unconsolidated concrete, and debonding in bridge decks (Yehia et al. 2007). Figure 6 and Figure 7 shows the schematic of a simplified GPR system and the response captured by a computer. Direct results from a radar system are shown in Figure 8. Weak and strong signals can be seen in this scan, and the responses are later mapped showing areas of concern.

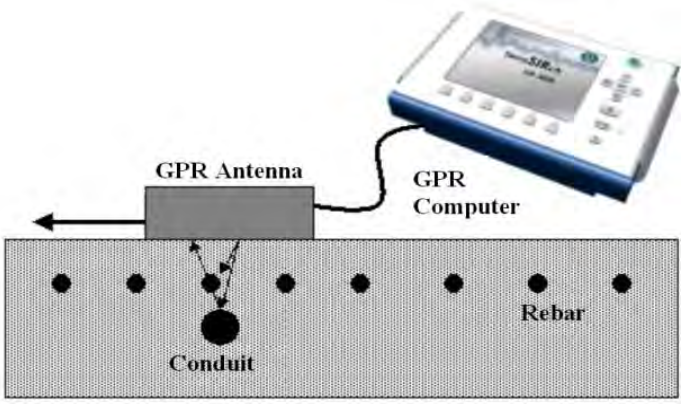

Figure 6: Schematic of GPR equipment and test setup (Olson Engineering).

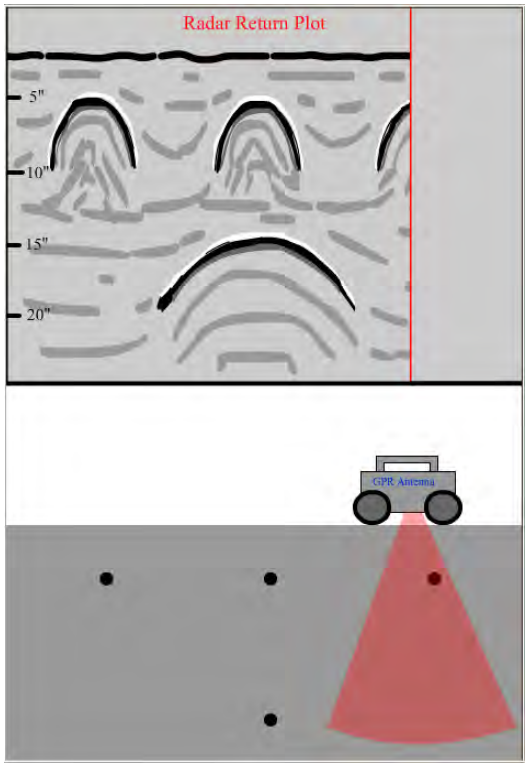

Figure 7: Simplified GPR system and response from The Masonry Society website (Coombs 2007).

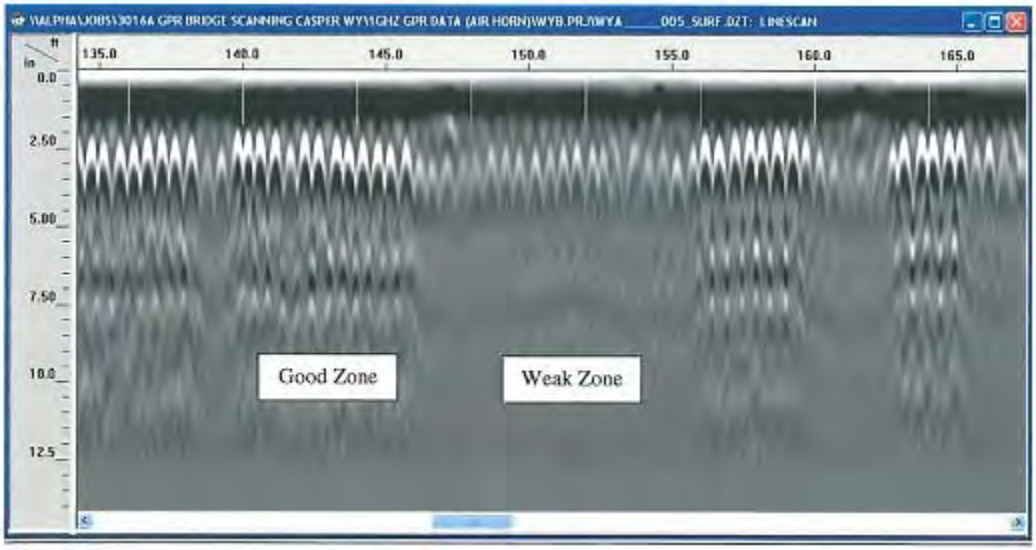

Figure 8: Characteristic radar returns (Olson Engineering).

3.5.1 Types of GPR Systems

The two main types of GPR systems are air-coupled systems, that are typically vehicle mounted, and ground-coupled systems, that rest directly on the surface of the ground.

Air-coupled systems were used in vehicle mounted systems as early as 1992 (Alongi et al. 1993). Two air-coupled systems were developed by the Lawrence Livermore National Laboratory for the Federal Highway Administration (FHWA) (Warhus et al. 1994). High-speed Electromagnetic Roadway Mapping and Evaluation System (HERMES) was designed to survey deck condition during normal traffic flow. Precision Electromagnetic Roadway Evaluation System (PERES) is slower and provides a more accurate survey (Davidson and Chase 1998; Scott et al. 2000). FHWA funded the PERES system, a second generation of the HERMES (Huston et al. 2007a, b). It is much simpler and uses one antenna, whereas the HERMES system uses 64 antennae to get a wider scan in a single pass (Scott et al. 2000). The PERES system consists of an air horn antenna mounted onto two A-frames moved manually along the road (Huston et al. 2007a, b). Images of the van-mounted system and the PERES system are shown in Figure 9. The air horn systems must be calibrated for the distance from the bridge deck to the antenna.

Figure 9: PERES II system and vehicle mounted systems (Huston et al. 2007b).

Maser (1995) created a radar van that tested over 150 pavement and bridge sections. Maser's system demonstrated ± 4.4% accuracy when 64 of the bridges were compared to ground truth evaluations. Many DOTs participated in this study, including WYDOT.

Ground-coupled systems rest directly on the roadway surface and transmit the impulses and return data in a form similar to that of the air-coupled system. Geophysical Survey Systems, Inc., (GSSI) developed and sells a self-contained, cart-based GPR system, which claims to accurately estimate repair costs (Figure 10). An optional GPS system can be integrated into the GPR in to ease data interpretation.

Figure 10: Typical GPR ground-coupled cart.

3.5.2 Previous Testing-General

Several groups have used GPR systems successfully and ASTM specifications exist (ASTM D 6087; ASTM D 6432; Clemena 1983; Warhus et al. 1994; Juranty 1995; Maser 1995; Warhus et al. 1995; Davidson and Chase 1998; Chase 1999; Huston et al. 1999; Barnes and Trottier 2002; Hugenschmidt 2002; Shroff 2005; Barnes et al. 2008; Belli et al. 2008; Yehia et al. 2008). Barnes and Trottier (2002) mentioned that epoxy coatings on reinforcing steel can cause problems with the accuracy of GPR. They also mention that when moisture and chlorides are present, the apparent deterioration is magnified and the accuracy of the test is lowered.

3.5.3 Bridge Decks with Overlays

Currently, WYDOT evaluations of asphalt-overlaid decks are limited to chloride sampling, coring, and visual inspection. GPR can be useful for these types of decks. An extensive discussion of the effects of asphalt on a GPR evaluation is presented by Barnes and Trottier (2002). Since radar can investigate multiple-layered materials, the concrete-asphalt combination will work well, according to these researchers. Barnes and Trottier report that, when the asphalt and concrete debond, the GPR signal will vary and be reflected. They also mention that, when moisture and chlorides are present, the apparent deterioration is magnified and the accuracy of the test is lowered. They also used GPR to find areas of corrosion and compared them to half-cell potential results. A New Hampshire DOT evaluation of asphalt covered decks had success with GPR, with researchers saying although GPR is not perfect, it far exceeds other forms of evaluation (Juranty 1995). Chung and Carter (1993) found signal reflection problems caused by multiple layers of asphalt and traffic induced variations in the asphalt.

3.5.4 Summary of GPR Capabilities

A summary of the capabilities of GPR is presented in Table 5 (Abudayyeh et al. 2004; Yehia et al. 2007). Section 3.6 provides tables of previous tests and important findings and comments from each.

Table 5: Summary of GPR (Abudayyeh et al. 2004; Yehia et al. 2007).

Uses	Advantages	Limitations
• Concrete mapping, mining, geotechnical, road, and bridge. • Forensics. • Detection of voids and honeycombing. • Delaminations. • Moisture content.	• Versatility. • Portability. • Effectiveness. • Low cost. • Good with overlays. • Minimum traffic control (vehicle-mounted system). • Prediction of repair quantities.	• Interpretation. • Complexity of results. • Can interfere with traffic (cart-mounted system).

3.6 Summary of Previous Tests

The following tables are a compilation of completed tests, either in the lab or in the field. Comments are included from each test discussing what lessons were learned or valuable tips in testing procedures. Table 6 lists the bridges that were evaluated by nondestructive means, while Table 7 contains previous research work on tests slabs in laboratories.

Table 6: List of bridge decks evaluated using NDE methods.

Location	Nondestructive procedure	Overlay	Comments	Researcher
Michigan	GPR, Chain Drag	Concrete	GPR more accurate than chain dragging.	Yehia et al. 2005
Nova Scotia	GPR	Asphalt	Epoxy-Coated Reinforcement may cause inaccuracies.	Barnes and Trottier 2002
Nova Scotia	GPR	None	Automated depth correction improved accuracy and precision.	Barnes et al. 2008
Virginia	Impact Echo	Concrete	IE can detect deck delamination but "precise interpretation of the measured parameters has yet to be fully automated."	Gucunski et al. 2008b
Eastern US	GPR	Asphalt	First known vehicle mounted GPR system.	Alongi et al. 1993
Eastern US	GPR/Impact Echo	Concrete/ Asphalt	Rough surfaces caused problems testing with the impact echo method.	Davis 1996
Ohio	GPR/Manual Sounding	Silica Fume	GPR overestimated the cracks/delamination.	Fitch and Abdulshafi 1998
Vermont	GPR	Concrete	Creation of a GPR cart system.	Huston et al. 1999
Ontario	GPR	Concrete	Developed their own radar van and discussed the logistics (operating) of operating the vehicle.	Carter, Chung et al. 1995
Illinois	GPR, Thermal Imaging	Concrete	Infrared technology cannot always differentiate between a delamination and a debond of the overlay.	Kunz and Eales 1985
NA	GPR	Asphalt	The waterfall method of interpretation was used and was successfully with an asphalt overlay.	Chung and Carter 1993
Mississippi	Chain Dragging		Developed a computerized system for chain dragging.	Henderson et al. 1999
New York	Impact Echo, Thermal Imaging, GPR	Concrete	Tested a long bridge in New York State, Good correlations from the NDE and ground trothing.	Shroff 2005

Location	Nondestructive procedure	Overlay	Comments	Researcher
New Jersey	Impact Echo, GPR	Concrete	IE can detect deck delamination but it is not fully automated yet.	Gucunski, Rascoe et al. 2008a
Illinois	Thermal	Concrete	Oil drippings, tire marks, and other markings showed up on the camera. They recommended to test between 8:00 a.m. and 2:00 p.m.	Knorr et al. 1983
California	GPR	Concrete	HERMES and PERES systems.	Davidson and Chase 1998
Switzerland	GPR	Concrete	Data was difficult to interpret.	Hugenschmidt 2002
Connecticut	Impact Echo, GPR	Asphalt overlay	Vehicle mounted system was used.	Gucunski, Romero et al. 2005
New Hampshire	Thermal Imaging, GPR	Asphalt overlay	Excellent summary table relating test methods to field conditions.	Juranty 1995

Table 7: Summary list of test slabs for different investigations.

Nondestructive Test Procedure	Defect in Slab	Comments	Researcher
GPR	24 x 24 x 6 in. slabs, air cracks, water-filled cracks, reinforcement	GPR is less sensitive to ambient conditions.	Halabe et al. 1997
GPR	Delamination with asphalt overlay	They claim GPR gives more promising results than most other types of test.	Chen et al. 1997
Thermal	Delaminations	ASTM D 4788 Standard Test Method for Detecting Delaminations in Bridge Decks Using Thermography.	Khan 1998
GPR	Cracks, Delaminations	They reported GPR overestimated the cracks/delamination.	Fitch and Abdulshafi 1998
Thermal	Voids, Delaminations	An approach was used to refine the thermal images.	Abdel-Qader et al. 2008
Impact Echo, Thermal Imaging, GPR	Surface Cracks, Voids, and Delaminations	General reference article regarding these three tests.	Yehia et al. 2007
GPR	Voids, Delaminations	HERMES and PERES radar systems were used.	Scott et al. 2000
GPR	Cracks, Voids, Delaminations	The thicker the specimen, the more accurate the test.	Yehia et al. 2005

Chapter 4 Field Testing and Methods

Three types of bridge decks were studied in Wyoming: a bare concrete bridge deck in Casper, a concrete deck with a latex modified concrete overlay in Douglas, and a concrete deck with an asphalt overlay near Buford. The methods used were chain dragging, half-cell potential evaluations, impact echo, thermal imaging, and GPR, (air-coupled and ground-coupled). Cores from all three bridges were also extracted and evaluated, and those results were compared with those obtained using the tools described above. This chapter describes the bridges studied, along with field testing and analysis procedures.

4.1 Casper Bridge

The first bridge, with a bare concrete deck, is located on First Street in Casper, Wyoming, at milepost 2.09. The bridge contains 4 spans over the North Platte River, and the deck was designed to be 7 in. deep. The centerline length is 360 ft with skewed ends and a radius of 955 ft. The tests were conducted during the week of June 15, 2009. Only the eastbound lanes were evaluated due to weather and time constraints. Figure 11 shows the bridge looking northeast. Figure 12 shows the underside construction of the bridge.

Figure 11: First Street Bridge in Casper, Wyoming.

Figure 12: First Street Bridge underside in Casper, Wyoming.

4.2 Douglas Bridge

The second bridge, which had a latex modified concrete overlaid deck, is located in Douglas, Wyoming on the southbound lanes of I-25 (structure AFY) at milepost 137.6. The bridge is 186' long with skewed ends and contains four spans. The deck was designed to be 7.25 in. deep; the overlay increased the depth to 8 in.

Tests were conducted during the week of August 3, 2009 with the overlay present. During the week of August 6, 2010, tests were conducted using a van-mounted GPR scanning device. The concrete overlay was then removed by milling 1 to 1.25 in. down. Tests were conducted without an overlay present during the week of August 27, 2010. Figure 13 shows the bridge looking north. Figure 14 shows the underside construction of the bridge.

Figure 13: Southbound I-25 (Structure AFY) Bridge in Douglas, Wyoming.

Figure 14: Southbound I-25 (Structure AFY) Bridge underside in Douglas, Wyoming.

4.3 Remount Bridge

The third bridge, the eastbound bridge of the Remount Interchange on I-80 (structure AYB), recently had an asphalt overlay applied after a traffic accident occurred. A silica fume overlay was present and partially milled off before the asphalt overlay was applied. Located at milepost 339.32, this bridge is three spans and is 93 ft long. Initial tests with the asphalt overlay

present were conducted during the week of May 24, 2010. After that, the overlay was removed. The milling depth was 3 to 3.5 in. of material, including all of the asphalt down to the top layer of reinforcing steel. Evaluations without the overlay occurred during the weeks of August 9, 2010 and August 30, 2010. Figure 15 and Figure 16 show the bridge looking northwest and the underside of the bridge.

Figure 15: Eastbound Remount Bridge (structure AYB), near Buford, Wyoming.

Figure 16: Eastbound Remount Bridge (structure AYB) underside, near Buford, Wyoming.

4.4 Field Procedures

The following sections discuss the procedures that were used to evaluate the bridge.

4.4.1 Chain Dragging and Half-cell Potential Procedures

WYDOT performed all chain dragging and half-cell potential evaluations on all three bridges. Chain dragging evaluations were set up on a 5 ft by 5 ft grid to help with documentation. The entire deck is then dragged by the evaluator. Whenever a dull or hollow sound was heard, the area was outlined for documentation at the end of the test. Figure 17 shows a WYDOT inspector conducting a chain drag test.

Figure 17: Chain dragging evaluation.

Half-cell data was collected according to ASTM C 876 and standard WYDOT practices. The sponge on the half-cell was wetted when needed to give a clearer voltage. Readings were taken at specific locations provided by WYDOT's computer software. Once the readings were taken, the data was entered into their software to produce voltage maps. Half-cell data was collected from the Casper and Douglas bridges. On the Remount Bridge, half-cell data could not be gathered because an epoxy coating on the rebar masked the signal.

4.4.2 Impact Echo Procedure

To gather data for the impact echo test, a digital sounding device was used to measure the depth of concrete decks (Olson Instruments Concrete Thickness Gauge CTG™). This device uses a solenoid that strikes the surface and a receiver that converts the reading to concrete depth via a Fast Fourier Transform. Figure 18 shows impact echo tests being carried out by the University of Wyoming researchers.

Figure 18: University of Wyoming researchers performing impact echo test.

The impact echo tests also utilized grids to collect and organize data. A 3 ft by 3 ft grid provided the resolution recommended by previous research (Gucunski et al. 2008b). The thickness gauge was calibrated to provide accurate thickness readings. A location was selected on the deck in which the depth of the concrete was known to set the wave velocity. From there, data was collected methodically, with every test point's number and location recorded to later produce a graphical representation. Data was transferred to a laptop in the field. Olson Engineering's rolling impact echo bridge scanner was also used to test all three bridges as part of their development program for the apparatus.

4.4.3 Thermal Imaging

It was unknown whether thermal imaging would be a viable WYDOT option; as a result infrared cameras were rented for thermal imaging. A FLIR T250 camera used for the Casper Bridge and the Douglas Bridge with the overlay with infrared resolution of 200 x 150 pixels and

accuracy of ± 3.6 °F. It should be noted that this level of accuracy was reduced due to lens that was used to increase the area the camera could cover in one photograph. The camera used for the Remount Bridge, with and without the overlay, and the Douglas Bridge, without the overlay, was a FLIR B200, which has the same resolution and accuracy as the T250, but with a narrower range of readable temperatures. A boom and cart were used to raise the camera and orient it perpendicular to the bridge deck surfaces. Figure 19 and Figure 20 show the camera and the setup that was used.

Figure 19: Thermal camera.

Figure 20: Thermal camera setup.

The same 3 ft by 3 ft grid that was used for the impact echo tests was used for thermal imaging. Metallic gold paint was used to clearly locate the marks using the thermal camera (Figure 21). A laptop was connected to the infrared camera to collect and store the images. Once the camera was in the air and oriented perpendicularly to the deck, it could be centered over the point and saved as the location on the deck. The images were later stitched together using photo editing software. When the deck is heating up, damaged areas will be at a higher temperature than those of sound areas. This typically occurs a few hours after sunrise with clear skies. In the evening when the deck cools off, damaged areas will cool faster and will appear darker than sound areas. This is due to air's low conductance of heat compared to concrete, which allows the air to heat and cool more rapidly than concrete.

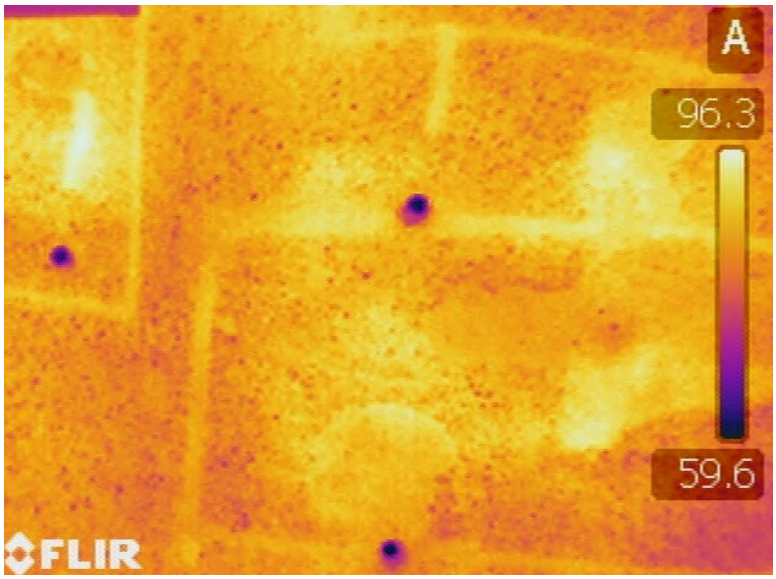

Figure 21: Metallic paint reflection in the infrared camera.

4.4.4 Ground Penetrating Radar

Ground penetrating radar tests were conducted by Olson Engineering and Resource International, Inc. (Rii).

4.4.4.1 Olson Engineering Tests

Olson Engineering of Wheat Ridge, Colorado conducted ground penetrating radar evaluations. They used both a ground-coupled system and a truck-mounted system to provide

a thorough evaluation. The ground-coupled system (Figure 22) was mounted on a cart similar to a jogging stroller. The antenna can also be used without a cart (Figure 23). The truck-mounted system (Figure 24) was used on a pickup truck. Both systems used a GSSI interface (Figure 25).

Figure 22: Ground-coupled GPR system.

Figure 23: Ground-couple GPR system without cart.

Figure 24: Truck-mounted GPR system.

Figure 25: GSSI interface that Olson Engineering uses.

Dr. Chris Barnes of Dalhousie University in Nova Scotia performed the signal analysis and produced the damage maps. Normalized rebar reflection amplitudes were later corrected for the influence of varying bar depth using Dr. Barnes' proprietary thresholds. This improved accuracy in predicting location and extent of delaminations and active corrosion.

A new GPR system from Ingeneria Dei Sistemi (IDS) was used by Olson Engineering on the Remount Bridge with the asphalt overlay. Known as the Aladdin System, this GPR setup

allows signals to be sent out in both parallel and perpendicular directions to provide a 3-dimensional scan. Both transverse and longitudinal bars can be seen with a single pass.

4.4.4.2 Resource International, Inc. Tests

Another GPR air-coupled test was performed by Resource International, Inc. (Rii) from Ohio for comparison purposes. This system was able to travel at 30 mi/h without impeding traffic. Figure 26 shows the vehicle mounted GPR setup on the Rii van. Douglas Bridge with the overlay was evaluated in this subcontract.

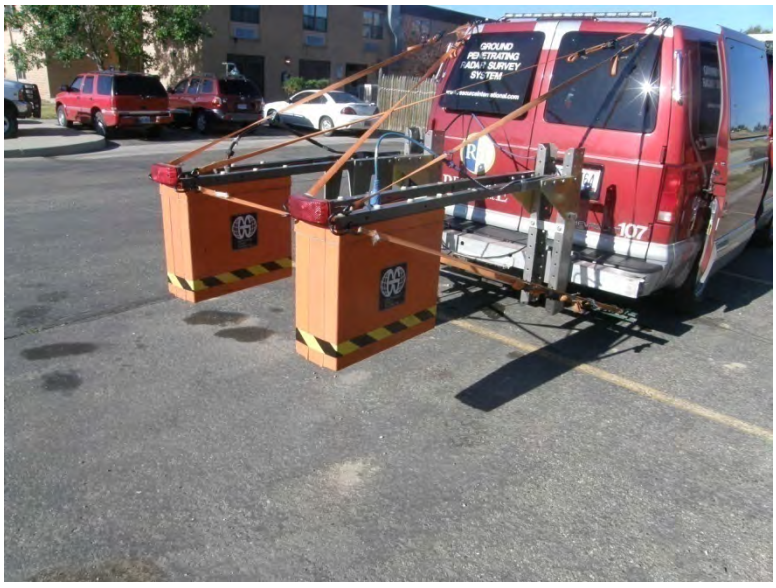

Figure 26: Radar apparatus on Rii's van.

4.4.5 Bridge Deck Damage Maps

Damage maps were created to visualize the results of each evaluation. All data was recorded and plotted using computational and computer-aided design (CAD) software. These plots were standardized by using editing software such as Microsoft Publisher to outline areas of concern. Each plot was color-coded for this project: chain dragging maps are grey; half-cell potential maps are purple and white; impact echo maps are red; thermal imaging maps are blue; GPR delaminations are green; and GPR corrosion maps are purple.

Each damage map was compared pair-wise to see how the locations of damage correlated to one another. An example for 9 data points is shown in Figure 27. Each map was evaluated using the 3 ft by 3 ft grid and values were assigned to each grid intersection (Table

8): a value of zero indicates no damage was predicted and a value of one indicates damage was predicted by this method. The process was repeated for the other method under consideration. The numerical ratings for both methods where then added together at each grid intersection. If both methods predicted no damage a value of zero was assigned to this grid point. If one method predicted damage and the other method did not, a value of one was assigned, and a value of two was assigned if both methods predicted damage (Table 9). In the combined summed values figure, squares rated 0 and 2 were equally weighted and squares rated 1 carried no weight. A percent correlation was calculated and this value is an indication of how many times the two methods aligned. For the example shown in Figure 27, there were seven matching values (0 or 2 in the summed values section) and two values that did not match (1 in the summed values section). The resulting correlation is 7/9 or 78%. Perfect agreement between two methods would result in a score of 100 percent.

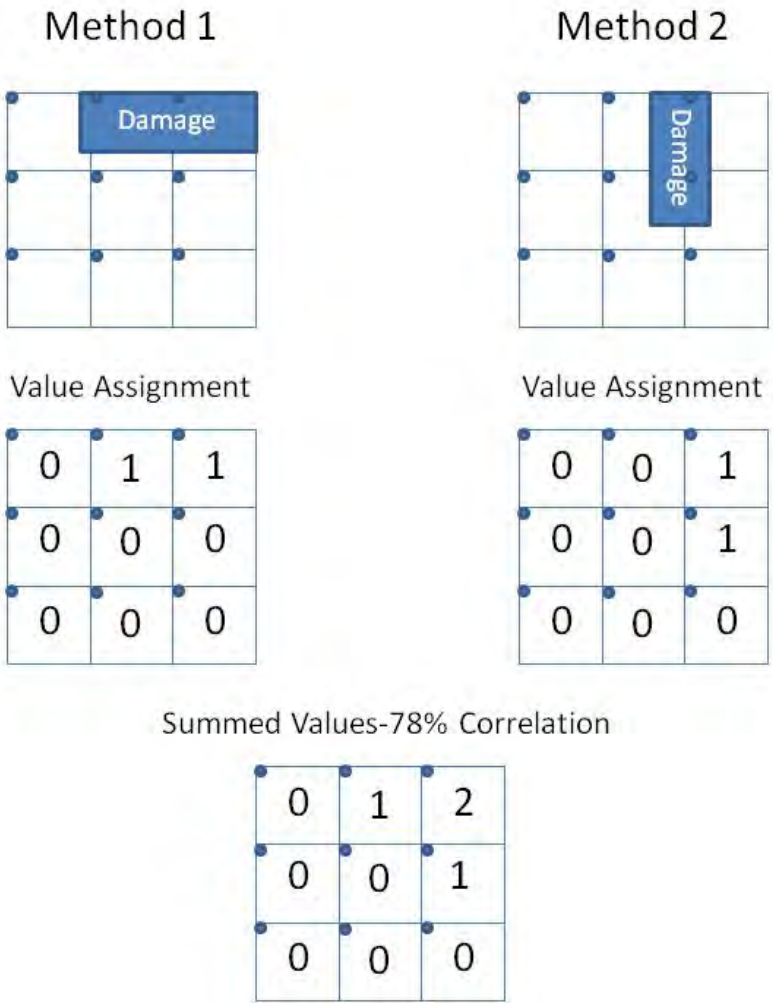

Figure 27: Pair-wise Correlation Example.

Table 8: Pair-wise value assignment indications.

Damage Indication	Value Assigned
No damage for a given point	0
Damage for a given point	1

Table 9: Pair-wise summed value indications.

Damage Indication	Summed Value
Neither method indicated damage	0
One method indicated damage	1
Both methods indicated damage	2

4.4.6 Core Evaluations

Cores were removed from each bridge to give a visual confirmation of the damage to the bridge deck in locations that had a range of methods indicating areas of concern. Areas that did not indicate damage were also taken to give a control core to compare with the others when possible. The overlay was present when the cores from the Douglas Bridge were removed whereas the coring on Casper and Remount bridges occurred on the bare concrete decks. The individual tests conducted on the cores are discussed in Appendix A for each of the bridges. Figure 28 shows the coring rig removing a core on the Casper Bridge. Although different crews were utilized to remove cores on each bridge, Tyler Robison was present for all coring.

Figure 28: Coring rig on Casper Bridge.

A correlation was conducted to evaluate the correctness of the predictions from each of the methods at each of the core locations. The cores from the Casper and Douglas Bridges were visually inspected and the percent correctness of the predictions was calculated in Equation 4-1. A percent was calculated for how many times the methods correctly predicted the state of the core. Remount cores were taken and visually inspected after the overlay was removed because it is difficult to core through asphalt overlay.

$$Percent\ Correlation = \frac{Times\ Method\ Correctly\ Predicted\ the\ Condition}{Total\ Cores} \qquad \textbf{Equation 4-1}$$

When the evaluation method predicted the condition of the core correctly, that core was given a point for that method. The points were added up and divided by how many cores were evaluated. This was then considered the percent correlation value, which can be found in Section 4.4.5.

4.5 Procedures Specific to each Bridge

The following sections discuss procedures that were unique to each bridge such as different grid spacing or additional testing performed on each bridge.

4.5.1 Casper Bridge

The Casper Bridge GPR studies utilized a grid of 1 ft in the transverse direction and 0.25 in. in the longitudinal direction. A 1600 MHz ground-coupled antenna and a 1000 MHz air horn were used. Readings were taken continuously along the longitudinal grid, with their positions recorded by using a distance wheel.

Cores from the Casper Bridge were removed for comparison between the methods. Beyond the visual inspections of the cores, ASTM C 39 Standard Test Method for Compressive Strength of Cylindrical Concrete Specimens was used to evaluate the compressive strengths of the cores.

4.5.2 Douglas Bridge

Olson Engineering's GPR tests on the Douglas Bridge utilized a grid of 1.5 ft in the transverse direction and 0.25 in. in the longitudinal direction. A 1600 MHz ground-coupled antenna and a 2000 MHz air horn were used. A distance wheel was used to take readings continuously along the longitudinal grid and record their positions.

The Douglas Bridge also utilized Rii's van-mounted system when the overlay was present. The test was conducted at 30 mph with scans taken every 1.5 ft transversely. Multiple passes were made to obtain accurate data. A WYDOT truck provided support by slowing traffic down behind the van with an arrow board. The antennas, from GSSI, were 1000 MHz. Figure 29 shows the van-mounted system in the field.

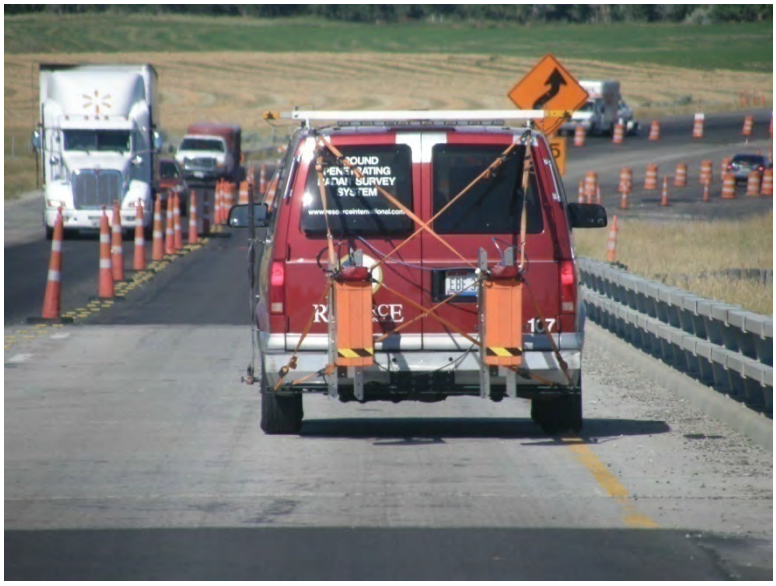

Figure 29: Rii's van-mounted system scanning the bridge.

Cores from the Douglas Bridge were also evaluated destructively as well as visual inspections. Compressive tests following ASTM C 39 were performed as well as splitting tension tests following ASTM C 496 Standard test Method for Splitting Tensile Strength of Cylindrical Concrete Specimens.

4.5.3 Remount Bridge

Olson Engineering performed an initial ground-coupled scan of the Remount Bridge deck using a procedure similar to that used on the Douglas Bridge. The scan revealed that the top reinforcing steel was oriented in the longitudinal direction. It is important to run the scans perpendicular to the top steel to get the most accurate measurement of corrosion and delamination. The closer the steel is to the top of the deck, the more likely it is to be corroded. After the initial scan, Olson Engineering returned to the bridge and moved the GSSI ground-coupled radar transversely across the deck at 30 cm. intervals.

The new GPR system from IDS was also used on the Remount Bridge (Figure 30). This system was moved across the transverse direction at 10 cm intervals. Carts were not utilized due to the short distances and the possibility of the cart sticking out into traffic.

Figure 30: IDS Aladdin ground-coupled radar system.

Cores from the Remount Bridge were also visually inspected and destructively tested. ASTM C 39 and ASTM C 496 were followed to evaluated selected core for compressive and splitting tensile strength, respectively.

Chapter 5 Results

This chapter discusses the results of the research project. Each individual bridge is considered, and overall conclusions are presented in Chapter 0. Results from the evaluations and reports from Olson Engineering and Rii are in the Appendix B.

5.1 Casper Bridge

Even though the Casper Bridge was curved, the results were fit to a straight bridge to compare the impact echo, thermal imaging, and GPR results to the chain dragging and half-cell potential results.

5.1.1 Damage Investigations

Chain dragging, impact echo, thermal imaging, and ground penetrating radar evaluations were compared. The collection of data went smoothly with one exception. Only the ground-coupled GPR system provided useable data. Data from the air-coupled system could not be used because the air horn radar did not have enough resolution to pick out individual reinforcing bar signatures (Section 5.1.4). Figure 31 presents a visual comparison of the damage maps for all four methods. Impact echo data was not collected directly on the curb due to interference with the signal response. When traffic flow was found to interfere with testing, thermal imaging was moved to 3 ft from the center line. Thermal imaging was carried out 3 ft from the centerline to permit travel in the adjacent lane.

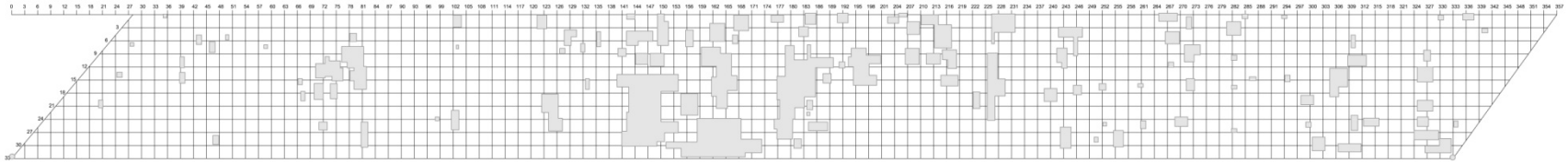

Chain Dragging

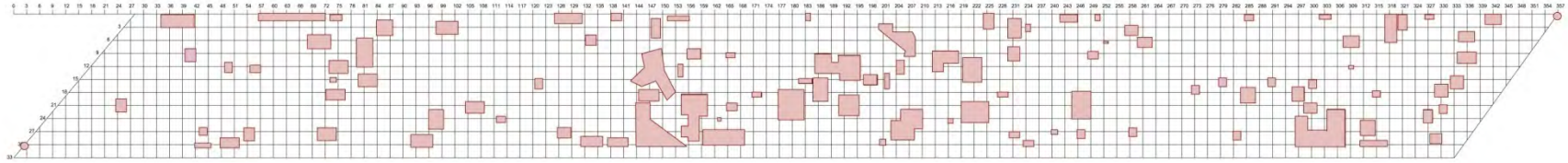

Impact Echo

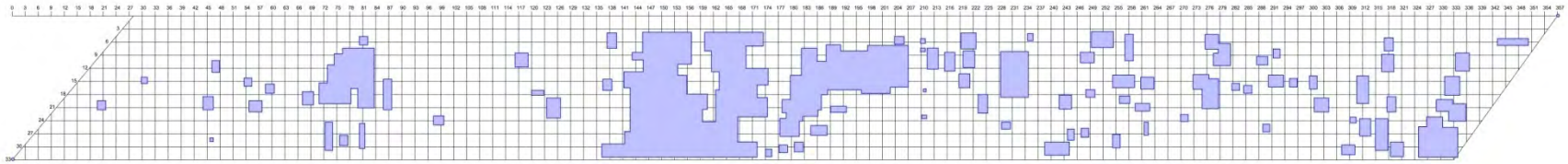

Thermal Imaging

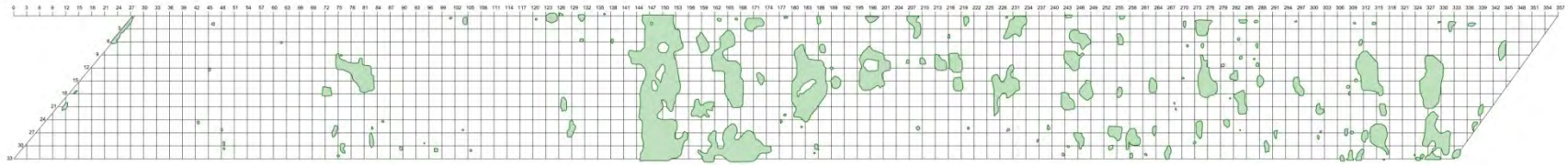

Ground Penetrating Radar

Figure 31: Direct comparison of Casper Bridge results.

The general areas of bridge damage determined by four different evaluation methods are shown in Figure 31. All four test methods indicated large areas of damage from 140 ft to 180 ft and scattered damage between 216 ft and 300 ft along the bridge. According to the results, thermal imaging indicated the highest amount of bridge delamination (17%), while GPR showed the least (11 %). This may be due to thermal imaging showing areas that are not actually delaminations from the data analyzer. Chain dragging, impact echo and GPR were within a 2% range. The pair-wise correlations, discussed in Section 4.4.5 between the delamination investigations, are shown in Table 10. For example, impact echo correlated 77% of the time with thermal imaging. This average correlation is 79%, which shows the methods were compatible with a bare concrete bridge deck.

Table 10: Casper Bridge methods correlations.

	Chain Dragging	**Impact Echo**	**Thermal Imaging**	**Ground-Coupled GPR**
Chain Dragging				
Impact Echo	78%			
Thermal Imaging	79%	77%		
Ground-Coupled GPR	82%	79%	81%	

5.1.2 Core Evaluation

A correlation was conducted to compare the findings from each method to the visual damage observed during coring (Table 11). The correlation of the cores shows the GPR method being a more accurate solution. Previous research had a 77% correlation level using GPR system to compare cores and the method (Yehia et al. 2008).

Table 11: Casper Bridge core correlations.

Test	Percent Correlated
Chain Drag	45%
Impact Echo	59%
Thermal Imaging	47%
Ground Penetrating Radar	73%

Compression tests of cores were conducted, but the results did not present any unique data as the cylinders all performed well because compression tests generally do not identify deterioration and delamination. The most accurate assessment of bridge damage would involve horizontal slicing of the surface, which is beyond the scope of this project and has few practical applications at this time.

5.1.3 Corrosion Investigations

The half-cell potential evaluations were compared to the GPR corrosion scans (Figure 32). The purple-filled regions of the half-cell potentials represent areas of -0.35 V or more negative, where, according to ASTM C 876, there is a greater than 90% probability of corrosion. The purple-outlined area represents a potential -0.2 V to -0.35 V.

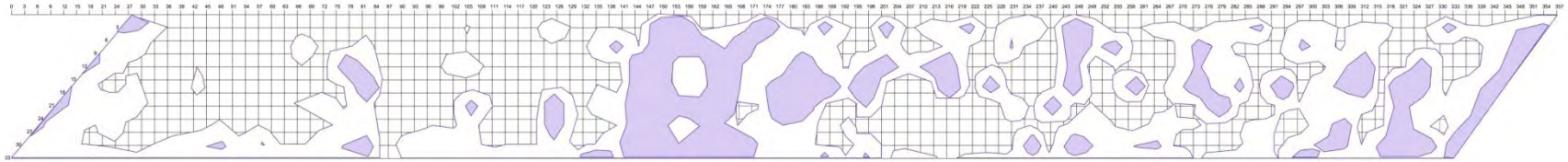

Half-cell Potential

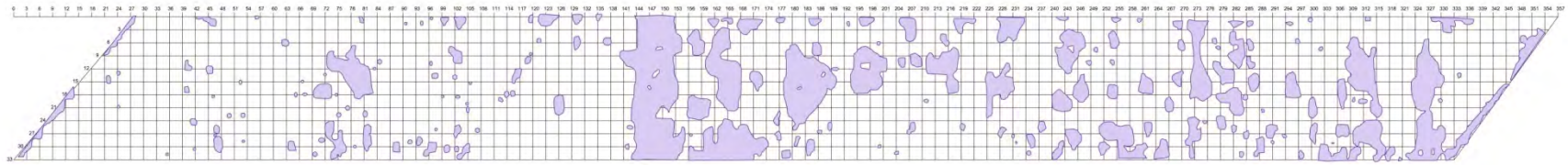

Ground Penetrating Radar Corrosion Evaluation

Figure 32: Comparison of Casper Bridge corrosion results.

When comparing the major regions of corrosion as indicated by GPR and half-cell potentials, it is clear that the basic shapes and positions of corrosion areas align. As shown in the results, the percentages between the half-cell potentials and the GPR evaluation differ by almost double. The 8.9% of potential corrosion from the half-cell evaluation is much lower than the 17% calculated from the GPR method. This may be caused due to GPR being able to differentiate the response amplitude and applying a sophisticated threshold system to the data.

5.1.4 Ground Penetrating Radar

This section presents a single scan of the ground-coupled cart and air-coupled systems from Olson Engineering. Section 3.5.1 describes the two GPR types. The ground-coupled system provided more detail in this case, whereas the air horn system did not produce useful data due to the wavelength of the signal and not discerning individual reinforcing bar signatures (Olson Engineering Report 3016A). Therefore, Olson Engineering's GPR analysis is based only on ground-coupled scans.

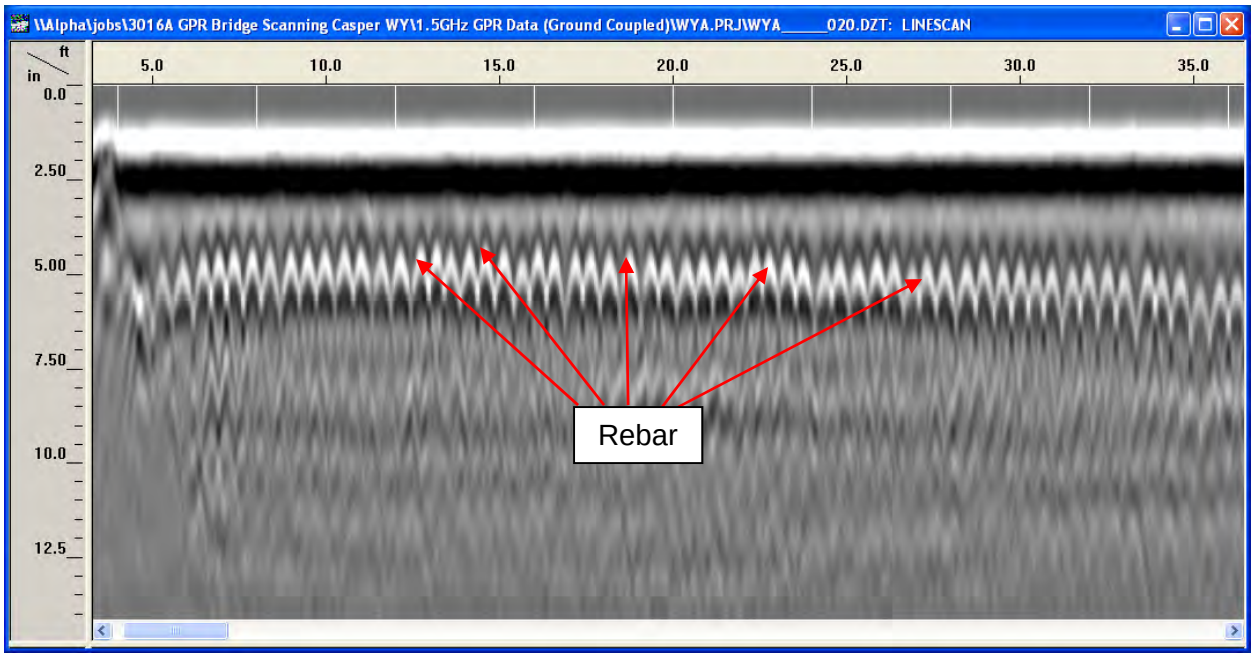

Figure 33: 1.5 GHz ground-coupled antenna GPR scan of Casper Bridge, 4.5 feet offset from south curb. The west joint is located at the far left of the plot (Olson Engineering Report 3016A).

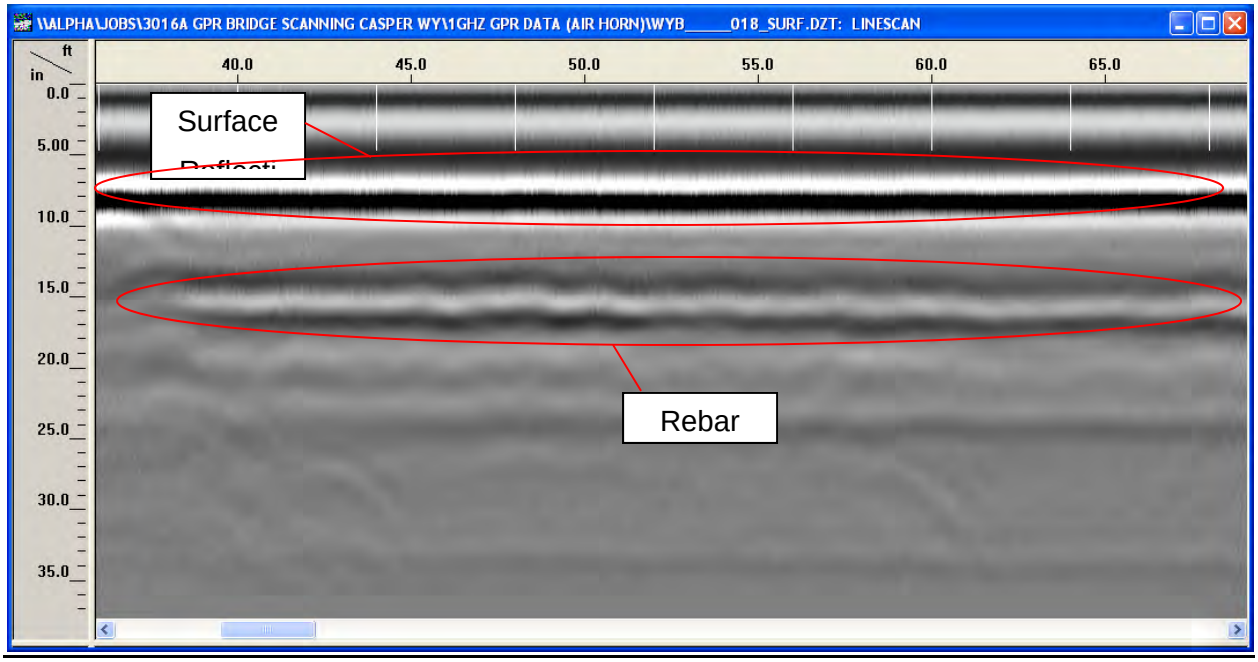

Figure 34: 1 GHz air horn antenna GPR scan 4.5 feet offset from south curb. The west joint is located at the far left of the plot (Olson Engineering Report 3016A).

5.1.5 Results from Milling of the Deck

The Casper Deck was milled for repairs, which revealed some areas of delamination. A visual inspection of the milled deck showed the most damaged area was from 142 ft to 180 ft (Figure 35 and Figure 36). This confirms the analysis from the other methods, as they also indicate large areas of damage in this zone. Differences in depths of damage could not be determined by these tests.

Repairs were classified into four categories: Class I-A (1/4 in. removal depth), Class I-B (2 in. removal depth), Class II-A (4 in. removal depth, typically half the thickness of the deck), and Class II-B (full depth removal). Actual repairs consisted of Class II-A over 18% of the bridge deck as shown in Table 12. The NDE methods predicted between 11 and 17% damage (Table 13) which correlates well with the actual repairs.

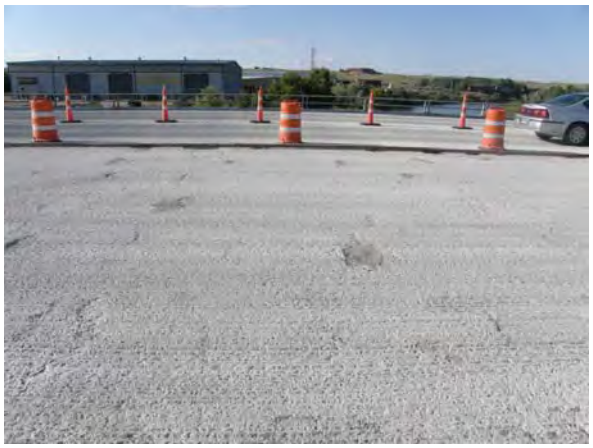

Figure 35: Casper Bridge milled surface (140 ft to 160 ft).

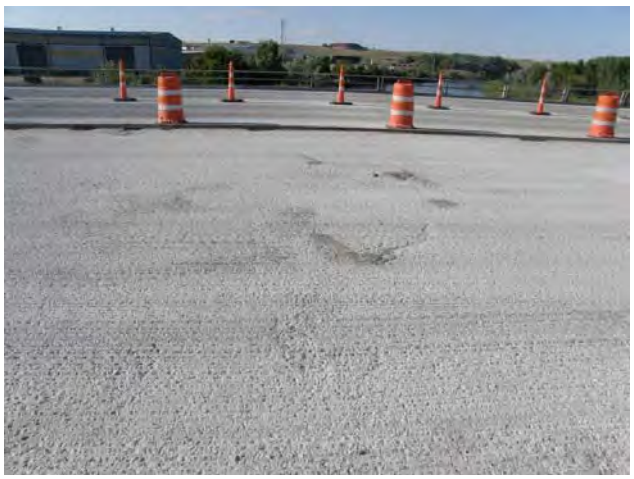

Figure 36: Casper Bridge milled surface (160 ft to 180 ft).

Table 12: Actual repairs for Casper Bridge.

Type of Repair/Areas	Area (ft^2)
Total Area	10990
Class II-A	2016
Class I-B	0
Class II-B	0
Total repair	2016
Percent of deck repaired	18%

Table 13: Percent damage predicted by NDE methods for Casper Bridge.

	Percent Damage
Chain Dragging	12
Impact Echo	13
Thermal Imaging	17
GPR without Corrosion Areas	11

5.2 Douglas Bridge

5.2.1 Delamination and Deterioration Evaluations

The following sections present the discussions of the evaluations for delamination and deterioration for the Douglas Bridge with and without the overlay present

5.2.1.1 Douglas Bridge with Overlay

Chain dragging, impact echo, thermal imaging, and ground penetrating radar evaluations were compared (Figure 37), including a ground-coupled and air horn GPR evaluations.

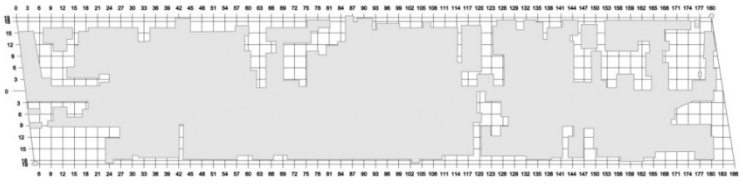

Chain Dragging

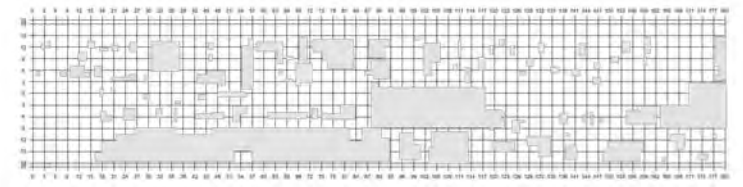

Secondary Chain Dragging

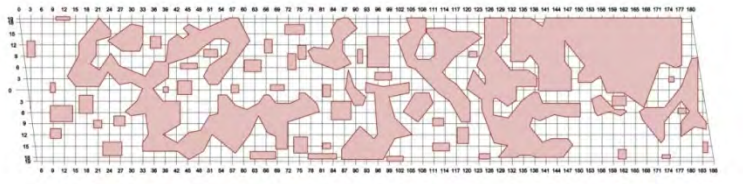

Impact Echo

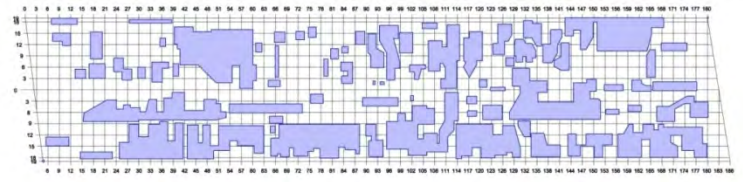

Thermal Imaging

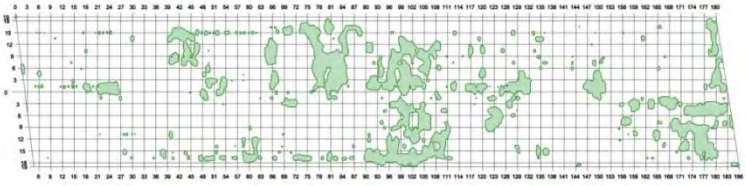

Ground Penetrating Radar-GSSI Ground-Coupled

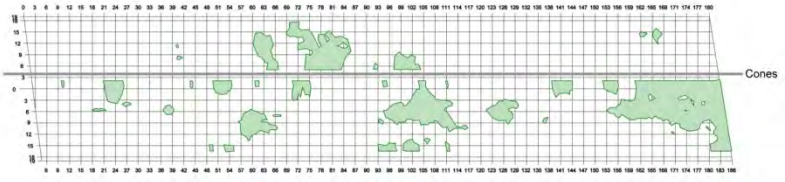

Ground Penetrating Radar-Rii Van Mounted

Figure 37: Comparison of delamination results of Douglas Bridge with overlay.

A great deal of damage in the Douglas Bridge complicated the comparison of methods, because the amount of damage did not give a control area to compare poor and adequate zones of the deck. It is also important to note the difference between the two chain drag evaluations conducted by two different WYDOT crews. This confirms the need for a simplified, nonbiased method for evaluating bridge decks. As shown in the results, the percent of damaged areas vary significantly, likely due to the extensive damage to the deck. GPR results were within 5% of each other, but the range from 11% for the ground-coupled GPR to 74% for one of the chain dragging evaluations signifies a wide range of results. The pair-wise correlations, discussed in Section 4.4.5 between the delamination investigations, are shown in Table 14. For example, impact echo correlated 57% of the time with thermal imaging. Most comparisons of methods yielded lower correlations than the Casper Bridge data. The two chain dragging correlation showed the variability in this method, while the two GPR systems correlation was the highest at 79%.

Table 14: Douglas Bridge with overlay methods correlations.

	Chain Dragging	2nd Chain Dragging	Impact Echo	Thermal Imaging	Ground-Coupled GPR	Air-Coupled GPR
Chain Dragging						
2nd Chain Dragging	48%					
Impact Echo	58%	50%				
Thermal Imaging	61%	55%	57%			
Ground-Coupled GPR	34%	63%	51%	50%		
Air-Coupled GPR	29%	68%	49%	48%	79%	

5.2.1.2 Douglas Bridge without Overlay

Chain dragging, impact echo, and thermal imaging results were compared (Figure 38). Useful GPR results were not available on the milled concrete surface due to direct coupling interference from the reflections from the top surface of the bridge deck and the signal from the reinforcing bars. This distortion made the reinforcing steel appear more corroded than during the evaluation including the overlay (Olson Report 3016B in Appendix B). This leads to overzealous estimations of damaged and corroded areas. Section 5.2.4 provides a direct comparison of sample scans showing the increased response of the steel from the deck with the overlay removed.

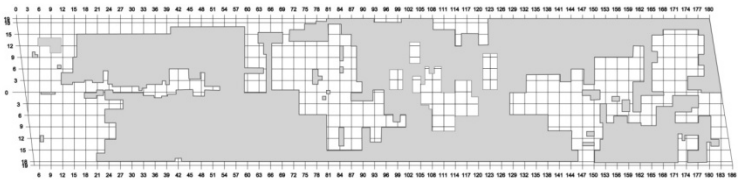

Chain Dragging

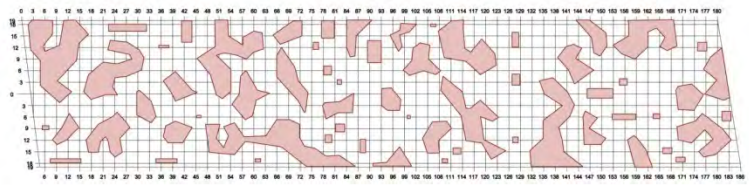

Impact Echo

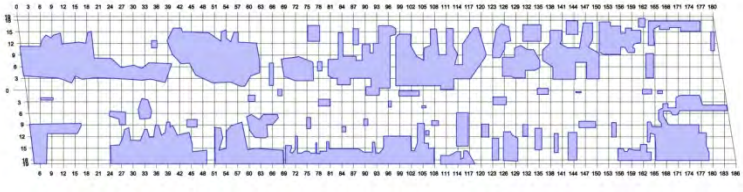

Thermal Imaging

Figure 38: Comparison of delamination results of Douglas Bridge without overlay.

With the overlay removed, the location of damage is still not fully aligned. Basic trends between thermal imaging and chain dragging seemed to compare well. Chain dragging results still indicated a high percentage of damage at 58.5%. The pair-wise correlations, discussed in Section 4.4.5 between the delamination investigations, are shown in Table 15. As observed with the Douglas Bridge with overlay, correlations were low for the Douglas Bridge without overlay.

Table 15: Douglas Bridge without overlay methods correlations.

	Chain Dragging	Impact Echo	Thermal Imaging
Chain Dragging			
Impact Echo	47%		
Thermal Imaging	62%	55%	

5.2.2 Core Evaluation

Neither compression nor split tension tests showed any bridge damage. All compression tests were 4000 psi or higher, which is beyond the 3750 psi concrete specified in the original plans. Splitting tension tests did not reveal any abnormalities either.

A correlation was conducted to compare the findings from each method to the visual damage observed during coring (Table 16). Overall the van-mounted system was best able to predict the damage the best at 78%. Previous research had a 77% correlation using GPR system to compare cores and the method (Yehia et al. 2008).

Table 16: Douglas Bridge core correlations.

Test	Percent Correlated
Chain Drag	77%
Impact Echo	68%
Thermal Imaging	73%
Ground Penetrating Radar-GSSI	59%
Ground Penetrating Radar-Rii Van Mounted	78%

5.2.3 Corrosion Evaluations

The following sections present the discussions of the evaluations for delamination and deterioration for the Douglas Bridge with and without the overlay present.

5.2.3.1 Douglas Bridge with Overlay

Half-cell potential evaluations were compared with GPR scans (Figure 39). The GPR corrosion evaluation utilizes the same data as delamination evaluations. The purple-filled regions of the half-cell potentials represent areas of -0.35 V or more negative, where there is a greater than 90% probability of corrosion according to ASTM C 876. The purple-outlined area represents a potential -0.2 V to -0.35 V.

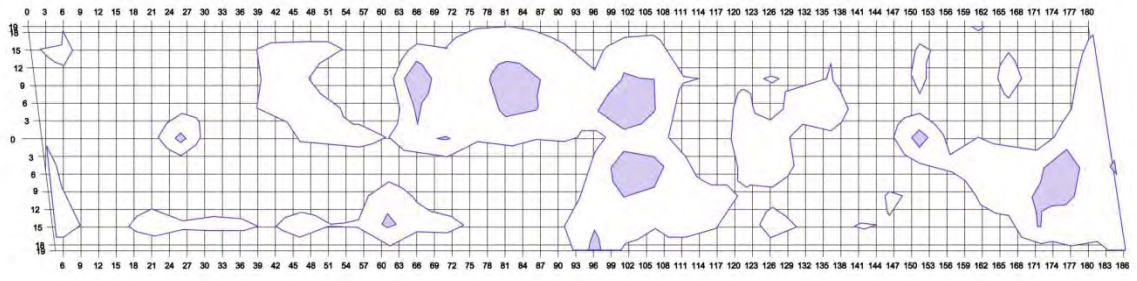

Half-cell Potential

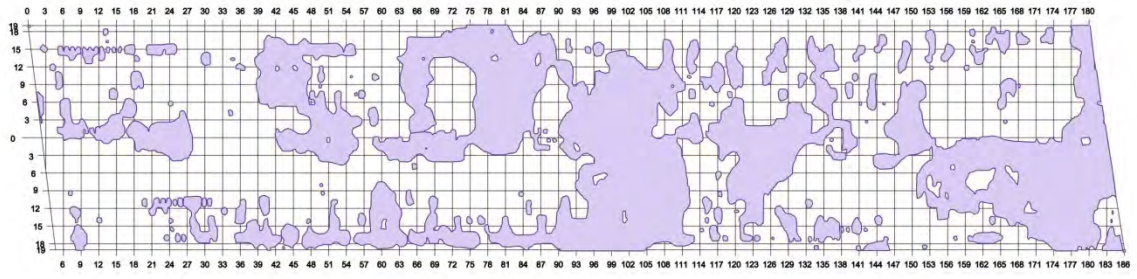

Ground Penetrating Radar Corrosion Evaluation

Figure 39: Comparison of corrosion methods for Douglas Bridge with overlay.

As with the Casper Bridge, the corrosion maps for the two methods align well. The GPR picked up the areas of lower potential indicated by the half-cell evaluation. As shown in the results, the percent probable corrosion area for -0.20 V and more negative and the GPR prediction were within 1% of each other; however the percent probable corrosion area for -0.35

V and more negative was 3.8%. This suggests the thresholds used by Dr. Barnes may have been too lenient for this bridge.

5.2.3.2 Corrosion Investigations without Overlay

The half-cell potential evaluation for the Douglas Bridge without the overlay is presented in Figure 40. ASTM C 876 was utilized identically to the corrosion investigations with the overlay present. The GPR corrosion evaluation was not available due to the ground coupling interference mentioned in Section 5.2.1.2. The half-cell results, however, show corrosion occurring. It was calculated that 69% of the deck had corrosion but there is less area showing the higher probability zones of corrosion, which was 0.4% of the total deck area. This is twice as much as was noted when the overlay was present.

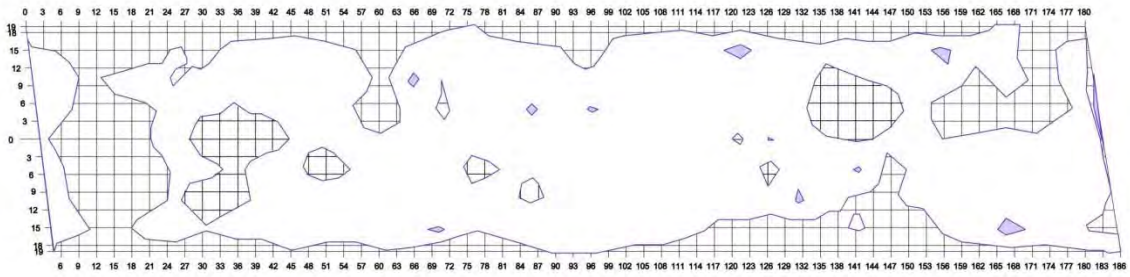

Figure 40: Half-cell potential results.

5.2.4 Ground Penetrating Radar

This section presents sample scans that allow comparison between the bridge deck with the overlay present and the overlay removed. Figure 41 shows Olson Engineering's scans from the GSSI ground-coupled cart of the Douglas Bridge with and without the overlay. The effects of shallow rebar, discussed in Section 5.2.1.2, have increased the reflections of the top layer of steel, causing problems evaluating the scans of the bridge without the overlay.

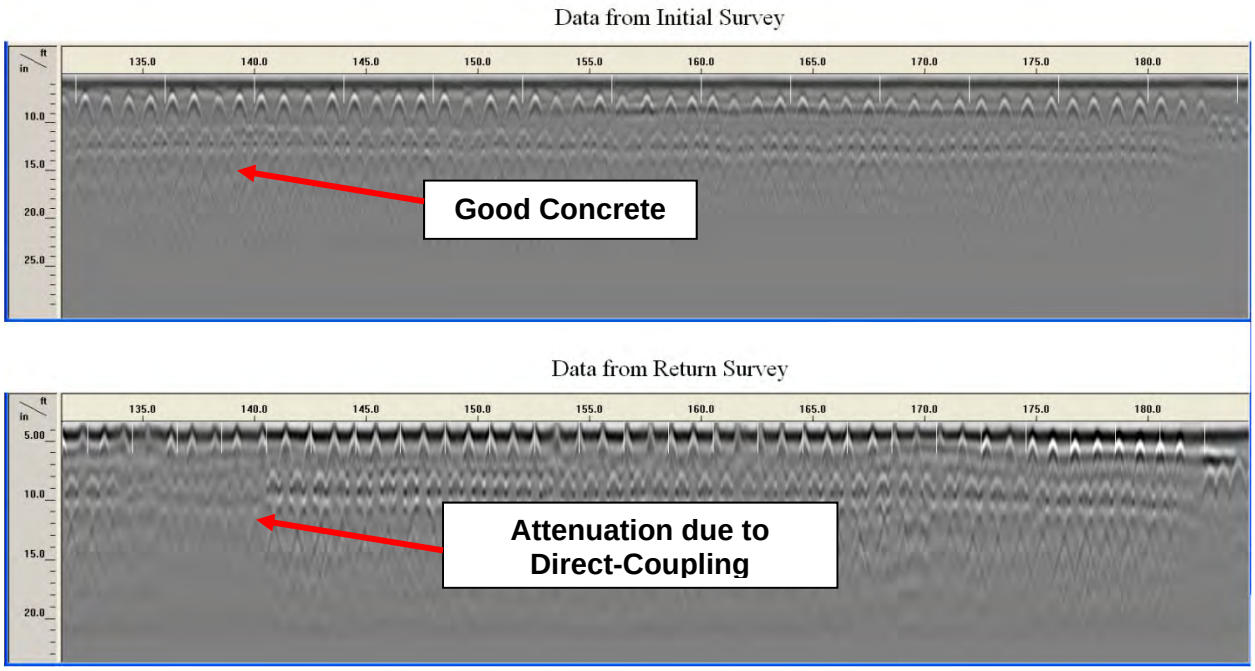

Figure 41: Direct comparison of ground-coupled cart (GSSI) data 6 feet south from the center of the bridge. Top scan is with the overlay and the bottom scan is without the overlay (Olson Engineering).

Sample scans from Rii's van mounted system are shown in Figure 42 and Figure 43. These scans provide a general view of how their system works and the details after data processing. The data, however, is not as crisp as the data from the ground-coupled systems.

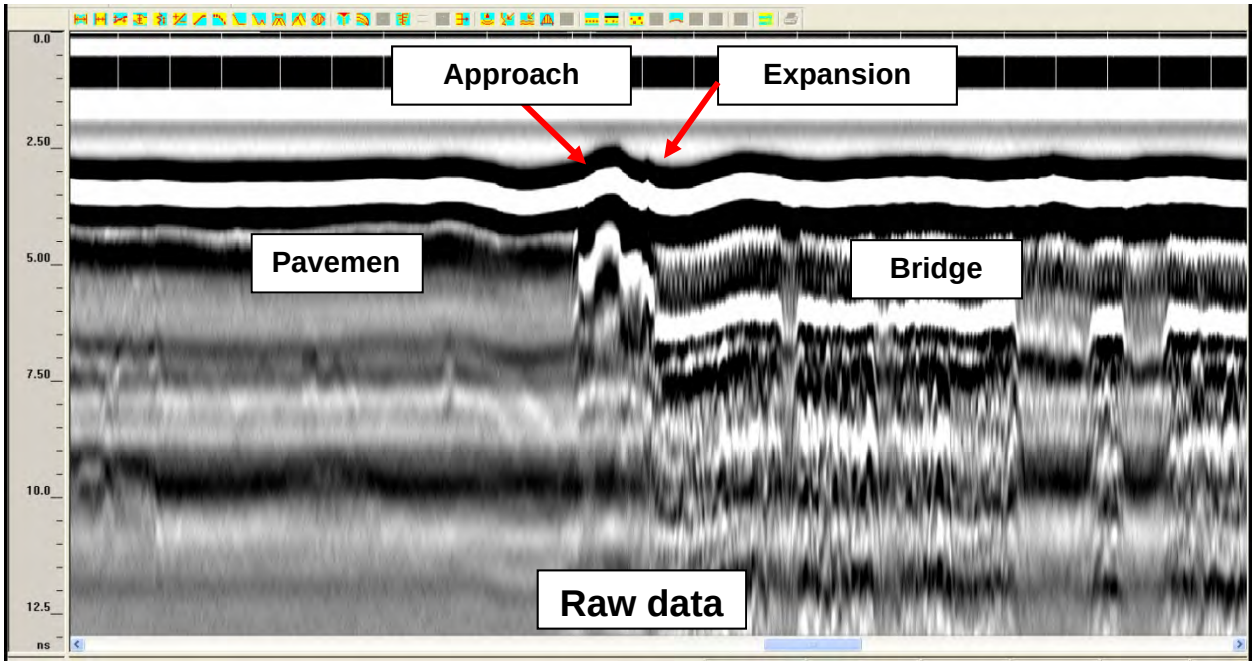

Figure 42: Raw data scan from Rii showing how the system determines where the bridge starts and pavement ends.

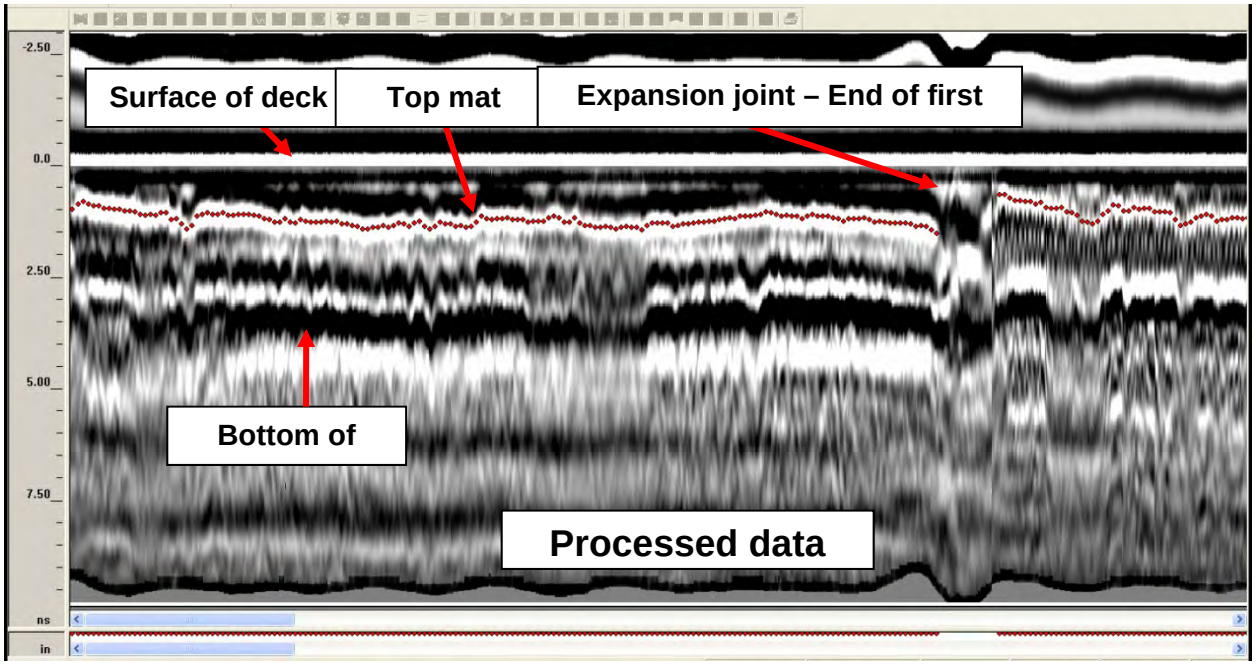

Figure 43: Processed data from Rii showing the details of a scan.

5.2.5 Results from Milling of the Deck

This section presents the actual repairs that were made to the Douglas Bridge. Every portion of this deck required milling and chipping. Figure 44 and Figure 45 show the extent of the necessary repairs.

Figure 44: Douglas Bridge chipping looking east.

Figure 45: Douglas Bridge chipping looking east.

These repairs were classified into four categories: Class I-A (1/4 in. removal depth), Class I-B (2 in. removal depth), Class II-A (4 in. removal depth, typically half the thickness of the deck), and Class II-B (full depth removal). Figure 46 shows the classification of the areas of removal. Actual concrete repair values are shown in Table 17. Damaged concrete based on NDE methods is shown in

Table 18. The repair value of 51.5% fell within the range of damage between 11% and 74%. The scatter in the data is discussed further in Chapter Chapter 6.

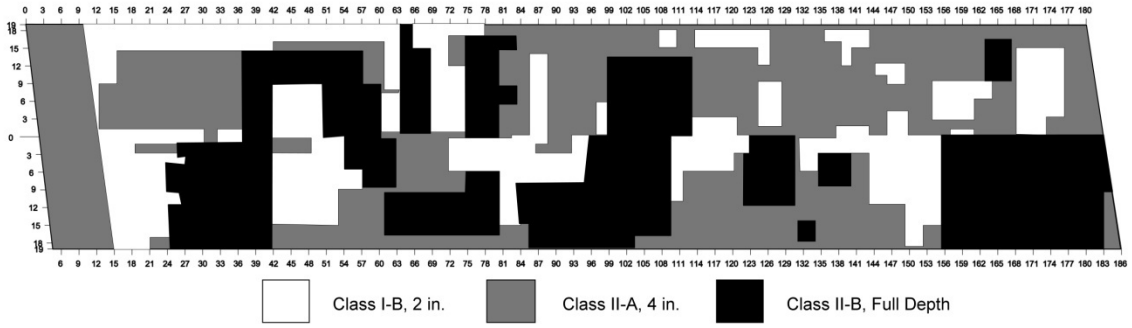

Figure 46: Douglas Bridge final repair schedule classification.

Table 17: Actual concrete repairs for Douglas Bridge.

Type of Repair/Areas	Area (ft^2)
Total Area	6840
Class II-A	371
Class I-B	1593
Class II-B	1557
Total repair	3521
Percent of deck repaired	51.5%

Table 18: Percent damage predicted by NDE methods for Douglas Bridge.

NDE Method	Percent Delaminated/Deteriorated
Chain Dragging	74%
Second Chain Dragging	19%
Impact Echo	45%
Thermal Imaging	39%
GPR Ground-Coupled Cart (without Corrosion Areas)	11%
Rii Van-Mounted System	17%

A comparison of the repair schedule was made to the half-cell potential results of the Douglas Bridge when the overlay was present (Figure 47). When the voltage potential was larger, a deeper repair was needed. The purple-filled areas represent the areas that have the largest voltage reading.

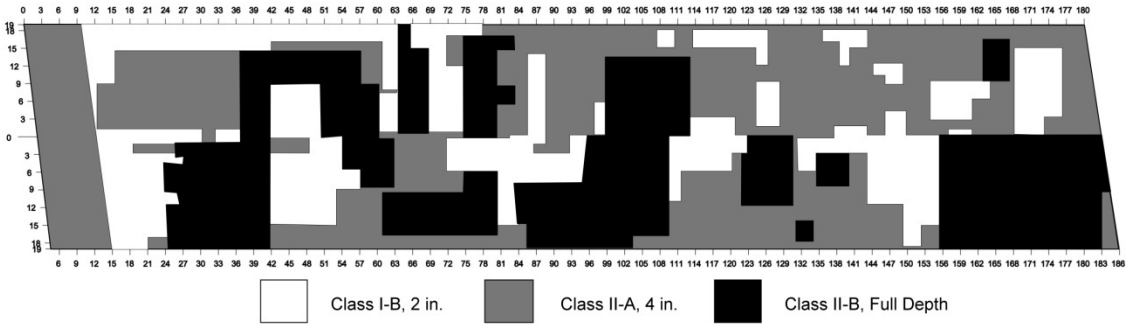

Repair Schedule

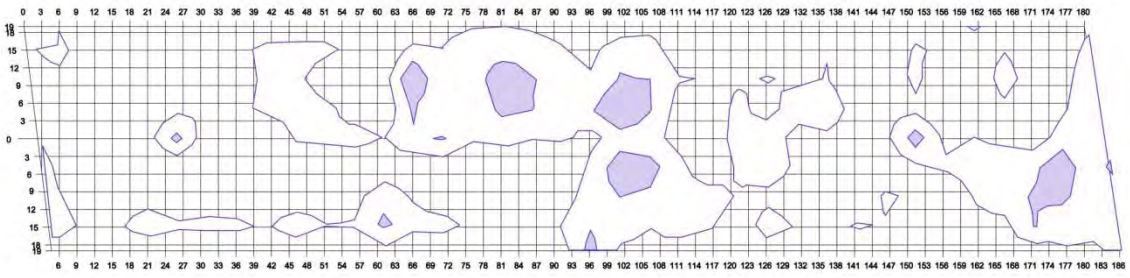

Half-cell Results with Overlay Present

Figure 47: Repair schedule and half-cell results comparison.

5.3 Remount Bridge

This section presents a discussion of the results of the Remount Bridge evaluation. Due to concerns over the effect of an asphalt overlay, a test slab was created to practice the impact echo and thermal imaging methods. Cold-pack asphalt was used which was not sufficiently stiff for the impact echo to work. The thermal imaging system also had difficulty to obtain useful data.

5.3.1 Delamination and Deterioration Evaluations

The following sections present the discussions of the evaluations for delamination and deterioration for the Remount Bridge with and without the overlay present.

5.3.1.1 Remount Bridge with Overlay

Impact echo, thermal imaging, and ground penetrating radar evaluations were compared (Figure 48). Chain dragging results were not available due to the method not working well with

asphalt overlay. Furthermore, chain dragging asphalt overlays is not a standard procedure for WYDOT.

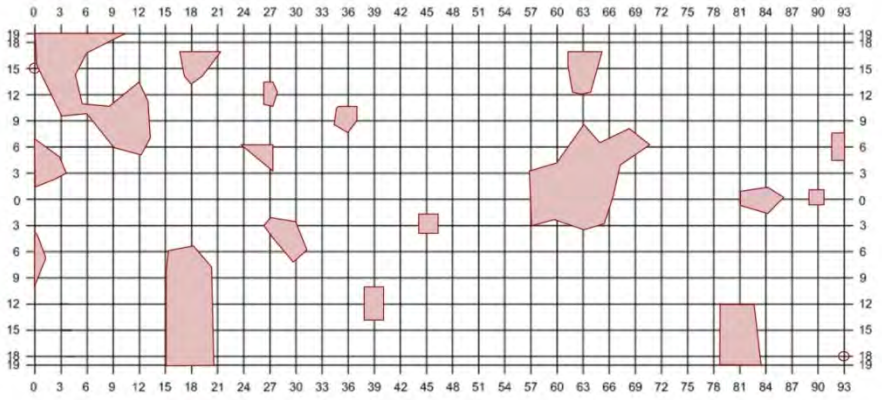

Impact Echo

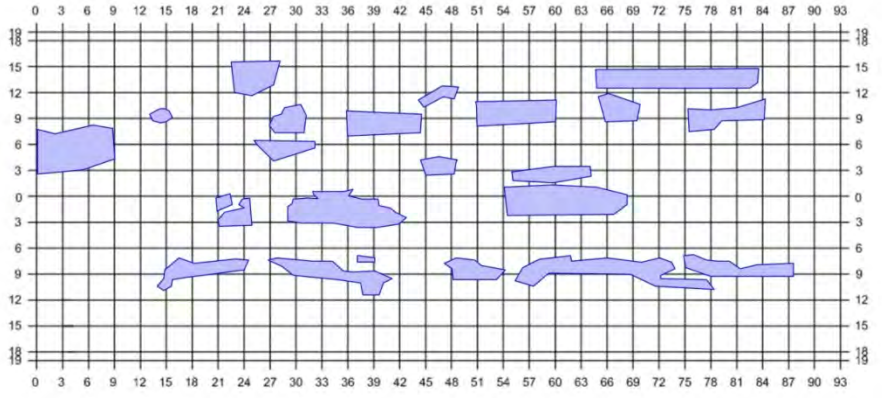

Thermal Imaging

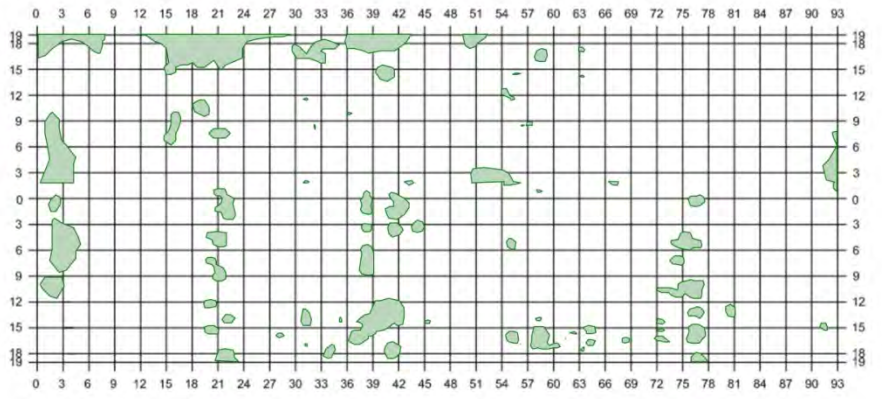

Ground Penetrating Radar-GSSI

Figure 48: Comparison of Remount Bridge with overlay delamination results.

The correlation of the data from the Remount Bridge is inconsistent. Although GPR and impact echo have similar patterns, the thermal imaging does not. This may be due to problems with the asphalt overlay masking the thermal emissivity for the thermal camera. The percent damaged and deteriorated followed the same pattern as well. The pair-wise correlations, discussed in Section 4.4.5 between the delamination investigations, are shown in Table 19. For example, impact echo correlated 76% of the time with GPR. The average correlation was 75%.

Table 19: Remount Bridge with overlay methods correlations.

	Impact Echo	**Thermal Imaging**	**Ground-Coupled GPR**
Impact Echo			
Thermal Imaging	75%		
Ground-Coupled GPR	76%	75%	

5.3.1.2 Remount Bridge without Overlay

Chain dragging, impact echo, and thermal imaging were compared (Figure 49). The same problems with the GPR and milled surface, discussed earlier with the Douglas Bridge, occurred on the Remount Bridge as well.

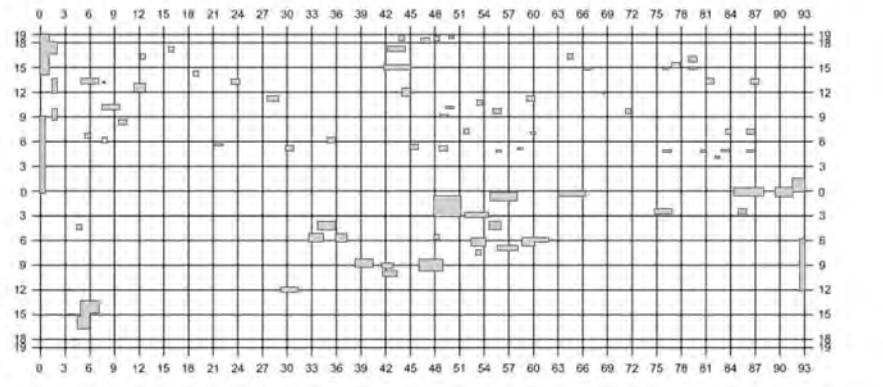

Chain Dragging

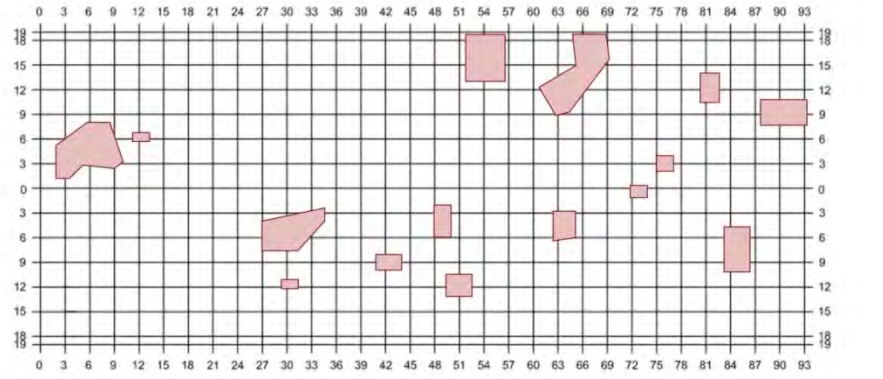

Impact Echo

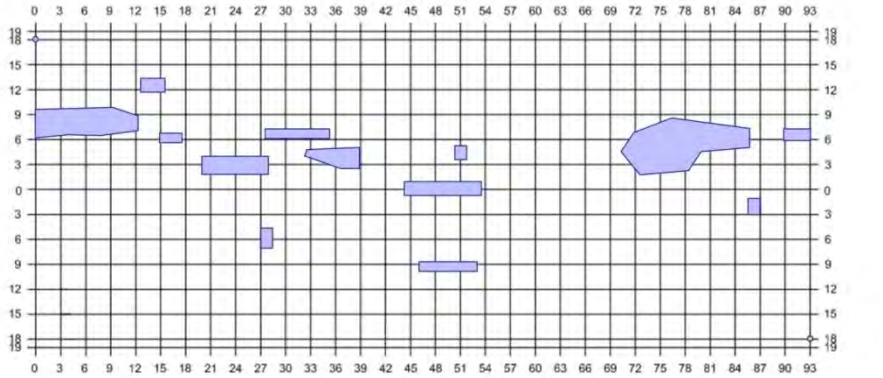

Thermal Imaging

Figure 49: Comparison of Remount Bridge without overlay delamination results.

The correlation of the data from the Remount Bridge without the overlay is inconsistent. The GPR and impact echo have similar patterns, but the thermal imaging does not follow the same trends. This may be due to environmental effects, as there were clouds occasionally

present during testing. The pair-wise correlations, discussed in Section 4.4.5 between the delamination investigations, are shown in Table 20. All methods converged between 85 and 86%.

Table 20: Remount Bridge with overlay methods correlations.

	Chain Dragging	Impact Echo	Thermal Imaging
Chain Dragging			
Impact Echo	85%		
Thermal Imaging	85%	86%	

5.3.2 Core Evaluation

Again, core testing provided results similar to those on the Douglas Bridge, that is, no damage was indicated. All compression tests were 5000 psi or higher, which are beyond the 3750 psi concrete specified in the original plans. Splitting tension tests did not reveal any abnormalities either. Corrosion Investigations with Asphalt Overlay.

5.3.3 Corrosion Evaluations

The following sections present the discussions of the evaluations for delamination and deterioration for the Douglas Bridge with and without the overlay present.

5.3.3.1 Remount Bridge with Overlay

The ground penetrating radar corrosion results from the GSSI ground-coupled cart are presented in Figure 50. No half-cell potential data was valid due to the reinforcement being epoxy-coated, which interferes with the voltage readings. It was found that 24% of the deck had corrosion.

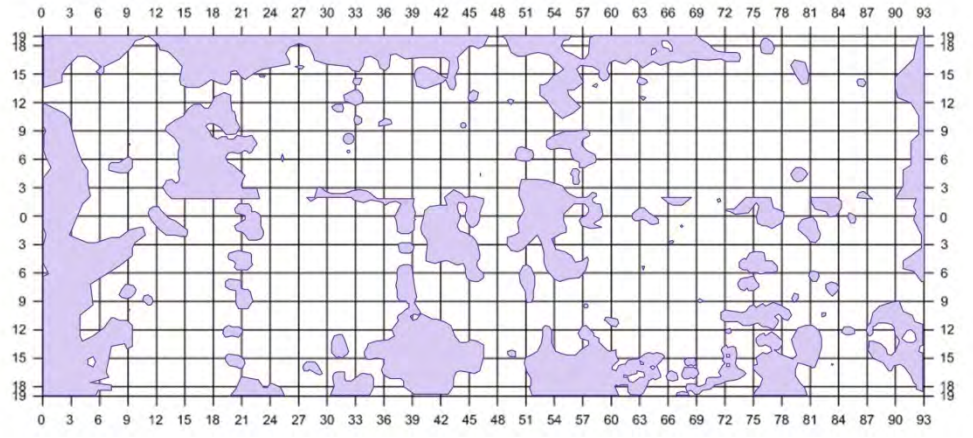

Figure 50: Ground Penetrating Radar Corrosion Evaluation.

5.3.3.2 Remount Bridge without Overlay

Due to the issues of interference with the GPR (Section 5.3.1.2) and the epoxy-coated rebar, no valid corrosion data was available for the Remount Bridge once the overlay was milled.

5.3.4 Ground Penetrating Radar

A select zone of GPR data for both the GSSI and IDS Aladdin systems were available on the Remount Bridge with the overlay (Figure 51). Figure 52 compares the two systems and it can be seen the two systems do not compare well. Olson Engineering and Dr. Barnes conclude the frequency of the antenna for the IDS Aladdin system was too high (2 GHz) for their data analysis software. The IDS system continues to be refined; it is expected to become a very powerful tool providing 3D scans of the bridge decks.

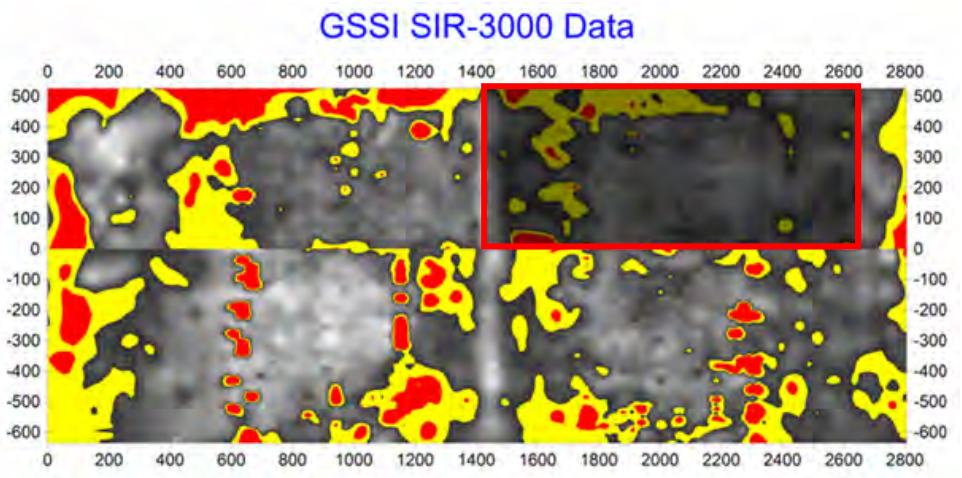

Figure 51: Highlighted zone of comparable GSSI and IDS Aladdin Data.

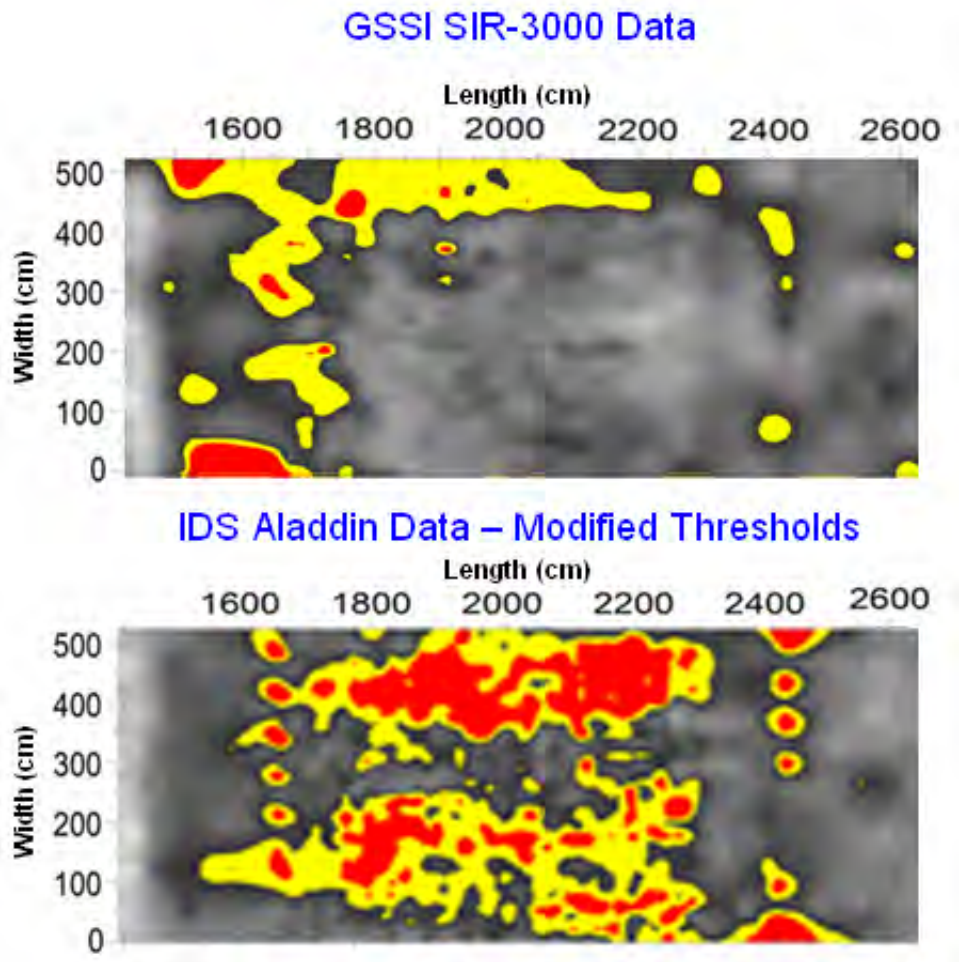

Figure 52: Direct comparison of GSSI and IDS Aladdin Data.

5.3.5 Results from Milling of the Deck

The following section discusses the actual repairs made to the Remount Bridge. Using the same classification for repairs on the Douglas Bridge, very few Class II-A repairs were made after the milling of Class I-A and I-B areas (Figure 53).

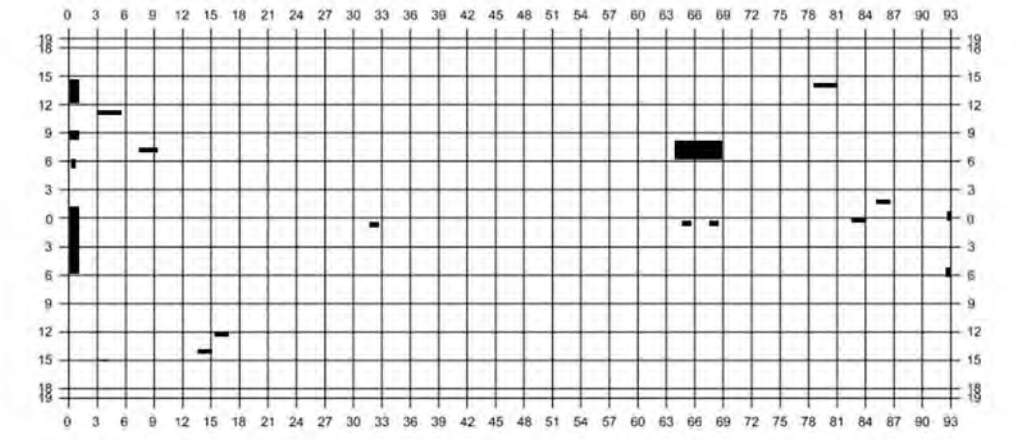

Figure 53: Remount Bridge final repair schedule (filled areas represent Class II-A repairs).

Overall, very little repair occurred beyond the milling and the total repair was 1% of the bridge deck as shown in Table 21. Figure 54 shows the northern lane of the bridge looking east. Most of the repair occurred where the approach slab met the bridge deck. Although the actual repair was considerably smaller than the predicted areas of damage as shown in Table 22, dealing with small percentages of damage always causes more variability. In addition, the following two factors with the reinforcement complicated the NDE.

- Reinforcing steel was coated which caused problems with the corrosion data collection and analysis using the half-cell potential method.
- Longitudinal reinforcing steel was placed above the transverse steel. This resulted in running the GPR system in the transverse direction rather than along the length of the bridge.

Figure 54: Remount Bridge reconstruction.

Table 21: Actual concrete repairs for Remount Bridge.

Type of Repair/Areas	Area (ft^2)
Total Area	3534
Class II-A	34.4
Class I-B	0
Class II-B	0
Total repair	34.4
Percent of deck repaired	1%

Table 22: Percent damage predicted by NDE methods for Remount Bridge.

NDE Method	Percent Delaminated/Deteriorated
Impact Echo	11%
Thermal Imaging	13%
Ground-Coupled GPR (without Corrosion Areas)	6.7%

5.4 Overall Comparison

The following figures and tables compare methods over the three bridges. Figure 55 through Figure 57 provide a visual comparison of field time and analysis time for the successful evaluations. The times were normalized to person hours per 100 ft of bridge deck from each of the tests. Table 23 and Table 24 compare the percentages of damage and corrosion, while tables in Appendix A identify the field time and analysis time back in an office. Even though the GPR systems took longer to complete, the analyses were more comprehensive and could detect both delamination and corrosion in the deck. GPR might eliminate the need for half-cell potential evaluations.

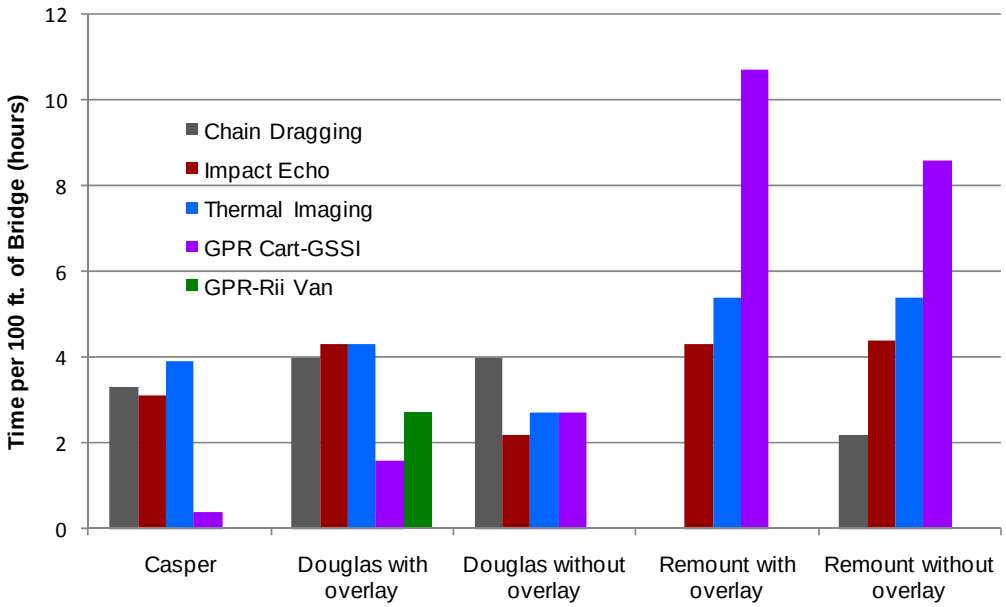

Figure 55: Comparison of testing time.

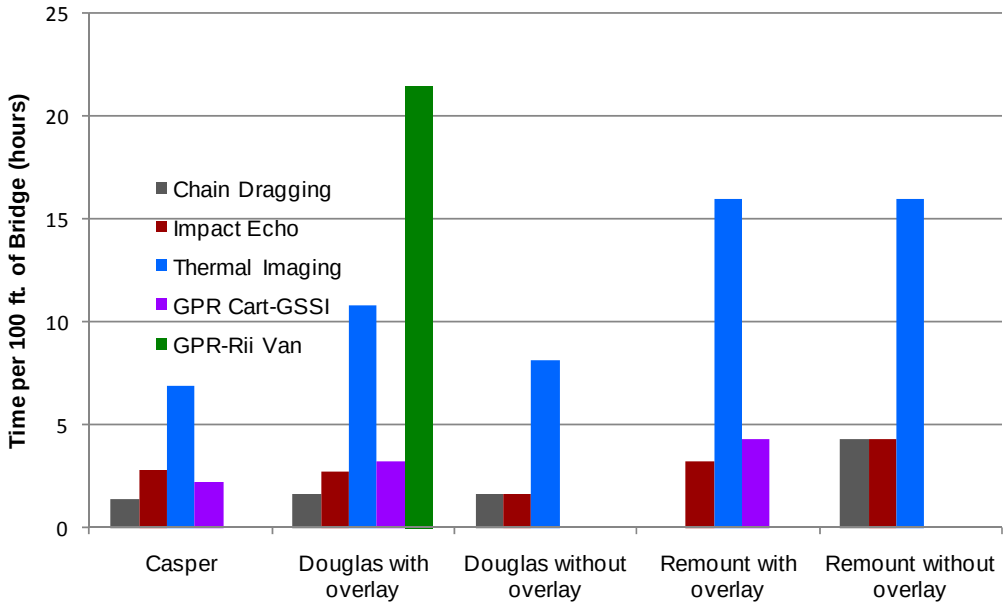

Figure 56: Comparison of analysis time.

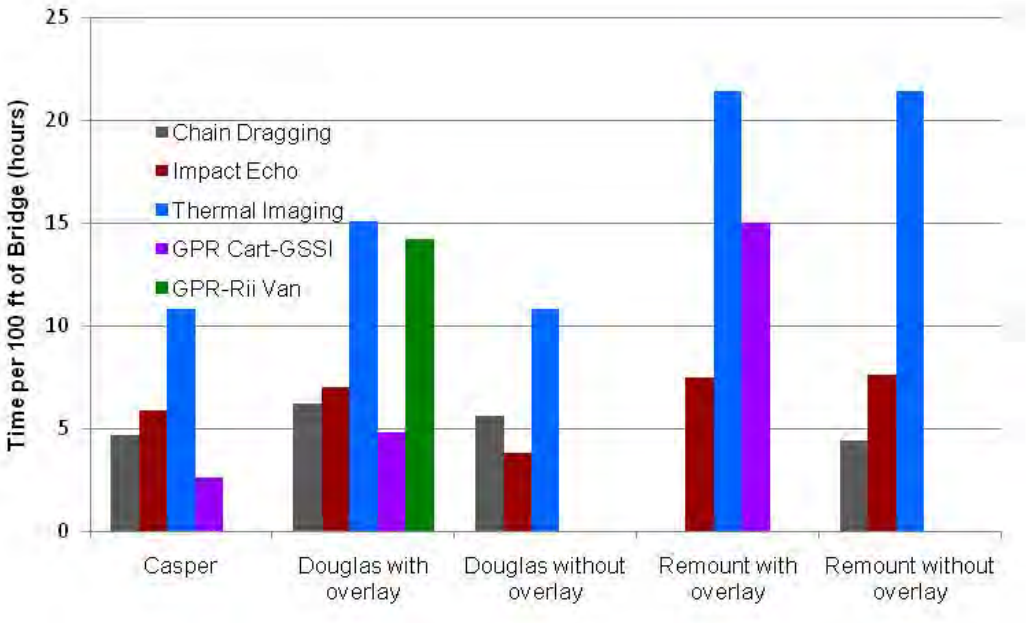

Figure 57: Comparison of the total time for evaluation and analysis.

Table 23: Comparison of percent damaged.

Method	Casper	Douglas with Overlay	Douglas without Overlay	Remount with Overlay	Remount without Overlay
Chain Drag	12%	74% 29%	58%	No Useful data	2.5%
Impact Echo	13%	45%	30%	11%	6.2%
Thermal Imaging	17%	39%	34%	13%	5.8%
GPR Cart-GSSI	11%	11 %	No Useful Data	6.7%	No Useful Data
GPR Cart-Aladdin	Not Used	Not Used	Not Used	No Useful Data	No Useful Data
GPR Vehicle Mounted	No Useful Data	No Useful Data	Not Used	Not Used	Not Used
GPR Vehicle Rii Van	Not Used	16.7%	Not Used	Not Used	Not Used

Table 24: Comparison of percent corrosion.

Method	Casper	Douglas with Overlay	Douglas without Overlay	Remount with Overlay	Remount without Overlay
Half-cell Potentials (-0.20 V -0.35 V)	31%	35%	69%	No Useful Data	No Useful Data
Half-cell Potentials (-0.35 V and more negative)	8.9%	11%	6.2%	No Useful Data	No Useful Data
GPR Ground-Coupled	17%	34%	No Useful Data	No Useful Data	No Useful Data

Chapter 6 Conclusions and Implementation Recommendations

General observations related to specific non-destructive evaluation methods are presented below.

- Chain dragging results are subjective based on the user and external factors such as highway noise. At times, the results varied by a factor greater than two. When the bridge deck damage was less than 20%, chain drag results correlated well with the other methods on bridge decks.
- Half-cell potential results and GPR corrosion results generally correlated well but half-cell readings are limited when coated reinforcing bars are used.
- Impact echo, thermal imaging, and GPR were successful in identifying damage to the concrete decks and results generally correlated well, even when concrete based overlays were present.
- Impact echo is more robust than thermal imaging because it is less subjective to weather conditions such as wet concrete surfaces, overcast skies, or small amounts of radiant energy that does not allow the heat differential to form on a bridge deck.
- Impact echo evaluations on a roughly milled surface may require extra field time to obtain results. A secondary impactor, such as a hammer or ice pick, may need to be used to induce an appropriate sound wave.
- Thermal imaging is dependent on more external variables, such as paint and oil drippings, shading from surrounding landscaping and structures, and changes in temperatures during the evaluation time. Variable weather conditions cause difficulty in obtaining an appropriate heat differential on the top and bottom of the bridge deck.
- GPR evaluations are used to locate steel and evaluate the concrete and steel conditions. This method was successful in determining that the longitudinal bars were placed above the transverse bars in the Remount bridge deck.

- GPR evaluations have problems when the deck has been milled and the reinforcing steel is located near the surface. GPR data should be compared to preliminary scans with overlays present to check for the possibility of the direct-contact interferences which results in over-diagnosing the repair schedule.
- Impact echo, thermal imaging and GPR methods are much less clear when an asphalt overlay is present. The overlay caused difficulty with each of these methods. In addition, the coated reinforcing bars located in Remount Bridge caused difficulty with half-cell potential readings.

Overall, the Casper Bridge deck and Remount Bridge decks yielded the highest correlations. These values were between 77 and 82% for Casper Bridge and ranged from 75-86 for Remount Bridge with the asphalt overlay and with the asphalt overlay removed. It should be noted that the milled surface does make data collection with the impact echo system more difficult.

When extensive bridge deck damage is present, confidence in the overall analysis is lower. The large percent damage in the Douglas bridge highlight this type of variation. Two separate chain dragging evaluations both performed based on ASTM standards yielded damage values that were off by a factor of more than two. While impact echo and thermal imaging gave similar results to the average of the two chain dragging results, there were not similar trends in location of damage. The corresponding correlations between methods performed on all bridge decks was always below 63%. Generally, it more economical to replace a bridge deck than repair such a large area of damage. When bridge damage is fairly light as in the case of Remount, the differences in actual repair percentages versus the predictions using may NDE become larger.

Correlation of cores was difficult because the compression test does not necessarily identify delaminations or areas of weak concrete. To accurately characterize all the damage it would be necessary to take horizontal slices of the bridge, which is impractical and beyond the scope of this study.

6.1 System Level Analysis Recommendations

One goal of this research project was to recommend a system-wide program for WYDOT that would save time while increasing safety, efficiency, and accuracy. The system that would best meet these three goals combined is a vehicle mounted system such as the one used by Rii. This system improves the safety of an evaluation because evaluators are in a vehicle with a following truck alerting other travelers to move around the inspection vehicle. The time required to perform scans would also be minimized if multiple evaluations occur at a single given time. Any vehicle mounted system needs to overcome the issue of recording where each data collection point begins and ends and estimate the positioning of the van based on the striping of the road. In the case of a rolling impact echo scanner such as that used by Olson Engineering, the accuracy would be improved due to the finer grid that could be obtained. On the other hand, the accuracy of GPR systems may be decreased when compared to direct contact methods. The cost of the Rii GPR system is estimated at 30 dollars per linear foot of a traditional 2-lane bridge. At this time a rolling impact echo scanner is not available. The authors recommend that WYDOT wait for systems to become commercially available and affordable before making a system-wide decision.

6.2 Local Level Analysis Recommendations

A local level analysis, or bridge by bridge evaluation, is the current method for WYDOT bridge investigation. Impact echo, thermal imaging, and GPR methods all have merits and concerns for daily use. At the current time, these three systems only minimally improve the safety or efficiency of the bridge deck evaluation process because they require personnel on the bridge at all times, but they do increase accuracy by removing the bias that can occur with chain dragging. Future work on a rolling impact echo scanner and GPR evaluation may change this. This research suggests that a combination of impact echo with GPR testing provides the most accurate predictions of delamination, debonding, and active corrosion on bridge decks.

6.2.1 Impact Echo Evaluations

The impact echo method can easily be implemented into a bridge deck analysis. A more accurate analysis could be completed using a smaller grid. Figure 58 and Figure 59 compare the levels of accuracy between Olson Engineering's Bridge Deck Impact Echo Scanner mentioned earlier in this report and the University of Wyoming's evaluation. Olson

Engineering's system has 18 times more data points than the University of Wyoming's scan. Olson's rolling bridge deck impact echo scanner, still in the developmental stage, may be a quicker and more accurate solution for this method. For bridges located far away from WYDOT headquarters this would require developing software that rapidly provides a plan view of damaged area in the field or hotel room.

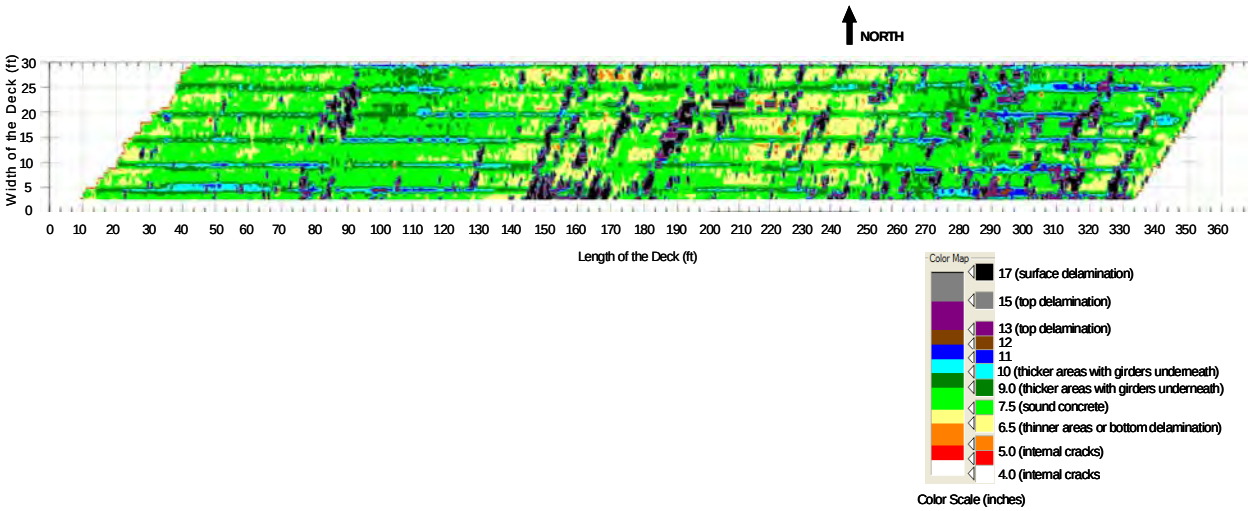

Figure 58: Olson Engineering truck mount Bridge Deck Scanner results from the Casper Bridge (Tinkey and Olson 2010).

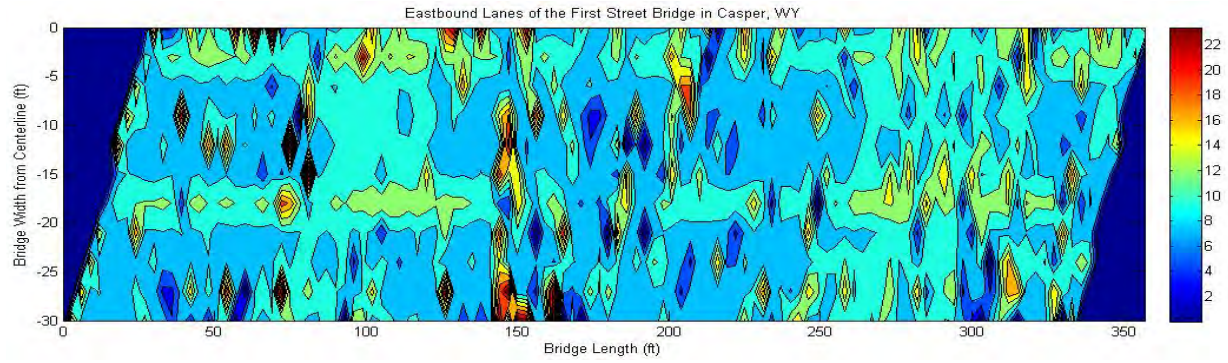

Figure 59: University of Wyoming impact echo results from the Casper Bridge.

The initial cost of a typical Concrete Thickness Gauge from Olson Engineering and training would be approximately 8,500 dollars. For immediate results using the impact echo method, which is one advantage of chain dragging, individual grid points could be marked immediately on the deck instead of waiting to analyzing the data in the office. In terms of field expense, the smaller the grid, the more expensive and time-consuming the investigation.

Figure 60 and Figure 61 compare grid size to time and costs. These charts are based on a 100 ft-long, two-lane bridge. Field time was estimated based on the number of points required to complete the evaluations. Total time is based on a two person crew in the field and a single engineer analyzing the data. The field cost is based on a supervisor at 40 dollars per hour and two laborers at 20 dollars per hour, with 200 dollars per day for additional travel and per diem expenses. Total time includes the field time as well as an engineer at 40 dollars per hour evaluating the data and writing a report.

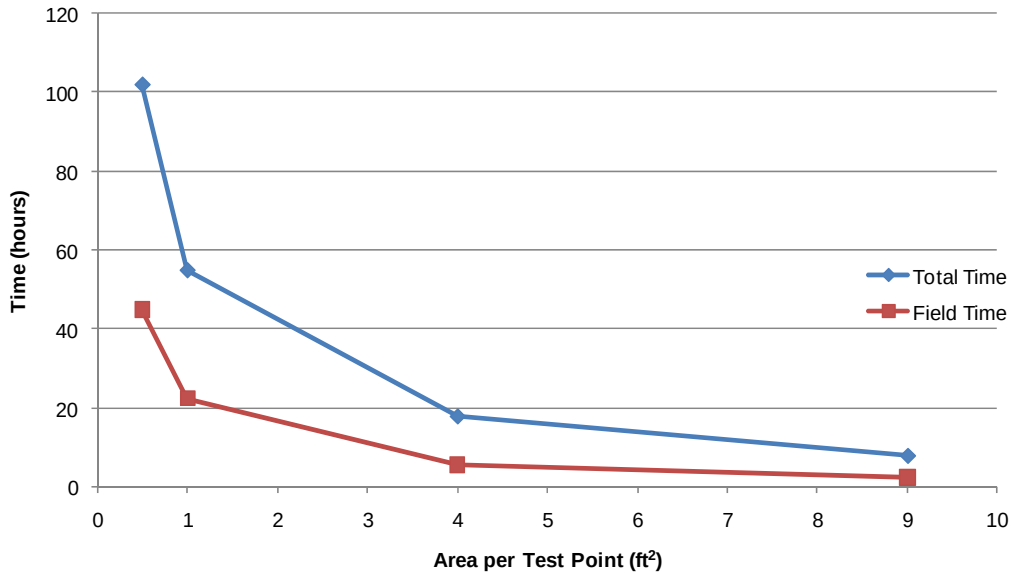

Figure 60: Impact echo grid size and time comparison.

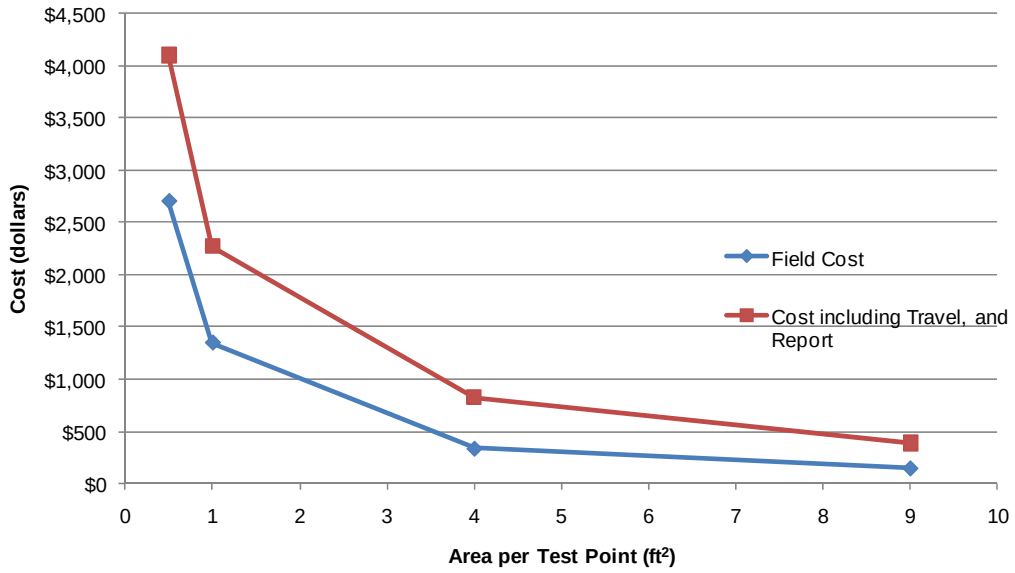

Figure 61: Impact echo grid size and cost comparison.

6.2.2 Thermal Imaging Evaluations

The thermal imaging method is not recommended for bridge investigations in Wyoming. The time to perform this test is much longer than the other methods, and it requires additional analysis to interpret the temperatures shown on the picture. The thermal camera is dependent on clear weather and eliminating surrounding obstructions. Neither of these two criteria is guaranteed for any particular testing date or bridge deck. The test is also subjective in that colors obtained may be dependent on a particular temperature. This issue could be resolved but the above criteria may still limit use of thermal imaging. The asphalt overlay on Remount seemed to compound this issue. There are solutions that will automatically scan the deck, but that technology starts at 90,000 dollars.

6.2.3 Ground Penetrating Radar Evaluations

The ground penetrating radar systems provide a detailed analysis of the bridge decks. Olson Engineering was able to provide a detailed analysis using the direct contact system. One output of this system and standard GSSI software is scans that can be viewed as cross-sections. With training, an operator could easily evaluate depth of problems in concrete. In the case of delamination, this could be confirmed by evaluating the depth of several cross-sections. The GSSI BridgeScan System is recommended. The base price for this system is 30,000 dollars including basic training. Using thresholds such as those developed by Dr. Chris Barnes,

corrosion in the deck can be quantified which can possibly remove the necessity for collecting half-cell potentials.

Rii was successful in evaluating locating the transverse reinforcing bars and some damage was detected on the Douglas Bridge. The percent damage was lower than that detected by impact echo and thermal imaging by a factor of two. It is difficult to assess if the damage was off due to the high level of damage in this bridge or if the faster speeds will continually yield lower percent damage. It is clear that some loss of accuracy occurs with the increased speed of a vehicle mounted system. To answer this question, it would be helpful to evaluate additional bridges with both systems. This study had limited availability of bridge decks and the second subcontract was out of the scope of the project.

Eventually a system will provide full three-dimensional views of the entire deck. Currently, a full lane dual-polarization system is still in the developmental stage and is very expensive. If a full lane GPR scanner becomes commercially available using similar technology to the IDS Aladdin System, the authors recommend considering this type of system. This should include a comprehensive study on several types of bridge decks with minimal damage to evaluate the limitations with asphalt overlays and milled surfaces. Such a study should consider technology transfer, detailed training costs and system upgrades for the first 10 years of operating this system.

References

Cited and Referenced Standards

ASTM C 39/C 39M Standard Test Method for Compressive Strength of Cylindrical Concrete Specimens

ASTM C 496 Standard test Method for Splitting Tensile Strength of Cylindrical Concrete Specimens

ASTM C 876 Standard Test Method for Half-Cell Potentials of Uncoated Reinforcing Steel in Concrete

ASTM C 1383 Standard Test Method for Measuring the P-Wave Speed and Thickness of Concrete Plates Using the Impact-Echo Method

ASTM D 4580 Standard Practice for Measuring Delaminations in Concrete Bridge Decks by Sounding

ASTM D 4788 Standard Test Method for Detecting Delaminations in Bridge Decks Using Infrared Thermography

ASTM D 6087 Standard Test Method for Evaluating Asphalt-Covered Concrete Bridge Decks Using Ground Penetrating Radar

ASTM D 6432 Standard Guide for Using the Surface Ground Penetrating Radar Method for Subsurface Investigation

Cited References

Abdel-Qader, I.; Yohali, S.; Abudayyeh, O.; and Yehia, S., 2008, "Segmentation of Thermal Images for Non-Destructive Evaluation of Bridge Decks," *NDE&E International*, V. 41, pp. 395-405.

Abraham, O. and Cote, P., 2002, "Impact-Echo Thickness Frequency Profiles for Detection of Voids in Tendon Ducts," *ACI Structural Journal,* V. 99, No. 3, pp. 239-247.

Abudayyeh, O.; Abdel-Qader, I.; Nabulsi, S.; and Weber, J., 2004, "Using Non-Destructive Technologies and Methods in Bridge Management Systems," *Journal of Urban Technology*, V. 11, No. 1, pp. 63-76.

Alongi, A. J.; Clemena, G. G.; and Cady, P. D., 1993, “Condition Evaluation of Concrete Bridges Relative to Reinforcement Corrosion, Volume 3: Method of Evaluating the Condition of Asphalt-Covered Decks,” *Strategic Highways Research Program Report SHRP-S-325,* Washington, D.C., National Research Council.

Annan, A. P., 2009, “Electromagnetic Principles of Ground Penetrating Radar,” *Ground Penetrating Radar: Theory and Applications*, ed. H. M. Jol, Elsevier.

Barnes, C. L.; Trottier, J.-F.; and Forgeron D., 2008, "Improved concrete bridge deck evaluation using GPR by accounting for signal depth-amplitude effects," *NDE & E International*, V. 41, No. 6, pp. 427-433.

Barnes, C. L. and Trottier, J.-F., 2002, "Phenomena and Conditions in Bridge Decks That Confound Ground-Penetrating Radar Data Analysis," *Transportation Research Record,* No. 1795, pp. 57-61.

Belli, K.; Wadia-Fascetti, S.; and Rappaport, C., 2008, "Model Based Evaluation of Bridge Decks Using Ground Penetrating Radar," *Computer-Aided Civil and Infrastructure Engineering,* V. 23, No. 1, pp. 3-16.

Carter, C. R.; Chung, T.; Reel, R.; Tharmabala, T.; and Wood. D., 1995, "Impulse Radar Evaluation of Reinforced Concrete Bridge Decks," *Proceedings of SPIE--The International Society for Optical Engineering,* V. 2456, pp. 174-185.

Cengel, Y. A. and Boles, M. A., 2006, *Thermodynamics: An Engineering Approach*, *5th Edition*, New York, McGraw-Hill.

Chase, S. B., 1999, “Tomographic Imaging of Bridge Decks using Radar,” *Structural Engineering in the 21st Century; Proceedings of the 1999 Structures Congress,* pp. 280-283.

Chen, H. L.; Halabe, U. B.; Pei, L.; and Allu, M., 1997, "Experimental Evaluation of Concrete Bridge Decks and Pavements Using Ground Penetrating Radar," *Building to Last; Proceedings of Structures Congress XV,* V. 2, pp. 1508-1512.

Chung, T. and Carter, C. R., 1993, "Impulse Radar Signatures of Selected Bridge Deck Structures," *IEEE,* pp. 59-63.

Clark, M. R.; McCann, D. M.; and Forde, M. C., 2002, "Infrared Thermographic Analysis of Bridges: Case Study," *Transportation Research Record*, No. 1813, pp. 242-248.

Clemena, G., 1983, "Nondestructive Inspection of Overlaid Bridge Decks with Ground-Penetrating Radar," *Transportation Research Record*, No. 899, pp. 21-32.

Coombs, J. M., 2007, *Enhancement of masonry curriculums through development of a virtual laboratory,* M.S., Department of Civil and Architectural Engineering, University of Wyoming, Laramie, WY.

Davidson, N. C. and Chase, S. B., 1998, "Radar Tomography of Bridge Decks," *SPIE--The International Society for Optical Engineering,* V. 3400, pp. 250-256.

Davis, A. G., 1996, "Impact-echo and Impulse Response Stress Wave Methods; Advantages and Limitations for the Evaluation of Highway Pavement Concrete Overlays," *Proceedings of SPIE--The International Society for Optical Engineering*, V. 2946, pp. 88-96.

FHWA, 2009, “Area of Bridges by Functional Classification,” http://www.fhwa.dot.gov/bridge/nbi/fcarea09.cfm (accessed: July 15, 2010).

Fitch, M. G. and Abdulshafi, O. A., 1998, "Field and Laboratory Evaluation of Silica Fume Modified Concrete Bridge Deck Overlays in Ohio," *Concrete in Construction*, No.1610, pp. 20-27.

Graybeal, B. A.; Rolander, D. D.; Phares, B. M.; Moore, M. E.; and Washer, G. A., 2001, "Reliability and Accuracy of In-Depth Inspection of Highway Bridges," *Transportation Research Record*, No. 1749, pp. 93-99.

GSSI, 2006, "What is GPR: A Short Description by GSSI," www.geophysical.com (accessed: May 2010).

Gucunski, N.; Romero, F. A.; Shokouhi, P.; and Makresias, J., 2005, “Complementary Impact Echo and Ground Penetrating Radar Evaluation of Bridge Decks on I-84 Interchange in Connecticut,” *Earthquake Engineering and Soil Dynamics* (GSP 133).

Gucunski, N.; Consolazio, G. R.; and Maher, A., 2006, "Concrete Bridge Deck Delamination Detection by Integrated Ultrasonic Methods," *International Journal of Materials & Product Technology*, V. 26, No.1-2, pp. 19-34.

Gucunski, N.; Rascoe, C.; Huston, D.; and Jalinoos, F., 2008, "Feature Condition Assessment of Bridge Decks by Complementary Impact Echo and Ground Penetrating Radar," *Materials Evaluation*, V. 66, No. 11, pp. 1125-1128.

Gucunski, N.; Slabaugh, G.; Wang, Z.; Fang, T.; and Maher, A., 2008, "Impact Echo Data from Bridge Deck Testing Visualization and Interpretation," *Transportation Research Record*, No. 2050, pp. 111-121.

Halabe, U. B.; Chen, H. L.; Bhandarkar, V.; and Sami, Z., 1997, "Detection of Sub-Surface Anomalies in Concrete Bridge Decks Using Ground Penetrating Radar," *ACI Materials Journal,* V. 94, No. 5, pp. 396-408.

Halabe, U. B.; Vasudevan, A.; GangRao, H.; Klinkhachorn, P.; and Shives, G. L., 2003, "Nondestructive Evaluation of Fiber Reinforced Polymer Bridge Decks Using Digital Infrared Imaging," *IEEE: IEEE Xplore*, pp. 372-375.

Henderson, M. E.; Dion, G. N.; and Costley, R. D., 1999, "Acoustic Inspection of Concrete Bridge Decks," *SPIE--The International Society for Optical Engineering*, V. 3587, pp. 219-227.

Henriksen, C., 1995, “Impact-Echo Testing,” *Concrete International,* V. 17, No. 5, pp. 55-58.

Hugenschmidt, J., 2002, "A One-to-One Comparison Between Radar Results and Reality on a Concrete Bridge," *Proceedings of SPIE--The International Society for Optical Engineering,* V. 4758, pp. 427-432.

Huston, D.; Hu, J. Q.; Maser, K.; Weedon, W.; and Adam, C., 1999, "Ground Penetrating Radar for Concrete Bridge Health Monitoring Applications," *SPIE--The International Society for Optical Engineering,* V. 3587, pp. 170-179.

Huston, D.; Fuhr, P.; Maser, K.; and Weedon, W., 2002, “Nondestructive testing of reinforced concrete bridges using radar imaging techniques,” The New England Transportation Consortium.

Huston, D.; Gucunski, N.; Maher, A.; Cui, J.; Burns, D.; and Jalinoos, F., 2007, “Bridge Deck Condition Assessment with Electromagnetic, Acoustic and Automated Methods,” *Proceedings of the 6th International Workshop on Structural Health Monitoring*.

Huston, D.; Cui, J.; Burns, D.; Gucunski, N.; Maher, A.; and Jalinoos, F., 2007, “Multisensor and Automated Measurement of Bridge Deck Condition,” *World Forum on Smart Materials and Smart Structure Technology* (SMSST07), Chongqing & Nanjing, China.

Jaeger, B. J.; Sansalone, M. J.; and Randall, W., 1996, "Detecting Voids in Grouted Tendon Ducts of Post-Tensioned Concrete Structures Using the Impact-Echo Method," *ACI Structural Journal,* V. 93, No. 4, pp. 462-473.

Juranty, M. W., 1995, "Ground Penetrating Radar Evaluation of Bridge Decks," *SPIE--The International Society for Optical Engineering*, V. 2456, pp. 59-67.

Khan, M. S., 1998, "Evaluation of Dual Band Infrared Thermography System for Bridge Deck Delamination Surveys," *Proceedings of SPIE--The International Society for Optical Engineering,* V. 3400, pp. 224-235.

Knorr, R. E.; Buba, J. M.; and Kogut, G. P., 1983, "Bridge Rehabilitation Programming by Using Infrared Techniques," *Transportation Research Record*, No. 899, pp. 32-34.

Kunz, J. T. and Eales, J. W., 1985, “Evaluation of Bridge Deck Condition by the Use of Thermal Infrared and Ground-Penetrating Radar,” *The Conference on Bridges Official Proceedings: 2nd Annual International Bridge Conference*, pp. 121-127.

Manning, D. G. and Holt, F. B., 1986, "The Development of Deck Assessment by Radar and Thermography," *Transportation Research Record,* No. 1083, pp. 13-20.

Maser, K, 1995, "Evaluation of bridge decks and pavements at highway speed using ground-penetrating radar," *SPIE--The International Society for Optical Engineering*, V. 2456, pp. 237-248.

Parillo, R. and Roberts, R., 2006, “Bridge Deck Condition Assessment Using Ground Penetrating Radar,” *9th European Conference on NDE*, Berlin, Germany.

Sansalone, M., 1997, "Impact-echo: The complete story," *ACI Structural Journal*, V. 94, No. 6, pp. 777-786.

Sansalone, M. and Carino, N. J., 1988, "Impact-Echo Method," *Concrete International*, V. 10, No. 4, pp. 38-46.

Sansalone, M. J. and Streett, W. B., 1997, *Impact-Echo Nondestructive Evaluation of Concrete and Masonry,* Ithaca, NY, Cayuga Press.

Scott, M.; Duke, J. C.; Davidson, N.; Washer, G.; and Weyers, R., 2000, "Automated Characterization of Bridge Deck Distress Using Pattern Recognition Analysis of Ground Penetrating Radar Data," *Materials Evaluation*, V. 58, No. 11, pp. 1305-1309.

Shroff, A. C., 2005, “Remote Sensing Techniques for Bridge Deck Evaluation,” *Bridge Management 5,* eds*.* G. A. R. Parke and P. Disney. London, ASCE: pp. 628-637.

Tawhed, W. F. and Gassman, S. L., 2002, “Damage assessment of concrete bridge decks using impact-echo method,” *ACI Materials Journal,* V. 99, No. 3, pp. 273-281.

Tinkey, Y. and Olson, L. D., 2008, "Applications and Limitations of Impact Echo Scanning for Void Detection in Posttensioned Bridge Ducts," *Transportation Research Record,* No. 2070, pp. 8-12.

Tinkey, Y. and Olson, L. D., 2010, “Vehicle-Mounted Bridge Deck Scanner,” NCHRP-IDEAS Program, In Press.

Warhus, J. P.; Mast, J. E.; Johanson, E. M.; and Nelson, S. D., 1994, "Advanced Ground Penetrating Radar," *SPIE--The International Society for Optical Engineering,* V*.* 2275, pp. 177-185.

Warhus, J. P.; Mast, J. E.; and Nelson, S., 1995, "Imaging radar for bridge deck inspection," *SPIE--The International Society for Optical Engineering,* V. 2456, pp. 296-305.

Yehia, S.; Abudayyeh, O.; Abdel-Qader, I.; and Zalt, A., 2008, "Ground-Penetrating Radar, Chain Drag, and Ground Truth: Correlation of Bridge Deck Assessment Data," *Transportation Research Record, No.* 2044, pp. 39-50.

Yehia, S.; Abudayyeh, O.; Nabulsi, S.; and Abdel-Qader, I., 2005, “A Comparison between Ground Penetrating Radar (GPR) and Impact Echo (IE) for Detection of Common Concrete Bridge Defects,” *Computing in Civil Engineering*.
Yehia, S., Abudayyeh, O.; Nabulsi, S.; and Abdel-Qader, I., 2007, "Detection of Common Defects in Concrete Bridge Decks Using Nondestructive Evaluation Techniques," *Journal of Bridge Engineering*, V. 12, No. 2, pp. 215-225.

Appendix A

This appendix presents the unabridged results from all nondestructive evaluations completed. The First Street Bridge located in Casper is discussed in Section A.1. Douglas Bridge with and without the overlay is discussed in Sections A.2 and A.3, respectively. Remount Bridge with and without the asphalt overlay is discussed in Sections A.4 and A.5, respectively. Results are broken down based on method and presented in the form of deck plan views, tables, and photographs. Detailed comments on the core results are also included. The final section for each bridge contains a comparison of damage for each non-destructive evaluation method.

A.1 First Street Bridge, Casper, Wyoming

Table A.1 presents the required time to complete and analyze the tests. Results from each method are provided in the following sections.

Table A.1: Time required for each NDE method performed on the Casper Bridge

Test	Time Performing Evaluation	Number of Workers	Time Performing Analysis
Chain Dragging	4 hours	3	5 hours
Impact Echo	5.5 hours	2	10 hours
Thermal Imaging	7 hours	2	25 hours
GPR-Ground-Coupled Cart	1.5 hours	1	8 hours
GPR-Air-Coupled	1 hour	1	N/A

A.1.1 Chain Dragging and Half Cell Potential Tests

This section presents the results of the chain drag and half cell potential tests, which were performed by the WYDOT bridge crew. Figure A.1 shows the detected damage and delaminations from the chain dragging test, which indicated that 12% of the deck was delaminated. Figure A.2 shows the half cell equipotential contour map. The purple-filled regions represent areas of -0.35 V or more negative, where there is a greater than 90% probability of corrosion according to ASTM C 876. The purple outlined area represents a potential -0.2 V to -0.35 V. The results, provided by WYDOT, have been overlaid on the grid to

standardize all of the tests for comparison. Table A.2 displays the percent potential corrosion corresponding to increasing voltage increments.

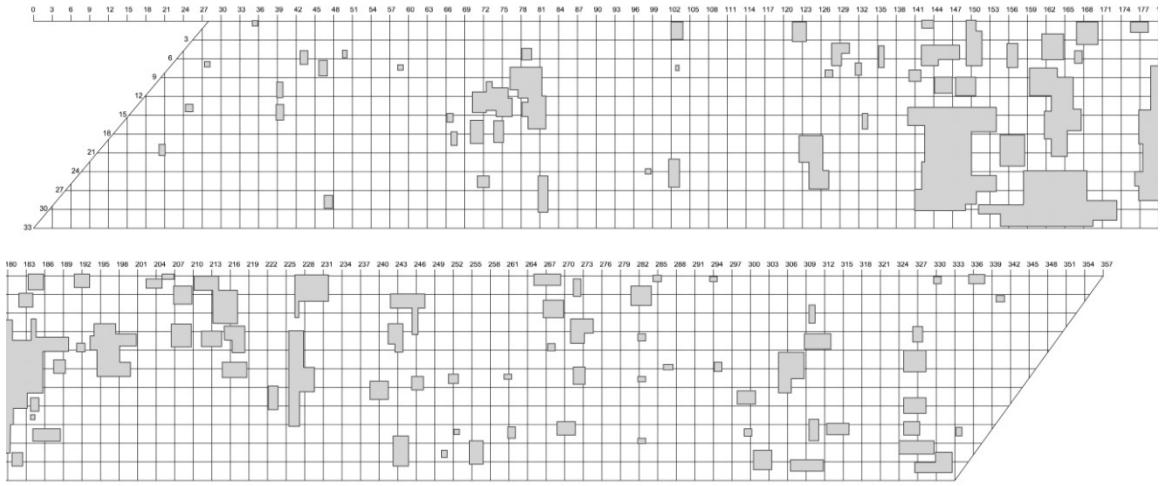

Figure A.1: Chain drag results outlining areas of delaminations

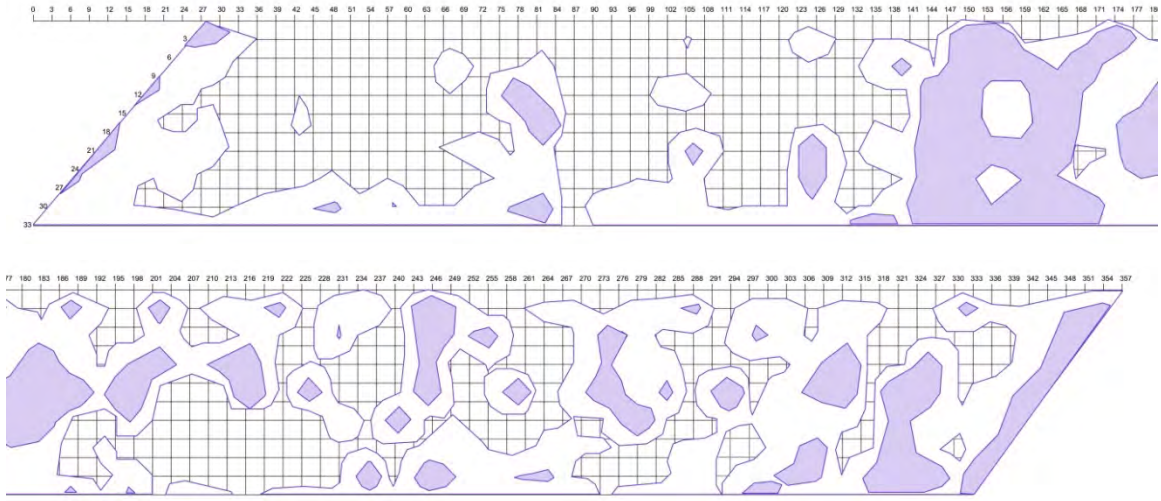

Figure A.2: Half cell potential results

Table A.2: Voltage increments and percent of deck corrosion potential

Voltage (V)	Percent of Total Damaged Area
Above 0.20	30.6%
Above 0.30	13.5%
Above 0.35	8.9%
Above 0.40	6.0%
Above 0.50	2.6%
Above 0.60	0.7%

A.1.2 Impact Echo

Results from the impact echo test are compiled below. All impact echo data was collected and analyzed by the University of Wyoming research team. In all grid figures, the top section is the north portion of the bridge. Figure A.3 was developed by plotting thickness readings from the CTG. The darker blue areas represent shallow bridge sections, and the darker red areas represent thicker sections. Deep regions represent potential areas of delamination. The dark blue regions on either side of the contour map represent the skewed ends of the deck. Figure A.4 is a simplified version of Figure A.3, only showing outlined damaged and delaminated zones. Impact echo test results indicated that 13% of the deck was delaminated.

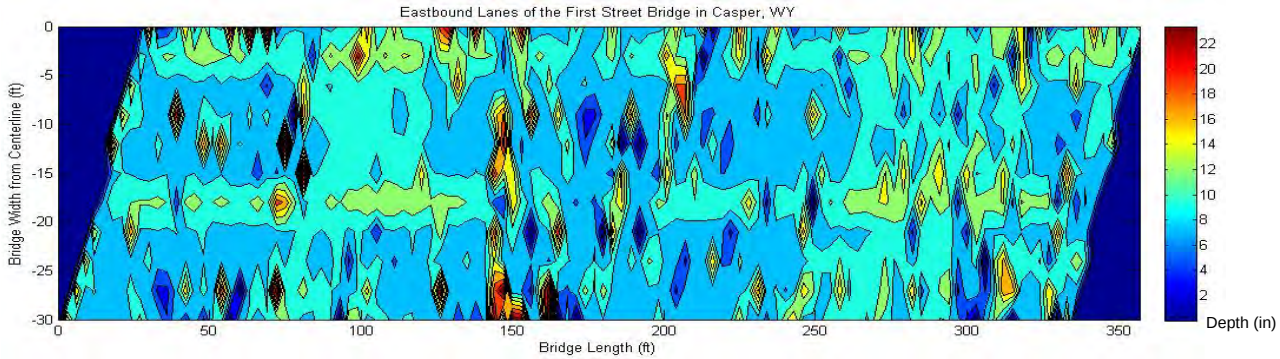

Figure A.3: Impact echo test contour map of damage

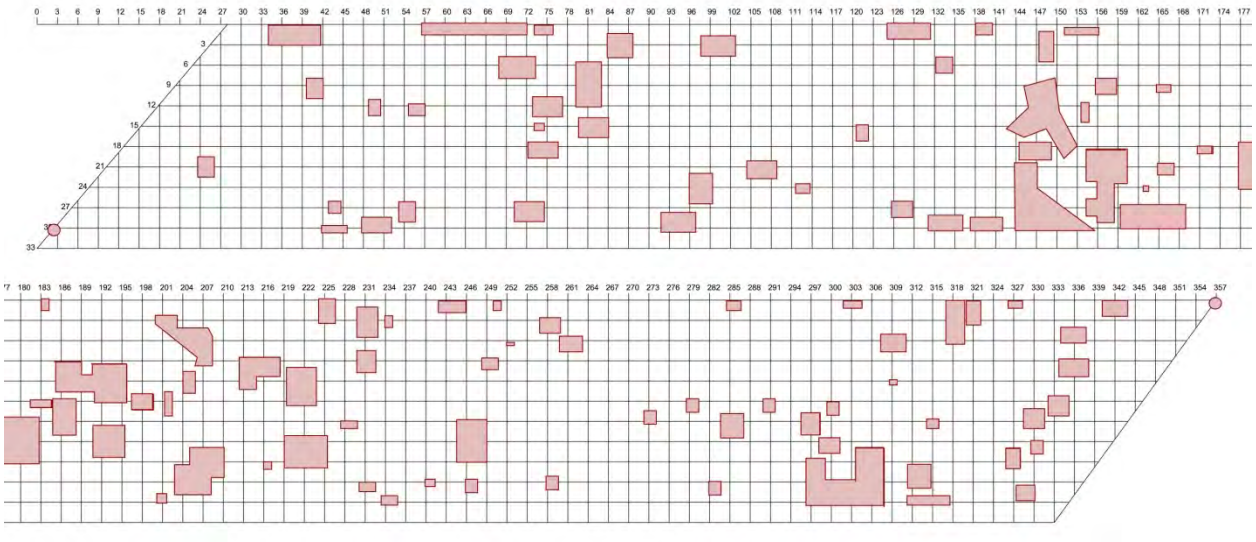

Figure A.4: Outlines of delamination/damage from impact echo test

A.1.3 Thermal Imaging

This section presents the results from thermal imaging testing and analysis performed by University of Wyoming researchers. Approximately 900 images were overlaid to produce Figure A.5. Yellow areas, which are warmer temperatures than the red areas, represent areas of delamination or damage. The same procedure from the impact echo test was used to outline damage and delaminations which are shown in both Figure A.5 and Figure A.6. Thermal imaging testing found 17% of the deck to be delaminated or deteriorated.

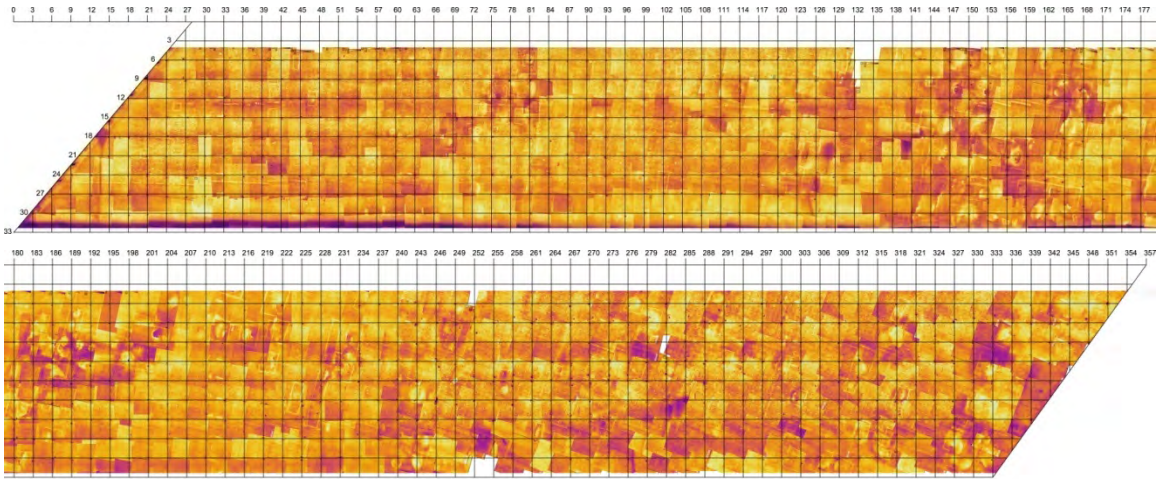

Figure A.5: Thermal images of the bridge deck

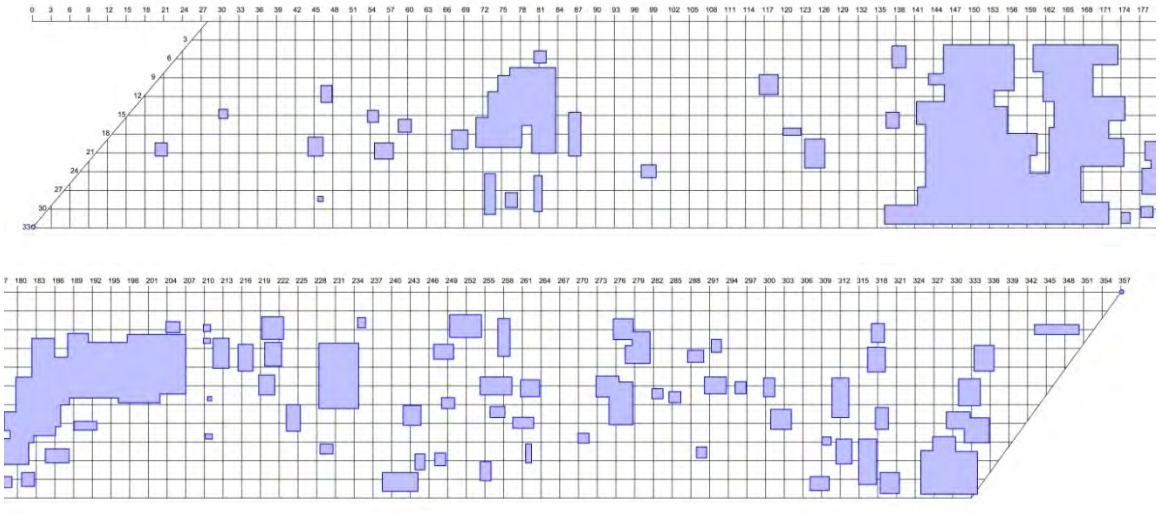

Figure A.6: Outlines of delamination/damage from thermal imaging test

A.1.4 Ground Penetrating Radar

Figure A.7 through Figure A.9 shows the damage maps produced by GPR evaluation. The air-coupled antenna used by Olson Engineering did not produce useful results because individual rebar signals were shown as a solid black line rather than individual responses. In Figure A.7, probable delaminations are shown in red and probable corrosion areas are shown in yellow. It was calculated that 11% of the deck was delaminated and 17% of the deck had corrosion.

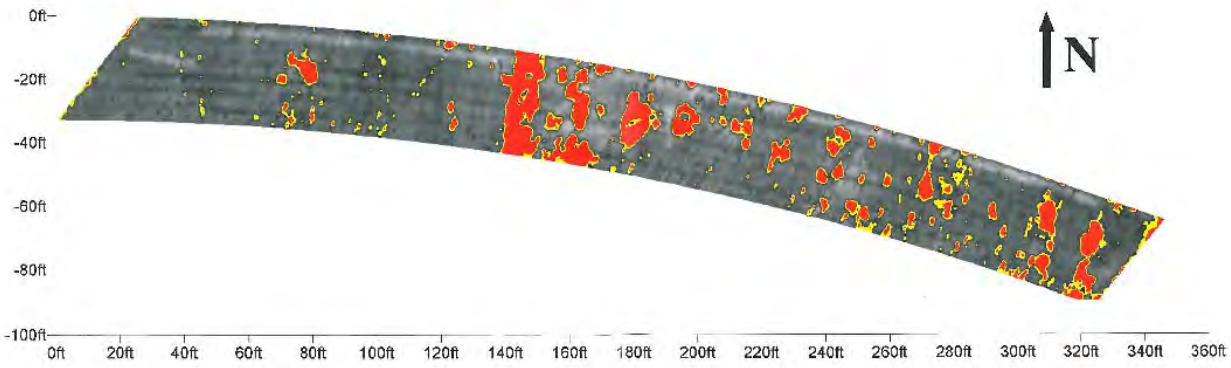

Figure A.7: Ground penetrating radar results from Barnes

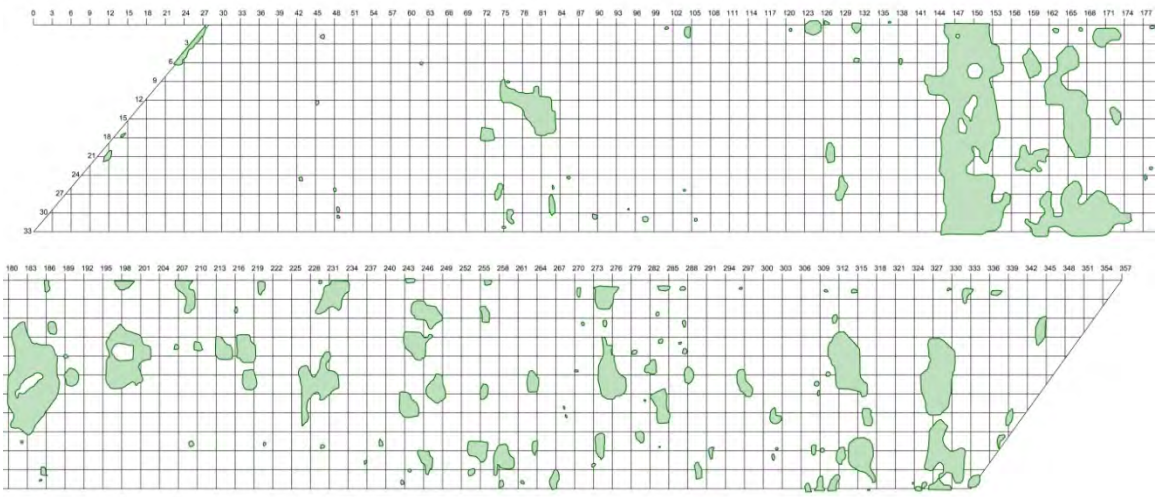

Figure A.8: Ground penetrating radar-probable delaminations

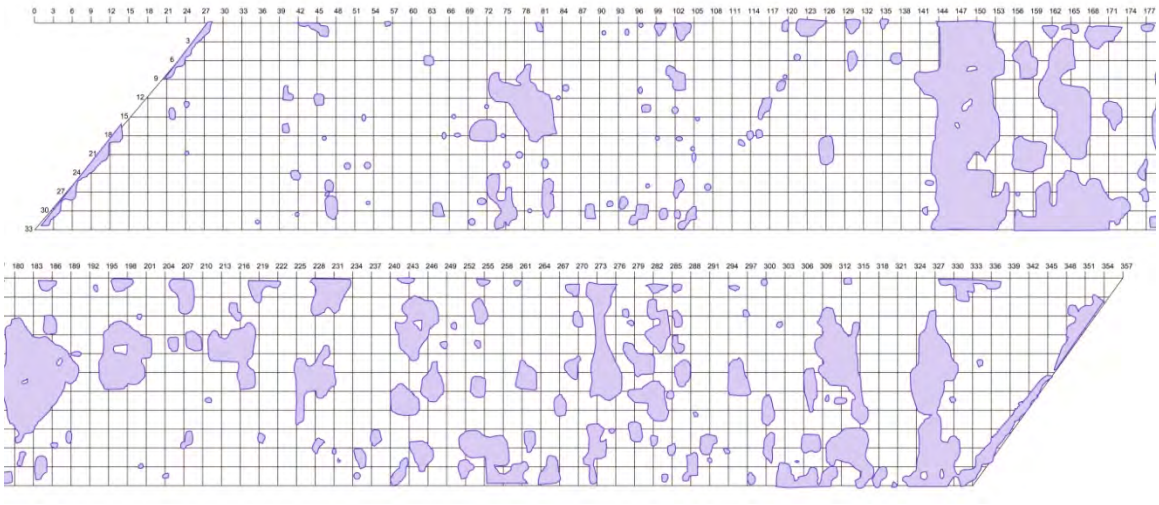

Figure A.9: Ground penetrating radar-probable corrosion

A.1.5 Summary of Damage

Table A.3 and Table A.4 summarize the previous results by showing the calculated areas of damage as a percentage of total bridge deck area for each NDE test performed on the Casper Bridge. Table A.3 shows percent delamination/deteriorated, while Table A.4 compares the percent of the deck that is predicted to be corroding.

Table A.3: Percent of Casper Bridge delaminated

NDE Method	Percent Delaminated/Deteriorated
Chain Dragging	12%
Impact Echo	13%
Thermal Imaging	17%
GPR (without Corrosion Areas)	11%

Table A.4: Percent of Casper Bridge with potential corrosion

NDE Method	Percent Potential Corrosion
Half Cell Potentials (-0.2 V and more negative)	31%
Half Cell Potentials (-0.35 V and more negative)	8.9%
GPR (Corrosion)	17%

A.1.6 Core Evaluations

Cores were taken from the deck from areas shown by the various evaluation methods to be damaged. GPR results were not available before cores were extracted, but were later correlated by overlaying the core locations on the GPR damage map. Figure A.10 shows where cores were removed from the bridge deck. A record of the cores removed is presented below in Table A.5.

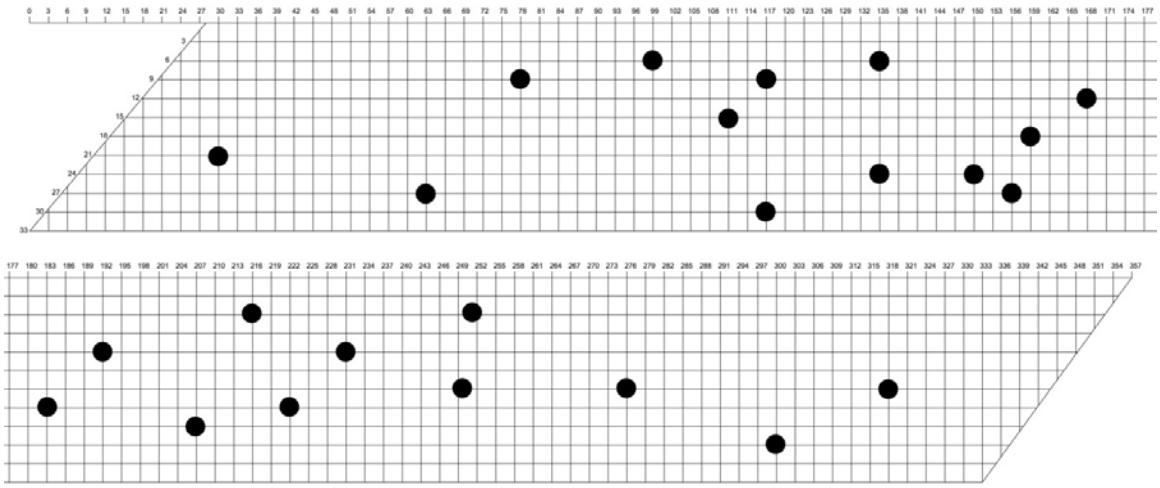

Figure A.10: Casper Bridge core locations

Table A.5: Casper Bridge core details

Number	Location	Method Showing Damage				Field Notes Pertaining to Deck Condition
		CD	IE	Ther.	GPR	
1	(30, 21)	x	x	x		Good
2	(63, 27)		x			2-Rebar 2A-Good
3	(78, 9)		x	x		3A-Rebar 3B-Good
4	(99, 6)	x				4A-Too Short 4B-Good
5	(111, 15)					5A-Too short 5B-Good
6	(117, 9)			x		6A-Rebar 6B-Good
7	(117, 30)	x	x	x		Good
8	(135, 6)	x				8A-8E-No Core
9	(135, 24)					9A-Rebar 9B-Good
10	(150, 24)	x		x	x	Good
11	(156, 27)	x	x	x	x	11A, B-Rebar 11C-No Core
12	(159, 18)	x	x	x		12A, B-No good 12C-Good
13	(168, 12)	x		x		Delamination
14	(183, 21)		x	x	x	Delamination
15	(192, 12)	x	x	x		Good
16	(207, 24)		x			Not deep enough
17	(216, 6)	x				17A-Rebar 12B-Good
18	(222, 21)		x			18A-No good 18B-Good
19	(231, 12)			x	x	Good
20	(250, 18)		x	x		Delamination
21	(251, 6)			x		Good
22	(276, 18)			x	x	Good
23	(300, 27)		x		x	Delamination
24	(318, 18)	x		x		Good

Table A.6 shows the percent correlations of each method prediction with deck condition as determined by cores.

Table A.6: Casper Bridge core correlations

Test	Percent Correlated
Chain Drag	45%
Impact Echo	59%
Thermal Imaging	47%
Ground Penetrating Radar	73%

A.2 Southbound I-25 Bridge, Structure AFY, in Douglas, Wyoming, with Latex Modified Concrete Overlay

Table A.7 presents the time required to complete and analyze the tests. Results from each testing method are provided in the following sections.

Table A.7: Time required for each NDE method performed on the Douglas Bridge with overlay

Test	Time	Number of Workers	Time Performing Analysis
Chain Dragging	2.5 hours	3	3 hours
Impact Echo	4 hours	2	5 hours
Thermal Imaging	4 hours	2-3	20 hours
GPR-Ground-Coupled Cart	3 hours	1	6 hours
GPR-Air-Coupled, Olson Engineering	3 hours	1	N/A
GPR-Air-Coupled, Rii	2.5 hours	2	21.5 hours

A.2.1 Chain Dragging and Half Cell Potential Tests

This section presents the results of the chain drag and half cell potential tests performed by the WYDOT bridge crew. Figure A.11 shows the detected damage and delaminations from chain dragging, from which it was calculated that 74% of the deck was delaminated. Figure A.12 shows a second chain drag evaluation conducted by another WYDOT crew. For the second evaluation 29% of the bridge was calculated to be damaged. It can be seen that this evaluation did not account for the skewed ends. Figure A.13 shows the half cell equipotential contour map. The purple-filled regions represent areas of -0.35 V or more negative, where there is a greater than 90% probability of corrosion according to ASTM C876. The purple outlined area represents a potential -0.2 V to -0.35 V. The results, provided by WYDOT, have been overlaid on the grid to standardize all of the tests for comparison. Table A.8 displays the percent potential corrosion corresponding to increasing voltage increments.

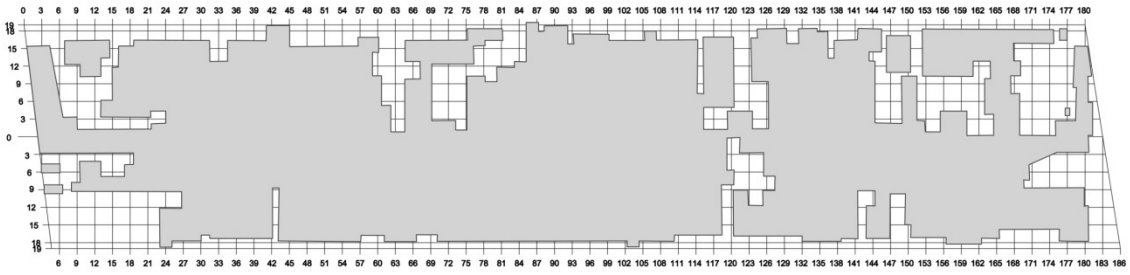

Figure A.11: Chain drag results outlining areas of delaminations

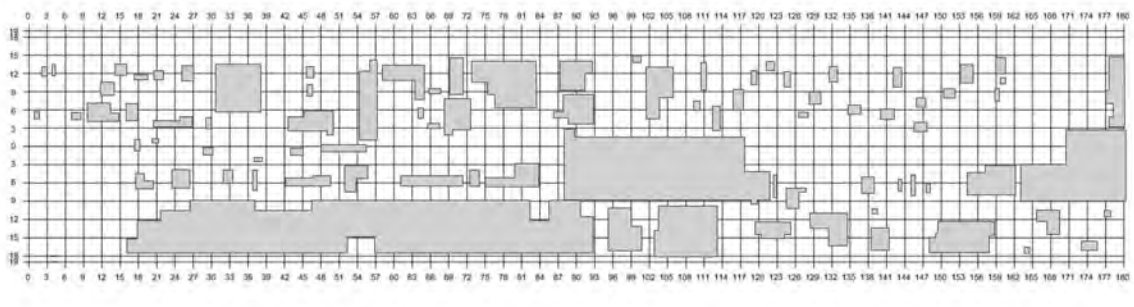

Figure A.12: Secondary chain drag results outlining areas of delaminations

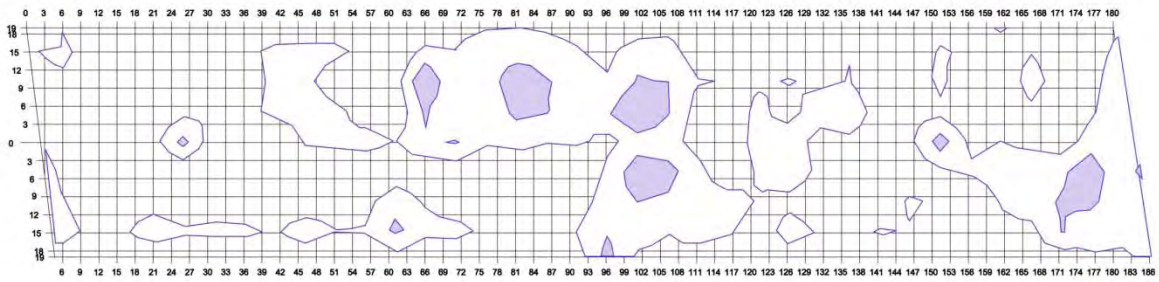

Figure A.13: Half-cell potential results

Table A.8: Voltage increments and percent of deck corrosion potential

Voltage (V)	Percent of Total Damaged Area
Above 0.20	35.5%
Above 0.30	10.6%
Above 0.35	3.8%
Above 0.40	1.0%

A.2.2 Impact Echo

The same procedure that was used for the Casper Bridge was used in producing the damage maps for the impact echo test. Figure A.14 shows the impact echo response of the concrete and Figure A.15 shows the outlines of the areas of delamination. Impact echo tests results indicated that 45% of the deck was delaminated.

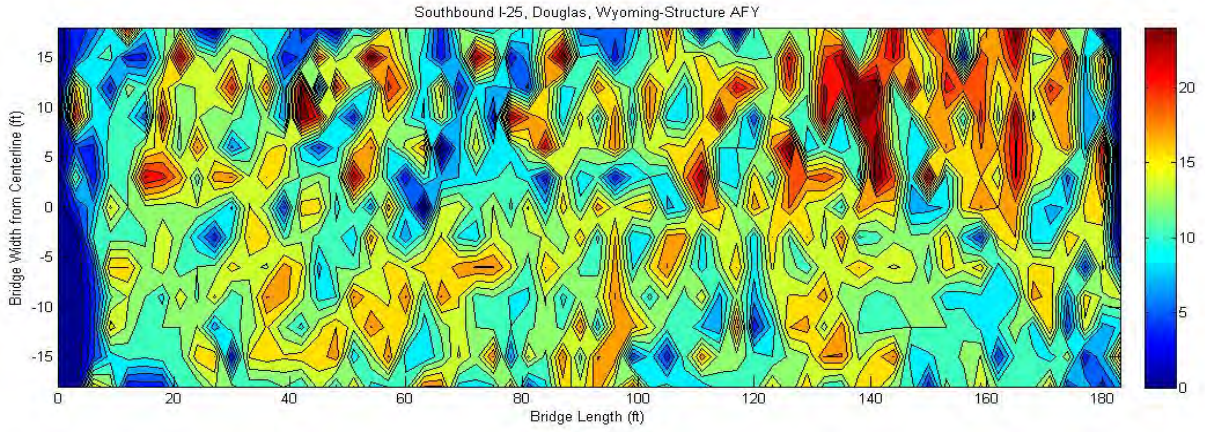

Figure A.14: Impact echo test contour map of damage

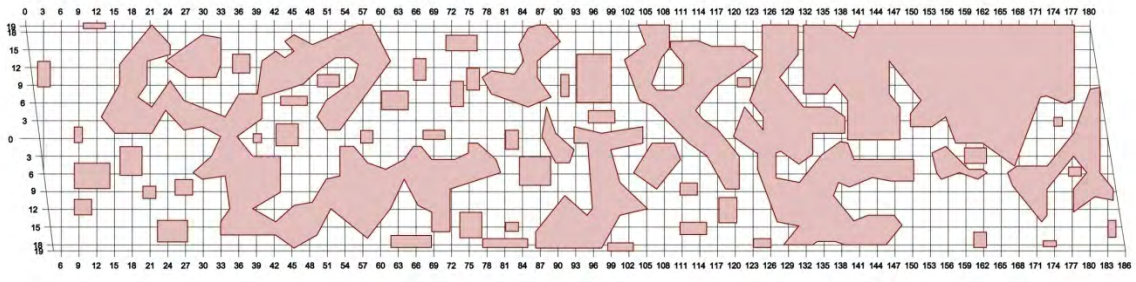

Figure A.15: Outlines of delamination/damage from impact echo test

A.2.3 Thermal Imaging

The same procedure as the Casper Bridge was used in producing the damage maps for the thermal imaging evaluation. Figure A.16 shows all of the thermal images stitched together while Figure A.17 shows the outlines of areas of delamination. Thermal imaging testing found that 39 % of the deck was delaminated or deteriorated.

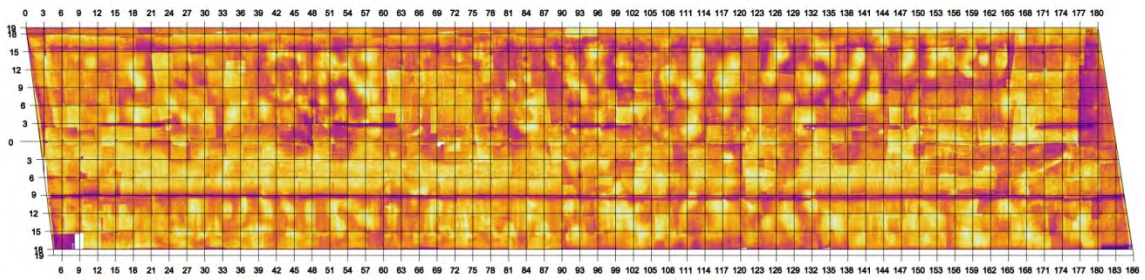

Figure A.16: Thermal images of the bridge deck

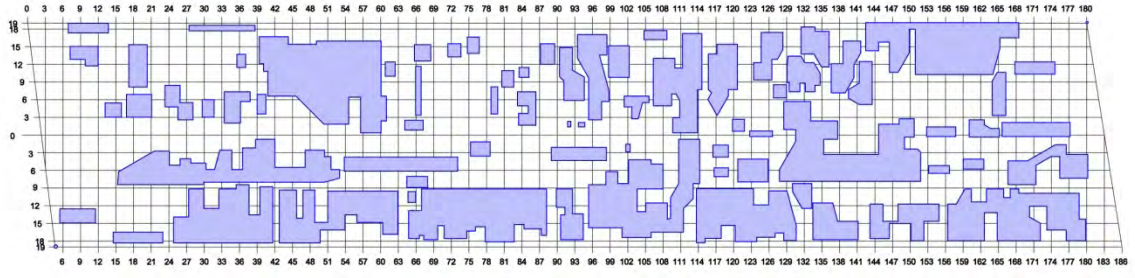

Figure A.17: Outlines of delamination/damage from thermal imaging test

A.2.4 Ground Penetrating Radar-Ground-Coupled

Figure A.18 through Figure A.20 shows the damage maps produced by the GPR evaluation. The air horn antenna used by Olson Engineering did not produce useful results, which contained rebar signals that were unresolvable. In Figure A.18, probable delaminations are shown in red and probable corrosion areas are shown in yellow. It was calculated that 11% of the deck was delaminated and 34% of the deck had corrosion.

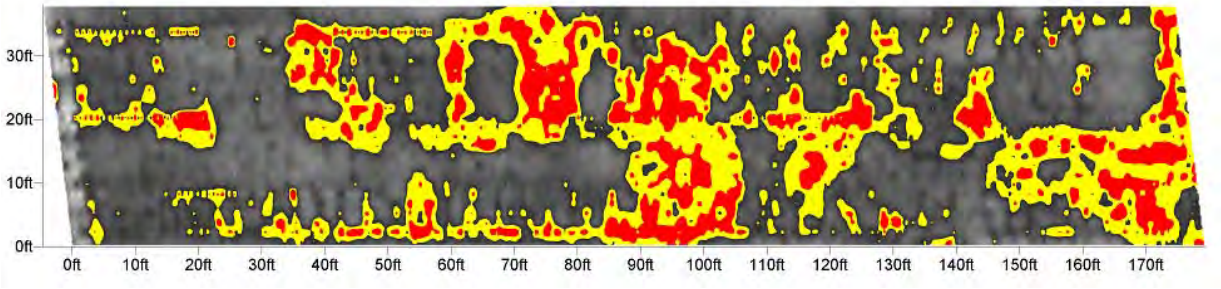

Figure A.18: Ground penetrating radar results from Barnes

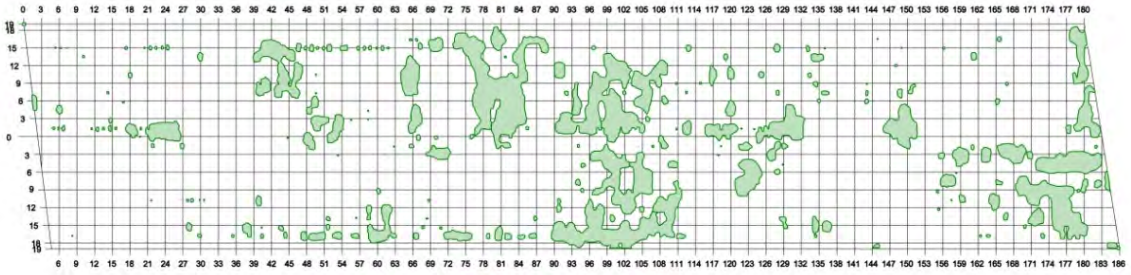

Figure A.19: Ground penetrating radar-probable delaminations

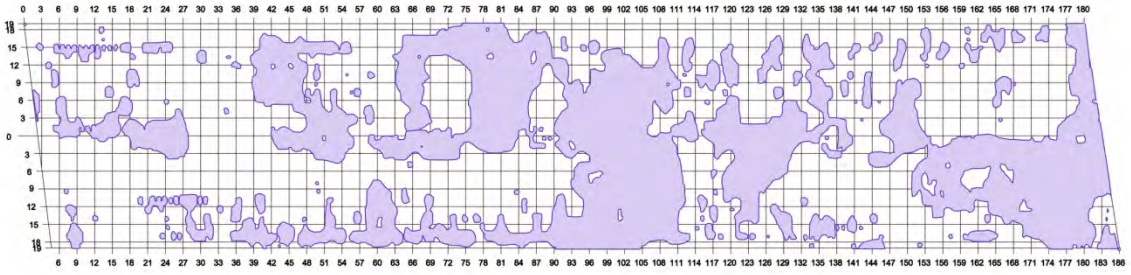

Figure A.20: Ground penetrating radar-probable corrosion

A.2.5 Ground Penetrating Radar-Air-Coupled

The following results show the damage maps that were calculated by Rii using the van-mounted GPR system. A pass along the cone line was not allowed due to construction constraints, which is visible in the damage maps (Figure A.21 and Figure A.22). It was calculated that 16% of the deck had deteriorated concrete.

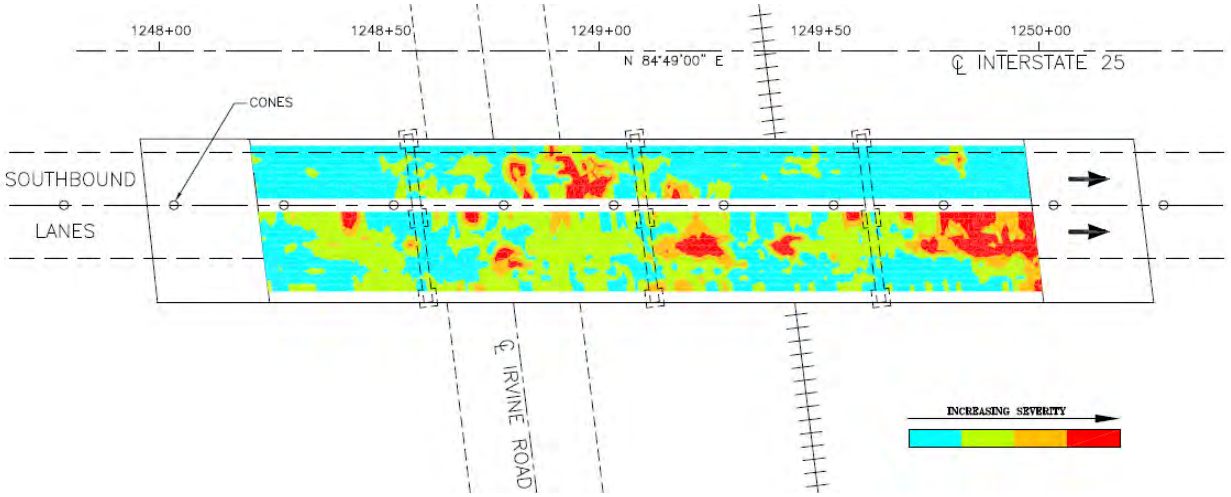

Figure A.21: Rii GPR plot

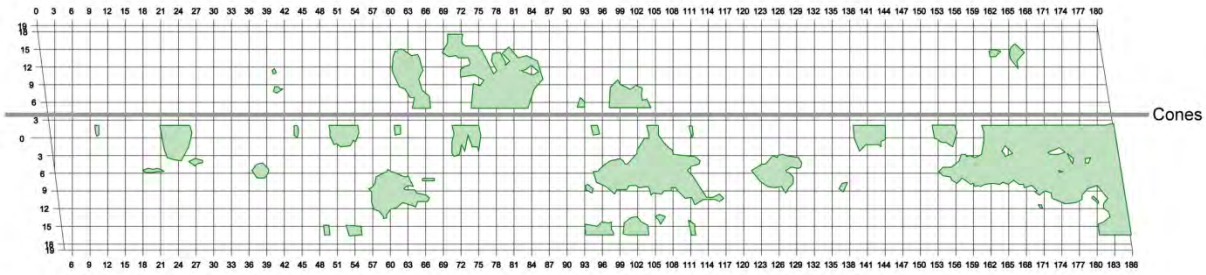

Figure A.22: Air-coupled GPR results from Rii

A.2.6 Summary of Damage

Table A.9 and Table A.10 summarize the previous results by showing the calculated areas of damage as a percentage of total bridge deck area for each NDE test performed in the Douglas Bridge. Table A.9 shows percent delaminated/deteriorated, while Table A.10 compares the percent of the deck that is predicted to be corroding.

Table A.9: Percent of Douglas Bridge with overlay delaminated/deteriorated

NDE Method	Percent Delaminated/Deteriorated
Chain Dragging	74%
Second Chain Dragging	19%
Impact Echo	45%
Thermal Imaging	39%
GPR Ground-Coupled Cart (without Corrosion Areas)	11%
Rii Van-Mounted System	17%

Table A.10: Percent of Douglas Bridge with overlay with potential corrosion

NDE Method	Percent Potential Corrosion
Half Cell Potentials (-0.2 V and more negative)	35%
Half Cell Potentials (-0.35 V and more negative)	4%
GPR (Corrosion)	34%

A.2.7 Core Evaluations

With the overlay present, cores were taken from areas of the deck where the evaluation methods showed damage. Although GPR results were not available before cores were extracted, they were later correlated by overlaying the core locations on the GPR damage map. Figure A.23 shows where cores were removed.

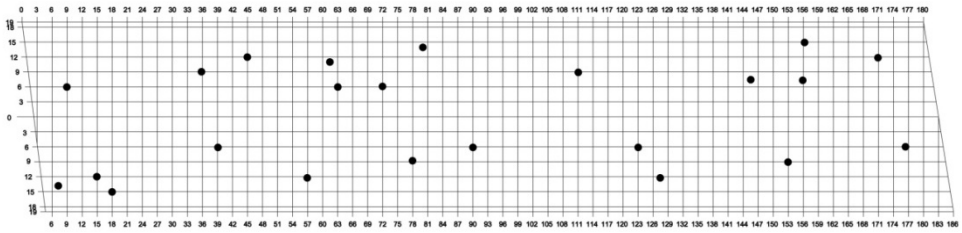

Figure A.23: Douglas Bridge core locations

Table A.11 presents the cores that were removed from the Douglas Bridge within two months after the evaluation of the overlaid deck was performed. Because different crews pulled cores and documented them for the three bridges, core details vary from bridge to bridge.

Table A.11: Core results from the Douglas Bridge with overlay

Number	Location	Method Showing Damage					Rebar Notes	Field Notes
		CD	IE	Ther.	GPR-GSSI	Rii		
1	(S7, 14)			x			Top of #6 at 5-3/8"	
2	(S15, 12)						Top of Long. #6 at 5-3/4"	Core broke off right above rebar
3	(S18, 15)						Core 3a: Hit #6 on left side 3" down, also hit vertical steel. Core 3b: Hit #6 on backside 2-1/2" down. Core 3c: Hit long. #6 at 3-1/4" down.	
4	(S, 39, 6)	x	x	x		x	Top of Long. #6 at 5" down.	Voids visible in hole between overlay and original concrete. Also, notice material between lifts.
5	(S, 57, 12)	x	x	x		x	Top of Long. #6 at 5-1/4" down.	Voids visible in hole on left side of core between overlay and original concrete.
6	(S, 78, 9)	x					No Steel	Cored completely through to the steel plate on the bottom of the deck at 6-3/4"
7	(S, 90, 6)	x					Top of Long. #6 at 5-1/4" down on left side of core.	
8	(S, 123, 6)		x	x	x	x	Top of Long #6 at 5-1/2" down.	Taken on concrete patch 2-1/2" thick. Original concrete under patch broke apart trying to remove it from hole. No voids visible in hole.
9	(S, 128,12)	x	x	x			Top of Long. #6 at 5-3/4" down.	Overlay separated from core. Hole shows void between overlay and original concrete. Void varies from 1/4" to 1" wide.
10	(S, 153, 9)	x					Trans. #6 at 6" on backside of core. Also hit vertical piece of steel. Only 1/4" of indentation visible on core. 2" of indentation is visible in the core hole.	
11	(S, 176, 6)		x	x	x	x	Hit #6 3" down and cut through bottom rebar.	
12	(N, 9, 6)						Nicked Trans. #6 at 2-1/2" down and marked with arrow.	Could not see any delamination.
13	(N, 36, 9)	x					Hit steel plate at 6"	

14	(N, 45, 12)	x	x	x	x		Hit Long. #6 at 5" down.	
15	(N, 62,11)			x		x	Hit Long. #6 at 5-1/2" down.	
16	(N, 63, 6)		x				Hit Long. #6 at 5-1/2" down.	
17	(N, 72, 6)		x				Hit Long. #6 at 5-1/4" down.	
18	(N, 80, 14)				x	X	Hit Long. #6 at 5-1/4" down.	
19	(N, 111, 9)	x	x	x			Hit Trans. #6 at 2-1/2" down.	3 attempts. All broke at overlay and original concrete. Delamination visible in holes.
20	(N, 146, 7)						Hit Long. #6 at 5-1/2" down.	
21	(N, 156, 15)	x	x	x			Hit Long. #6 at 5-1/4" down.	Delamination visible around hole and between overlay and original concrete.
22	(N, 156, 7)		x				Hit vertical steel at 2-1/2" down	Looks like chair support for rebar.
23	(N, 171, 12)		x	x			Hit Long. #6 at 4-3/4" down.	

A correlation was conducted to evaluate the findings from each method at each of the core locations (Table A.12).

Table A.12: Douglas Bridge core correlations

Test	Percent Correlated
Chain Drag	77%
Impact Echo	68%
Thermal Imaging	73%
Ground Penetrating Radar-GSSI	59%
Ground Penetrating Radar-Rii Van Mounted	78%

Compression and split tension evaluations were conducted on cores from areas where multiple methods showed damage. Compression tests followed ASTM C 39, as mentioned earlier, and split tension tests followed ASTM 496 Standard Test Method for Splitting Tensile Strength of Cylindrical Concrete Specimens. The results of the tests are shown in Table A.13 and Table A.14.

Table A.13: Compression test results from Douglas Bridge

Core	f_c (psi)
11	4840
14	5290
23	4090
Average	4740
Standard Deviation	± 12.7%

Table A.14: Splitting tension results from Douglas Bridge

Core	Splitting Tensile Strength (psi)
4	500
5	750
8	700
9	590
21	640
Average	640
Standard Deviation	± 15.4%

A.3 Southbound I-25 Bridge, Structure AFY, in Douglas, Wyoming, without Latex Modified Concrete Overlay

Once the overlay was removed, the Douglas Bridge was retested. Table A.15 presents the time required to complete and analyze each of the evaluation techniques. Results from each testing method are provided in the following sections.

Table A.15: Time required for each NDE method performed on the Douglas Bridge without overlay

Test	Time	Number of Workers	Time Performing Analysis
Chain Dragging	2.5 hours	3	3 hours
Impact Echo	2 hours	2	3 hours
Thermal Imaging	2.5 hours	2	15 hours
GPR-Ground-Coupled Roller	5 hours	1	8 hours

A.3.1 Chain Dragging and Half Cell Potential Tests

This section presents the results of the chain drag and half cell potential tests, which were performed by the WYDOT bridge crew. Figure A.24 shows the detected damage and delaminations from the chain dragging test, which indicated that 58% of the deck was delaminated. Figure A.25 shows the half-cell equipotential contour map. The purple-filled regions represent areas of -0.35 V or more negative, where there is a greater than 90% probability of corrosion according to ASTM C 876. The purple outlined area represents a potential -0.2 V to -0.35 V. The results, provided by WYDOT, have been overlaid on the grid to standardize all of the tests for comparison. Table A.16 displays the percent potential corrosion corresponding to voltage increments from the results.

Figure A.24: Chain drag results outlining areas of delaminations

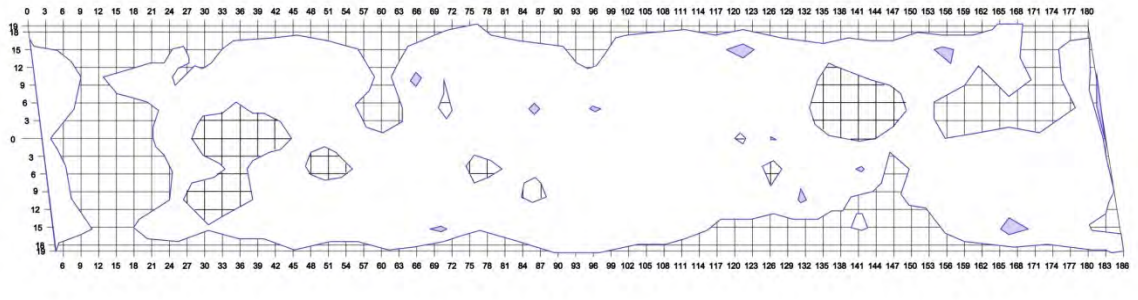

Figure A.25: Half-cell potential results

Table A.16: Voltage increments and percent of deck corrosion potential

Voltage (V)	Percent of Total Potential Area
Above 0.20	68.7%
Above 0.30	6.2%
Above 0.35	0.4%
Above 0.40	0.1%

A.3.2 Impact Echo

Again, the same procedure was carried out to produce the damage maps from the impact echo evaluation as with the Douglas Bridge with the overlay present (Figure A.26 and Figure A.27). Impact echo test results indicated that 30% of the bridge was delaminated or deteriorated.

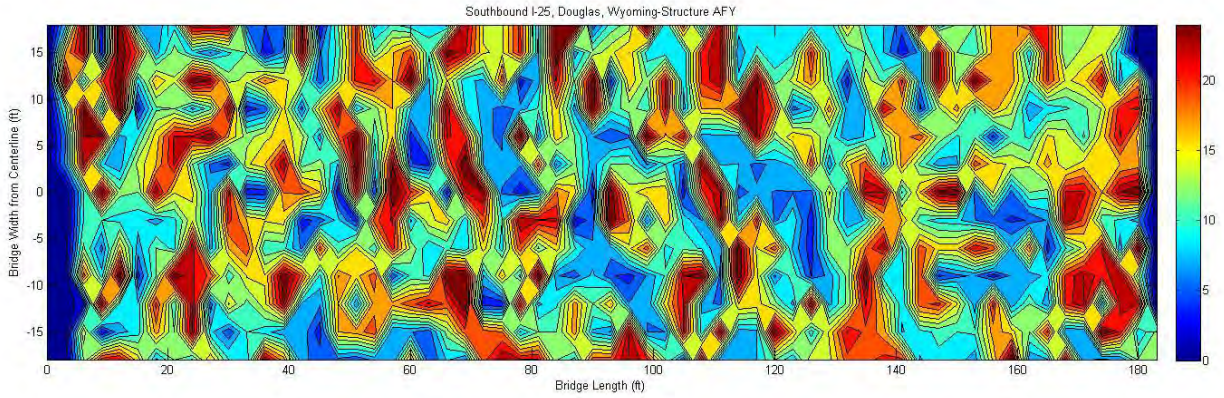

Figure A.26: Impact echo test contour map of damage

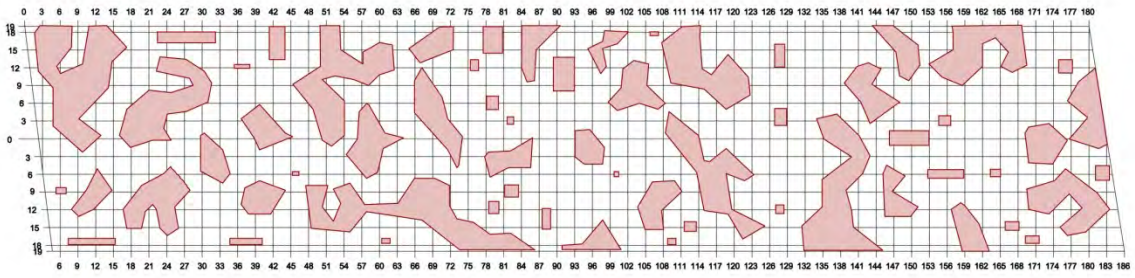

Figure A.27: Outlines of delamination/damage from impact echo test

A.3.3 Thermal Imaging

Again, the same procedure was carried out to produce the damage maps from the thermal imaging evaluation as with the Douglas Bridge with the overlay present (Figure A.28 and Figure A.29). Thermal imaging testing found that 34% of the bridge to be delaminated or deteriorated.

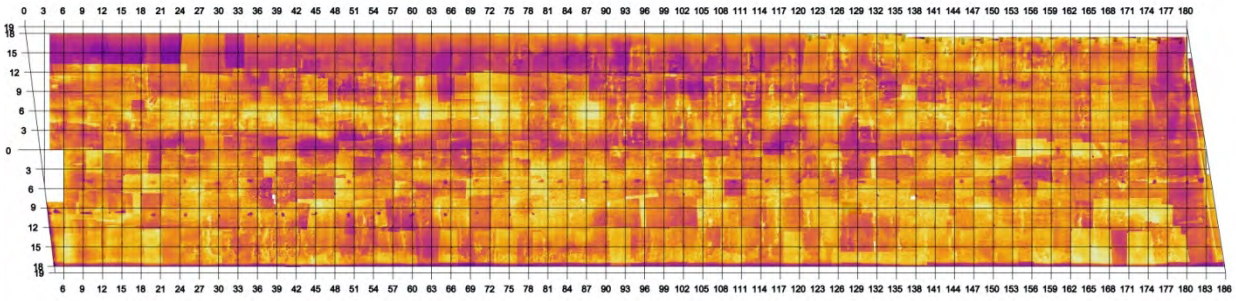

Figure A.28: Thermal images of the bridge deck

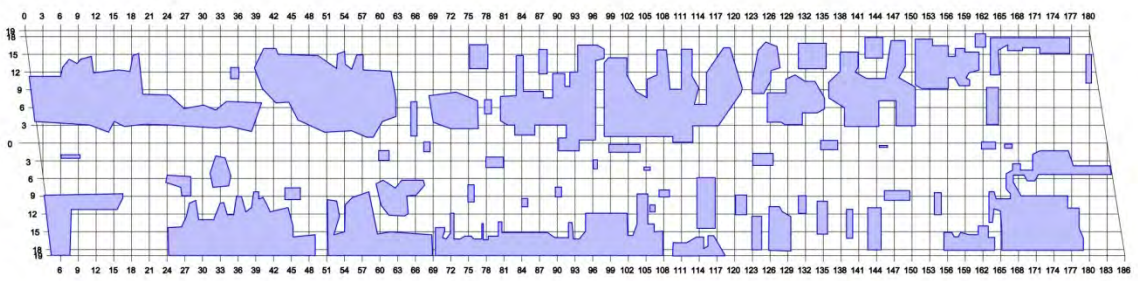

Figure A.29: Outlines of delamination/damage from thermal imaging test

A.3.4 Ground Penetrating Radar

Useful GPR results were not obtained on the milled concrete surface due to direct coupling interference from the reflections from the top surface of the bridge deck and the signal from the reinforcing bars. This distortion made the reinforcing steel appear more corroded than during the evaluation including the overlay (Olson Report 3016B in Appendix B).

A.3.5 Summary of Damage

Table A.17 summarizes the previous results by showing the calculated areas of damage as a percentage of total bridge deck area for each NDE test performed on the Douglas Bridge without the overlay.

Table A.17: Percent of Douglas Bridge without overlay delaminated/deteriorated

NDE Method	Percent Delaminated/Deteriorated
Chain Dragging	58%
Impact Echo	30%
Thermal Imaging	34%

A.4 Remount Bridge, near Buford, Wyoming, with Asphalt Overlay

Table A.18 presents the required time to complete and analyze the tests and description of each method is provided in the following sections. Results from each method are provided in the following sections.

Table A.18: Time required for each NDE method performed on the Remount Bridge with overlay

Test	Time	Number of Workers	Time Performing Analysis
Impact Echo	2 hours	2	3 hours
Thermal Imaging	2.5 hours	2	15 hours
GPR-Ground-Coupled Roller	5 hours	2	4 hours
GPR-Aladdin System	8 hours	1	6 hours

A.4.1 Chain Dragging and Half Cell Potential Tests

Although WYDOT does not perform chain dragging and half cell potentials on bridge decks with asphalt overlays, it was attempted on the Remount Bridge for purposes of consistency and comparison with the other bridge decks. WYDOT was not able to collect useful chain dragging or half cell potential data. Chain dragging results were inconclusive due to the nonhomogenous nature of the asphalt and concrete deck combination.

Half cell potentials were taken, but it was later realized the reinforcement was epoxy-coated which gives extremely high readings which are not valuable.

A.4.2 Impact Echo

The same procedure that was used for the Casper Bridge was used in producing the damage maps from the impact echo test. A test hole was drilled and the impact echo device was calibrated to it with the asphalt overlay. Figure A.30 shows the impact echo response of the deck and Figure A.31 shows the outlines of the areas of delamination. Impact echo test results indicated that 11% of the bridge to be delaminated or damaged.

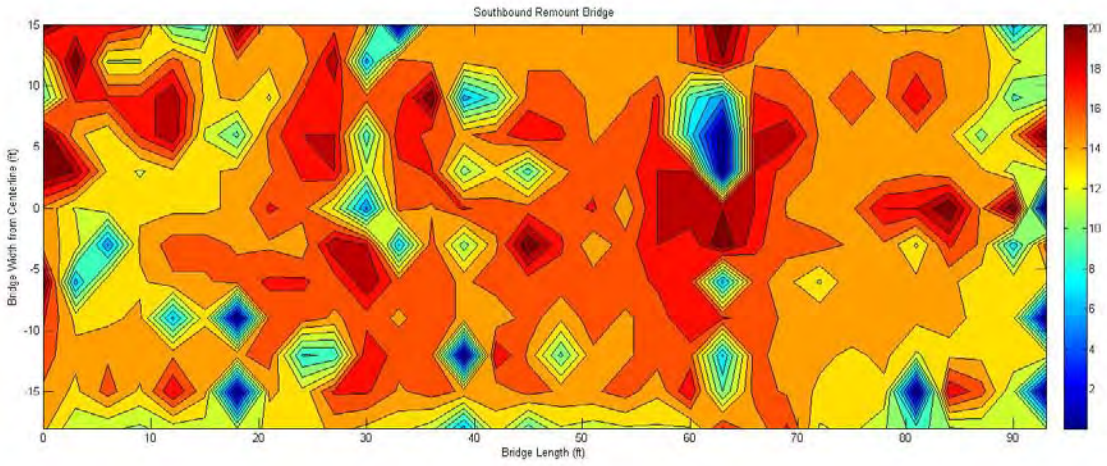

Figure A.30: Impact echo test contour map of damage

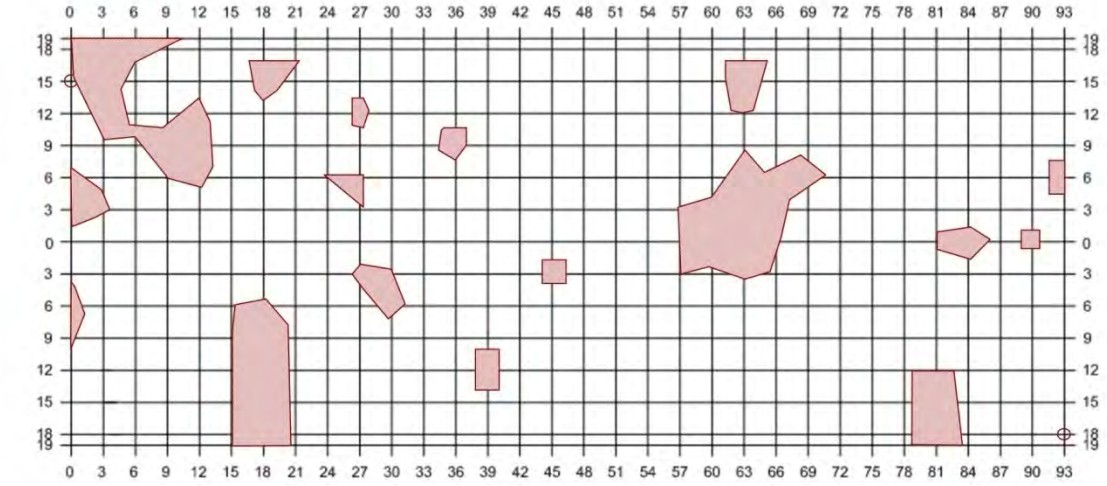

Figure A.31: Outlines of delamination/damage from impact echo test

A.4.3 Thermal Imaging

The same procedure as the Casper Bridge was used in producing the damage maps for the thermal imaging evaluation. Figure A.32 shows all of the thermal images stitched together while Figure A.17 shows the outlines of areas of delamination. Thermal imaging testing found that 13% of the bridge to be delaminated or deteriorated.

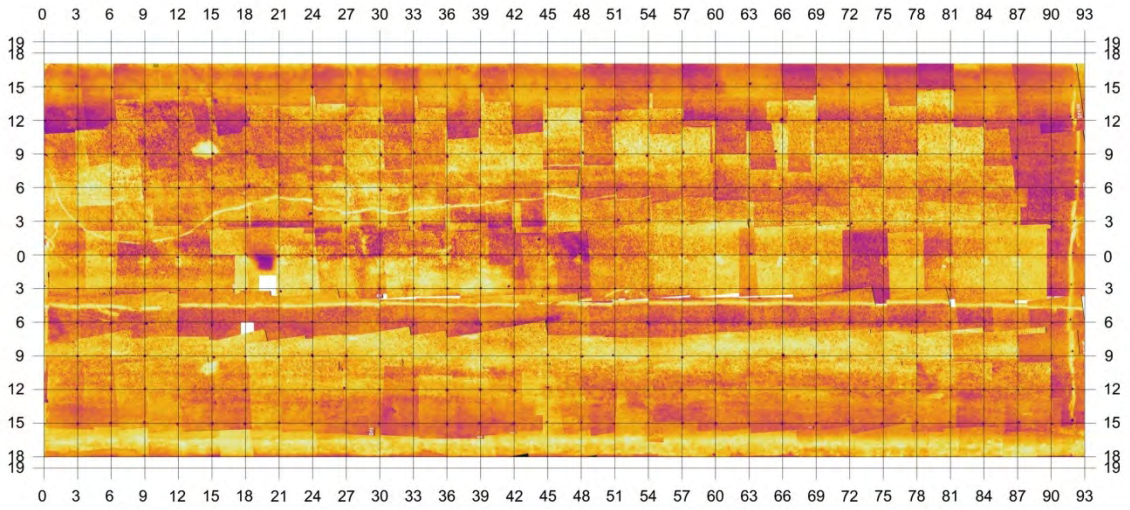

Figure A.32: Thermal images of the bridge deck

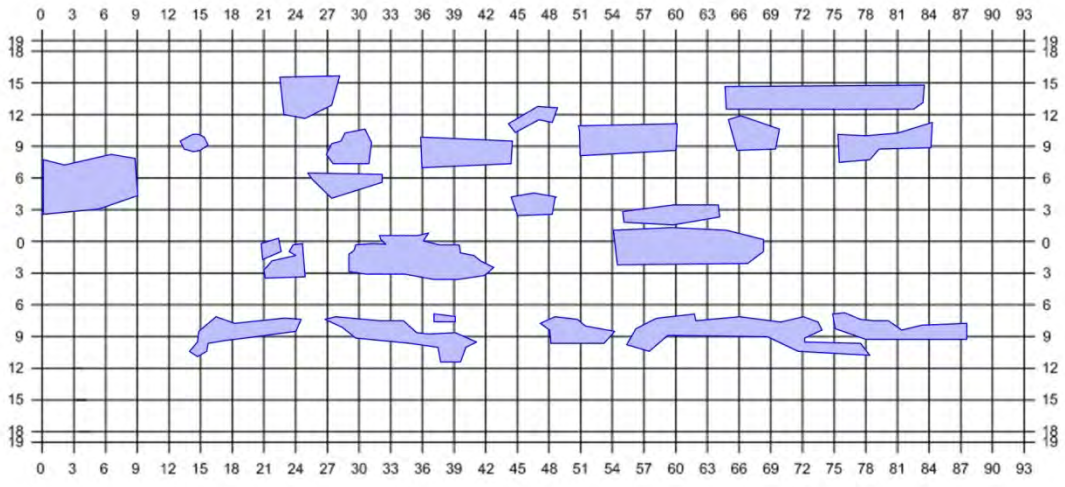

Figure A.33: Outlines of delamination/damage from thermal imaging test

A.4.4 Ground Penetrating Radar

Figure A.34 through Figure A.36 show the damage maps produced by the ground penetrating radar evaluation. In Figure A.34, probable delaminations are shown in red and probable corrosion areas are shown in yellow. It was calculated that 6.7% of the deck was delaminated and 24% of the deck had corrosion. Figure A.35 and Figure A.36 were created to split the two areas out into a probable delamination map and a probable corrosion map, respectively.

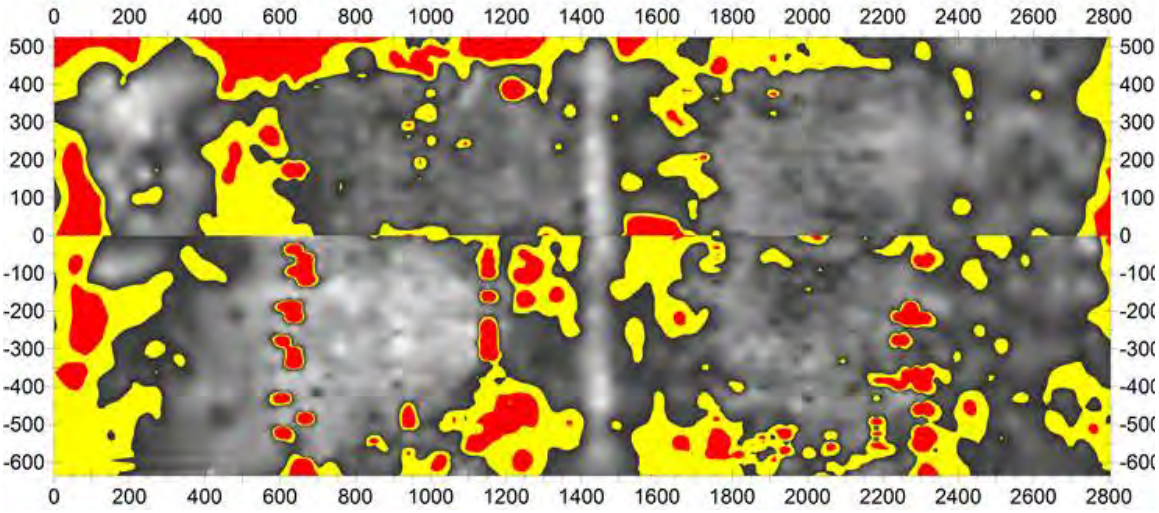

Figure A.34: GSSI ground penetrating radar results from Barnes

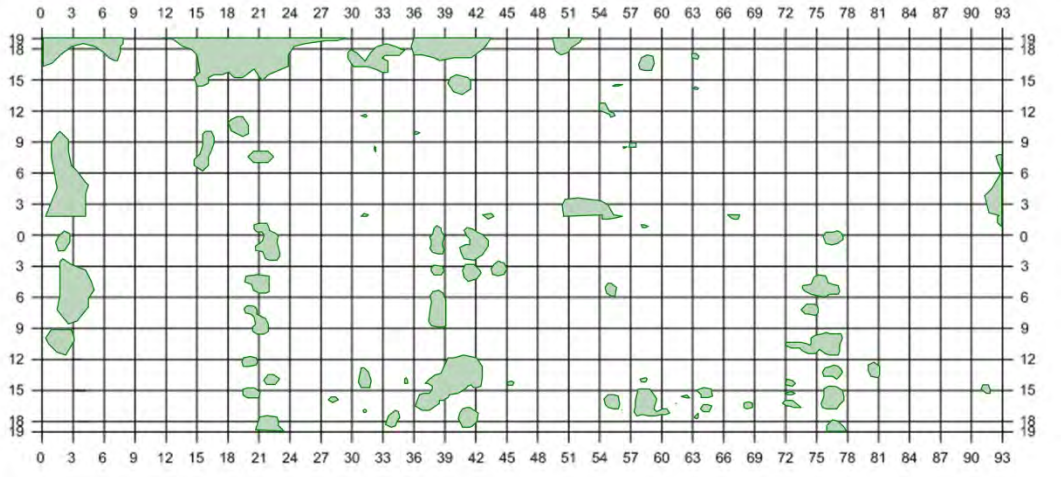

Figure A.35: GSSI ground penetrating radar-probable delaminations

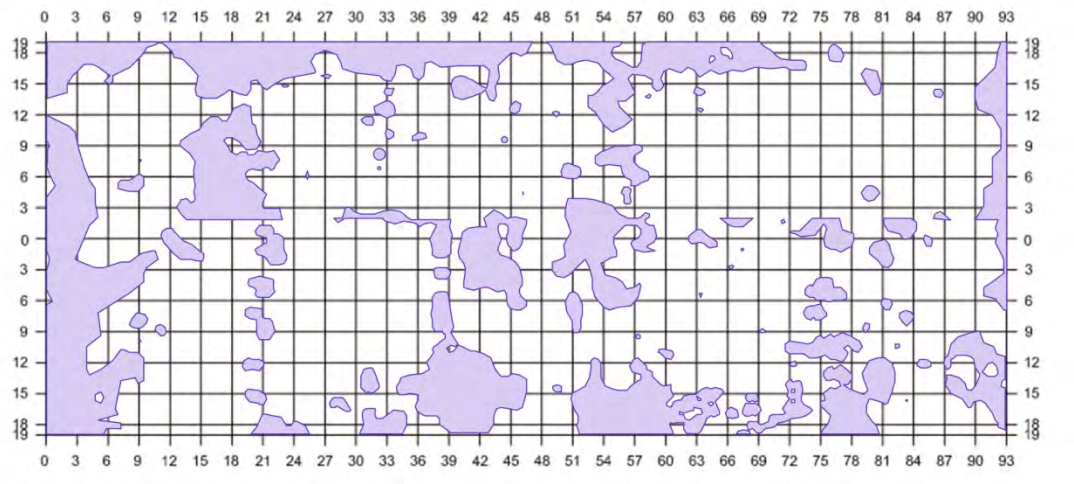

Figure A.36: GSSI ground penetrating radar-probable corrosion

The IDS Aladdin Data was not fully available due to issues with the new system. A comparison between the GSSI and Aladdin systems is available in reports 3106C submitted by Olson Engineering located in Appendix B.

A.4.5 Summary of Damage

Table A.19 summarizes the previous results by showing the calculated areas of damage as a percentage of total bridge deck area for each NDE test performed on the Remount Bridge with the overlay.

Table A.19: Percent of Remount Deck with overlay delaminated/deteriorated

NDE Method	Percent Delaminated/Deteriorated
Impact Echo	11%
Thermal Imaging	13%
Ground-Coupled GPR (without Corrosion Areas)	6.7%

A.5 Remount Bridge, near Buford, Wyoming, without Asphalt Overlay

Once the overlay was removed, the Remount Bridge was retested. Table A.20 provides the time requirements of each evaluation method and description of each method is provided in the following sections.

Table A.20: Time required for each NDE method performed on the Remount Bridge without overlay

Test	Time	Number of Workers	Time Performing Analysis
Chain Dragging	1 hour	2	2 hours
Impact Echo	2 hours	2	3 hours
Thermal Imaging	2.5 hours	2	15 hours
GPR-Ground-Coupled Roller	4 hours	2	4 hours
GPR-Aladdin System	3.5 hours	1	3 hours (1 side)

A.5.1 Chain Dragging and Half Cell Potential Tests

With no asphalt overlay, WYDOT performed a chain drag evaluation and found the following areas of damage as seen in Figure A.37. Half cell potentials were omitted again, as the epoxy coating gives extremely high readings which are not valuable.

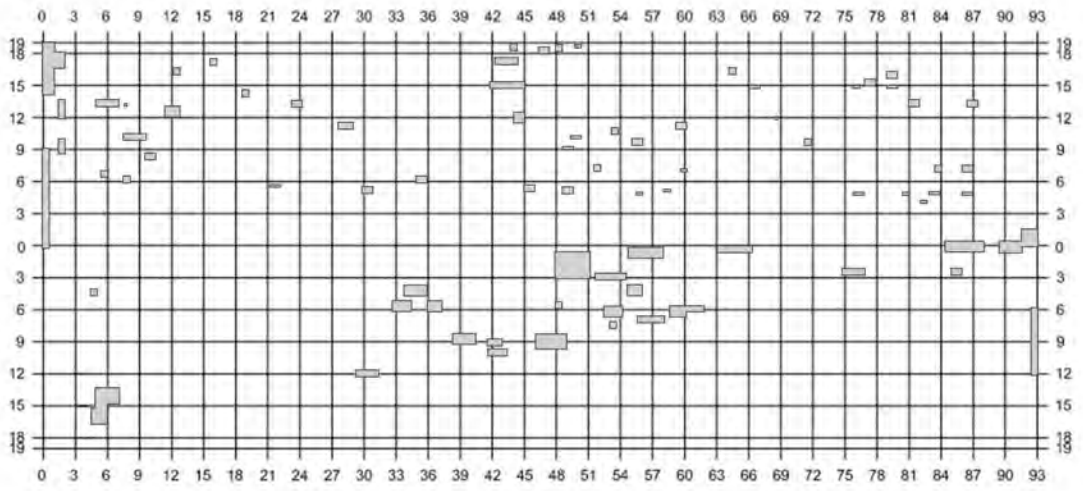

Figure A.37: Chain drag results outlining areas of delaminations

A.5.2 Impact Echo

Again, the same procedure was carried out to produce the damage maps from the impact echo evaluation as with the Remount Bridge with the overlay present (Figure A.38 and Figure A.39). Impact echo test results indicated that 6.2% of the bridge was delaminated or damaged.

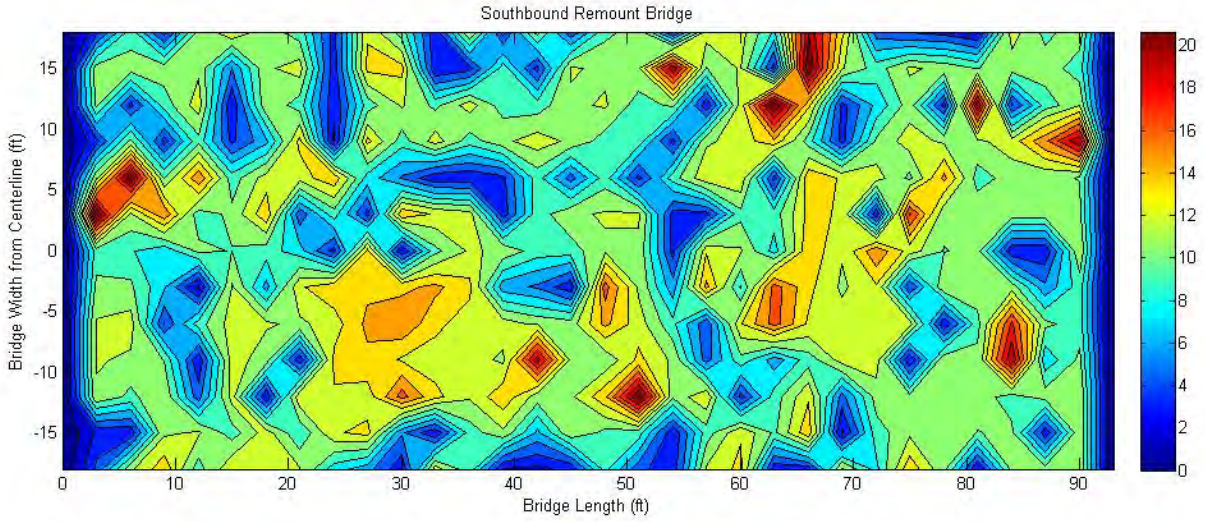

Figure A.38: Impact echo test contour map of damage

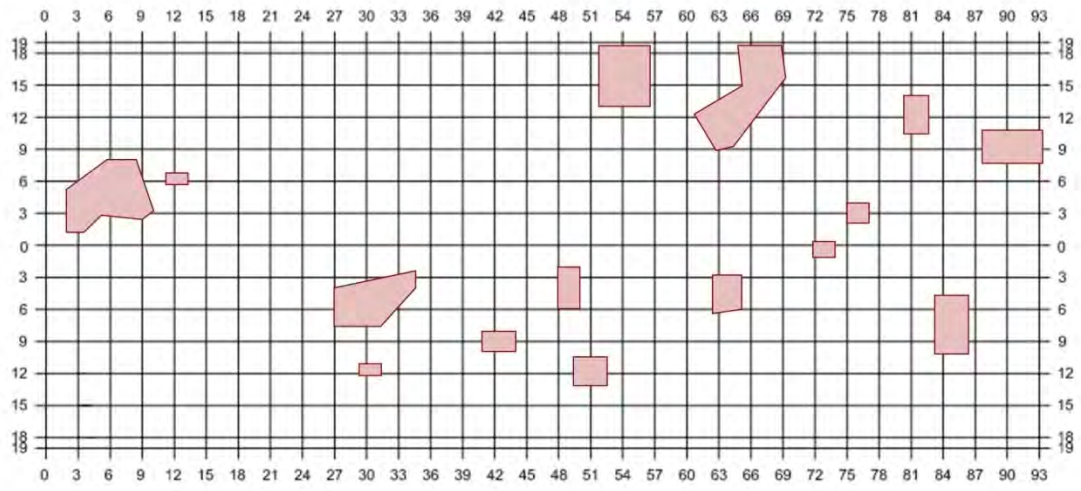

Figure A.39: Outlines of delamination/damage from impact echo test

A.5.3 Thermal Imaging

Again, the same procedure was carried out to produce the damage maps from the thermal imaging evaluation as with the Douglas Bridge with the overlay present (Figure A.40 and Figure A.41). Thermal imaging results found that 5.8% of the bridge was delaminated or damaged.

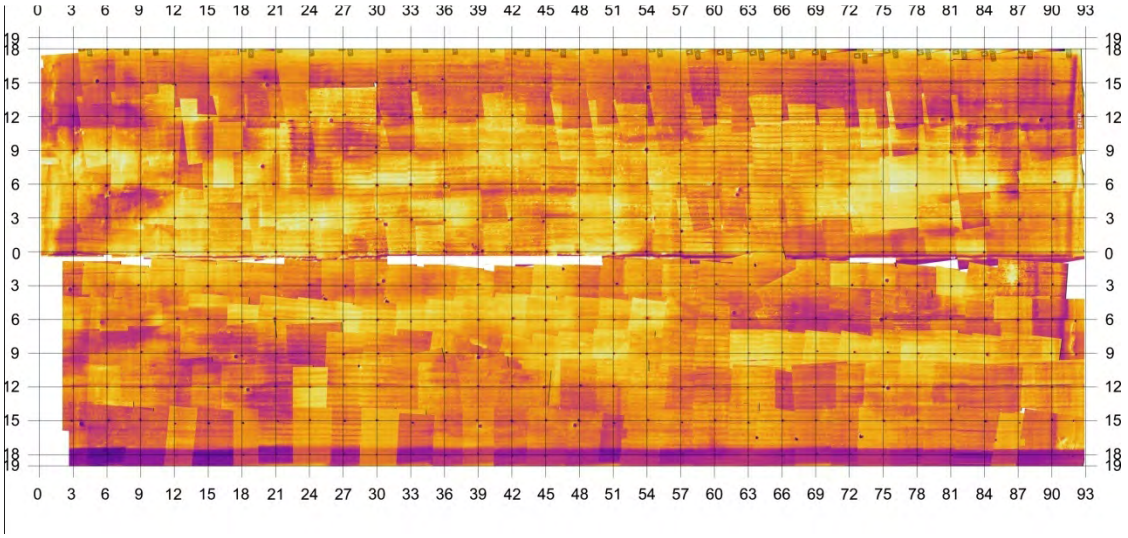

Figure A.40: Thermal images of the bridge deck

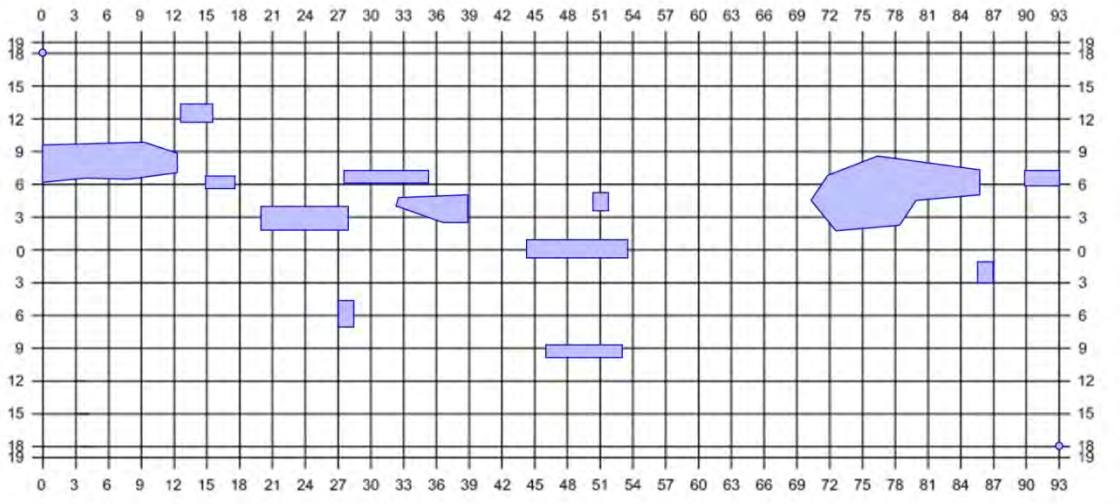

Figure A.41: Outlines of delamination/damage from thermal imaging test

A.5.4 Ground Penetrating Radar

Useful GPR results were not obtained on the milled concrete surface due to direct coupling interference from the reflections from the top surface of the bridge deck and the signal from the reinforcing bars. This distortion made the reinforcing steel appear more corroded than during the evaluation including the overlay (Olson Report 3016C in Appendix B).

A.5.5 Core Evaluations

Cores were taken from the Remount Bridge after the overlay was removed. This, however, removed most of the damaged areas, so the cores could not visually be correlated accurately. Compression and splitting tension were conducted on select cores following ASTM C 39 and ASTM C 496 respectively. Since all of the cores pulled from Remount were complete and did not show any damage, these tests were conducted to see if any correlations could be drawn. Figure A.42 shows where the cores were removed from the deck. Table A.21 and Table A.22 present the results of the core evaluations.

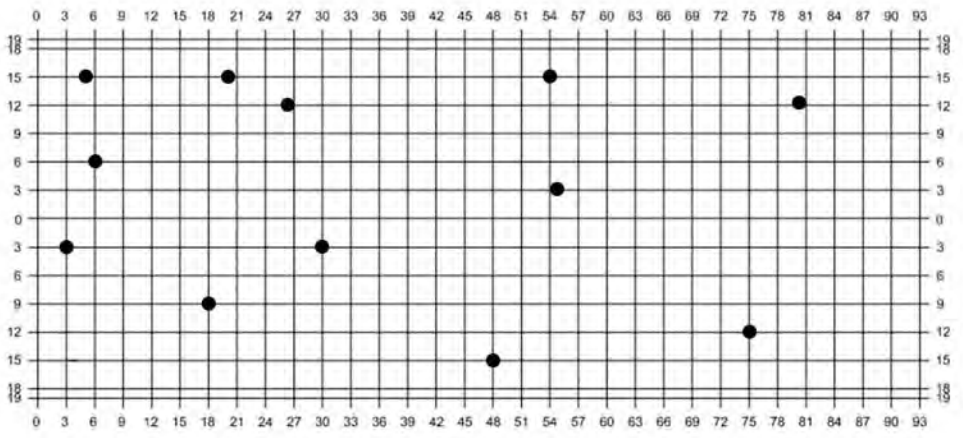

Figure A.42: Remount Bridge core locations

Table A.21: Compression results from Remount Bridge

Core	Location	f_c (psi)
1	N5-15	7380
2	N26-12	7240
3	N54-15	5820
4	S18-9	5730
5	S30-3	6020
6	S48-15	5040
Average		6210
Standard Deviation		± 14.8%

Table A.22: Splitting tension results from Remount Bridge

Core	Location	Splitting Tension Strength (psi)
7	N20-15	970
8	N55-3	790
9	N80-12	870
10	N6-6	940
11	S3-3	740
12	S75-12	800
Average		850
Standard Deviation		± 10.6%

Visual inspections and correlation to the methods were not available due to the asphalt and concrete milling. This lead to the removal of possible areas of delaminations and no conclusive information was revealed.

A.5.6 Summary of Damage Percentages

Table A.23 summarizes the previous results by showing the calculated areas of damage as a percentage of total bridge deck area for each NDE test performed on the Remount Bridge with the overlay.

Table A.23: Percent of Remount Deck with overlay delaminated/deteriorated

NDE Method	Percent Delaminated/Deteriorated
Chain Dragging	2.5%
Impact Echo	6.2%
Thermal Imaging	5.8%

Appendix B - Subcontractor Reports

NONDESTRUCTIVE TESTING AND EVALUATION INVESTIGATION GROUND PENETRATING RADAR FOR BRIDGE DECK OF 1ST STREET BRIDGE CASPER, WYOMING

Prepared for:
University of Wyoming
Department of Civil & Architectural Engineering
Dept 3295
1000 E. University Ave
Laramie, WY 82071

Attn: Professor Jennifer Tanner
Tel: 307.766.2073
Fax: 307.766.2221
Email: TannerJ@uwyo.edu

Olson Engineering Job No. 3016A

August 4, 2009

1.0 EXECUTIVE SUMMARY

Olson Engineering was contracted by the University of Wyoming to provide a nondestructive testing and evaluation (NDE&E) investigation of a concrete bridge deck of the 1st Street Bridge over the North Platte River located in Casper, WY. The Ground Penetrating Radar (GPR) test method was used in the investigation. The NDE investigation was performed by Mr. Matthew Hergert, Project Engineer, of Olson Engineering, Inc., in June 2009. Summaries of the data collection procedures and investigation findings are given below.

Field NDE&E Investigation

Ground Penetrating Radar (GPR) tests were conducted using a Geophysical Survey Systems, Inc., 1500 MHz ground coupled antenna and a 1 GHz air horn along the length of the deck. The tests were performed on the top of the deck. The objective of the GPR test was to locate possible areas of delamination within the bridge deck due to the corrosion of the top layer of the rebar mat. The bridge deck was scanned using a grid spacing of 1 foot along the N-S direction and 0.25 inch along the E-W direction (along each scan line).

The data from the 1 GHz air horn investigation was not useful for analysis by Dr. Barnes because all of the rebar signals appeared as one mass instead of individual points. The location of areas of corrosion in concrete using GPR and the analysis technique employed by Dr. Barnes requires that the rebar reflections be clear and discrete. Only general magnitude changes were evident in the 1 GHz air horn data. However, the testing performed with the 1500MHz ground coupled antenna was found to be very useful.

The results from the GPR investigation are presented in Section 5.0. The areal quantity of probable concrete delaminations was estimated to be 1,167.8 ft2, or 10.8 percent of the deck surface area. The areal quantity of probable active corrosion was estimated to be 1,798 ft2, or 16.7 percent of the deck surface area. Please note that the GPR investigation for delamination area is most accurate for bridge deck areas with no previous repairs. This is because the reflections of radar electromagnetic waves from all the rebar are used for grading purposes.

2.0 GROUND PENETRATING RADAR (GPR) METHOD

The GPR method involves moving an antenna across a test surface while periodically pulsing the antenna and recording the received echoes, as shown in Figure 1. Pulses are sent out from the GPR computer driving the antenna at a frequency range centered on the design center frequency of the antenna; in this case 1500 Megahertz (MHZ) equal to 1.5 Gigahertz (GHz), and 1000 Megahertz (MHZ) equal to 1.0 Gigahertz (GHz). These electromagnetic wave pulses propagate through the material directly under the antenna, with some energy reflecting back whenever the wave encounters a change in electrical impedance, such as at a rebar or other steel embedment or air-filled void. The antenna then receives these echoes, which are amplified and filtered in the GPR computer, and then digitized and stored. A distance wheel records scan distance across the test surface and embedded features can be located as a given distance from the scan start position. For repetitive scanning, a standard survey is designed and adhered to as field conditions allow to minimize mistakes and maximize data quality.

The scans for this investigation were created from pulses sent out at lateral intervals of approximately 30 pulses per foot (2.5 pulses per inch). The resulting raw data is in the form of echo amplitude versus time. By inputting the dielectric constant, which defines the material velocity, and by estimating the signal zero point, the echo time data can be converted to echo depth. The following equations explain this conversion:

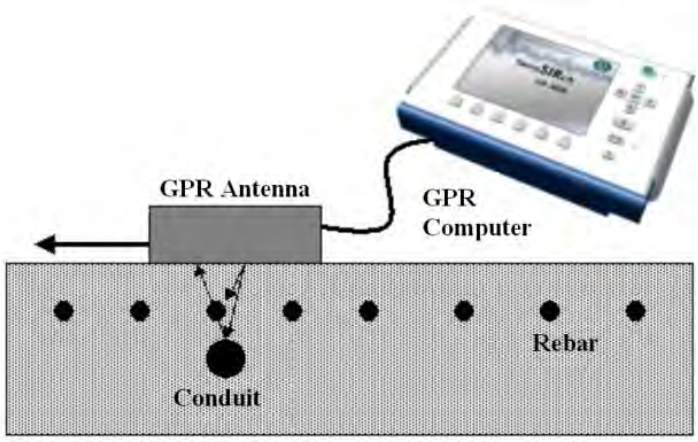

Figure 1: GPR Method Schematic

$V_{EM} = c / {}_r^{0.5}$ $D = (V_{EM} * T) / 2$

where V_{EM} is the material electromagnetic velocity, c is the speed of light (in air), $_r$ is the material relative dielectric constant, D is depth, and T is the two-way radar pulse travel time. If more accurate depth data is required, a depth calibration can be done if an embedment of a

known depth is available to scan over (or the backside reflection of the slab). The scans are then typically plotted as waterfall plots of all of the individual data traces collected, with the lightness or darkness (or color) of each point in the plot being set by the amplitude and polarity (positive or negative) of the data at a given depth in each trace. Further, if data are collected along evenly spaced gridlines, a 3-D interpolation can be performed to generate a cubic display of data. This data cube can then be sliced along certain planes (typically XY, XZ, and YZ) to enhance recognition and display of target features. Also, amplitude threshold constraints can be set to allow display of GPR reflections within the given threshold values. Regional features are often more easily recognized when viewing a slice of 3-D interpolated data.

Figure 2 - SIR-3000 GPR system with a 1500MHz ground coupled antenna mounted on a cart.

3.0 FIELD INVESTIGATION

The GPR tests were performed using a Geophysical Survey Systems, Inc., 1500 MHz ground coupled antenna as well as a 1 GHz (1000MHz) air horn antenna along the length of the concrete bridge deck. The tests were performed on the top of the deck (Figure 3) per drawings provided by the Wyoming Department of Transportation (WYDOT). Traffic control for the testing was also provided by WYDOT. The deck was scanned with the 1500 MHz antenna using a grid spacing of 1.5 feet along the N-S direction (width of the bridge) and 0.25 inch along the W-E direction (along a scan line). GPR data files were recorded in the eastbound direction, in one and a half foot transverse intervals from the centerline of the bridge to the south curb edge. The 1 GHz air horn antenna data was collected from 4.5 feet inside the centerline to 4.5 feet from the curb due to limitations based on the width of the truck the radar antenna was mounted on. The objective of the GPR tests was to determine areas of the bridge deck with potential corrosion or delamination (cracks) at the top layer of steel reinforcement.

Figure 3 - GPR testing with the 1500MHz ground-coupled antenna over the North Platte River in Casper, Wyoming.

4.0 EXAMPLE DATA

Data collected with the 1500 MHz antenna contained clear reflections from each individual rebar in the deck. The raw data shows evidence of some variance in signal attenuation within the concrete, which is normally due to corrosion and/or delaminations. The areas undergoing corrosion show up as weaker signals compared to areas in good condition (Figure 4). The data from the 1500 MHz antenna was of good quality as shown in the figures below.

Data from the 1 GHz air horn was accurate for depth but lacked the resolution (due to the wavelength of the signal) to pick out individual rebar. Figures 5 and 6 show data collected over the same location with the 1500 MHz antenna and the 1 GHz air horn. Both plots show the depth and amplitude of the signal, but only the 1500 MHz data allows precise locating of the reinforcement.

1500 MHz Ground Coupled Antenna

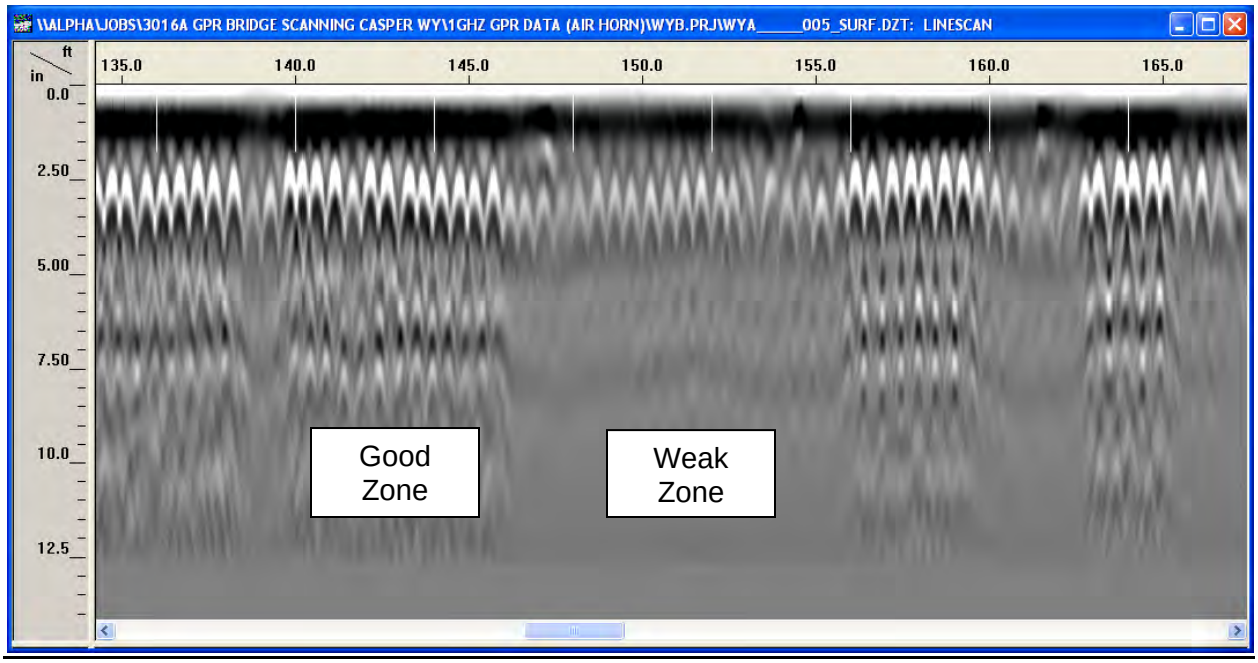

Figure 4 - GPR Scan 6 feet offset from the Bridge centerline. Note the variance of the signal strength as the radar passed areas of suspected corrosion.

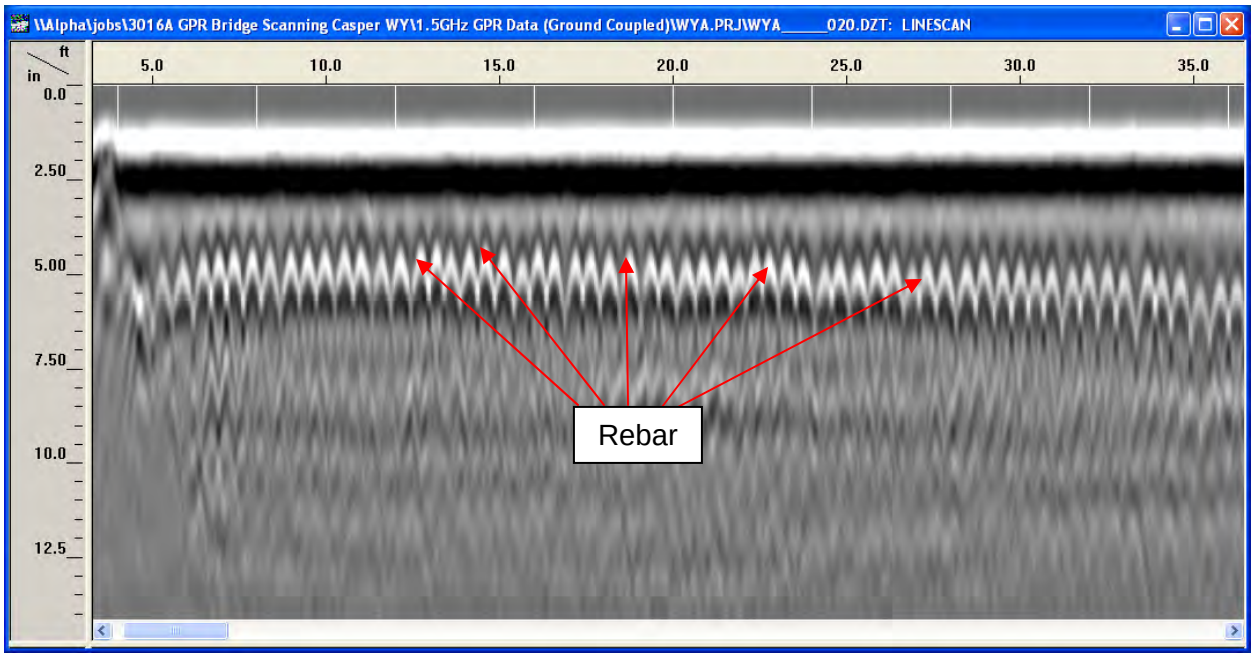

Figure 5 – 1500MHz ground coupled antenna GPR Scan 4.5 feet offset from South curb. The West joint is located at the far left of the plot.

1000MHz Air Horn Antenna

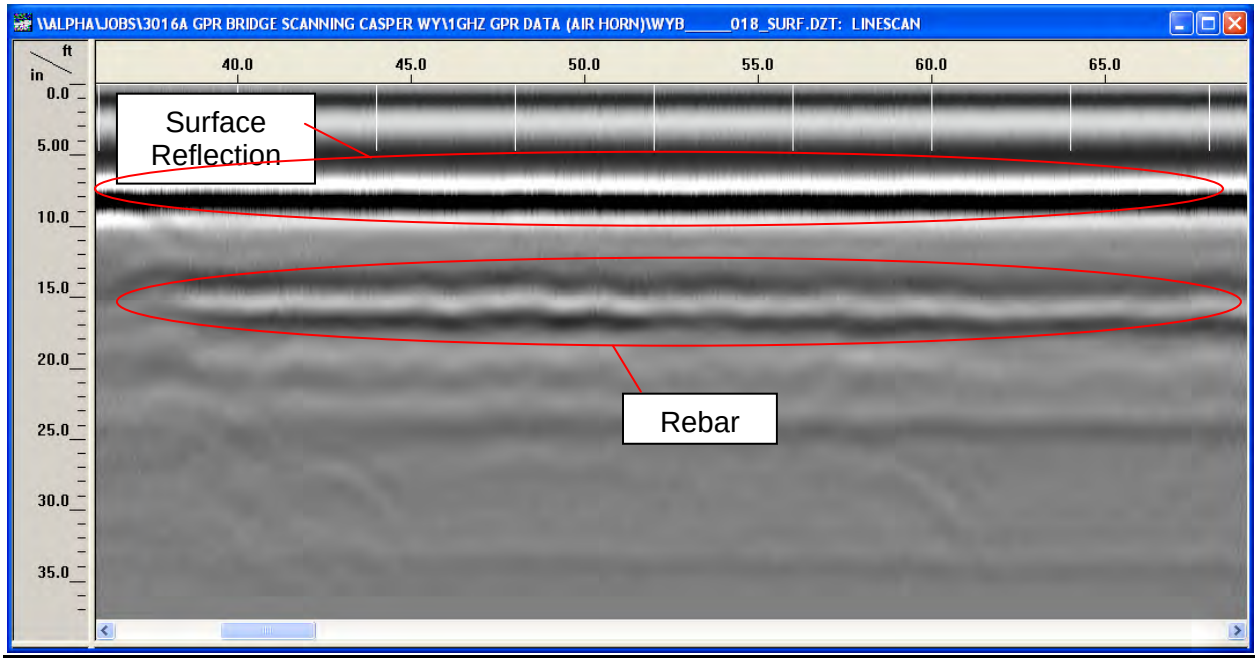

Figure 6 – 1GHz air horn antenna GPR Scan 4.5 feet offset from South curb. The West joint is located at the far left of the plot.

5.0 TEST RESULTS

The GPR data from the asphalt overlaid deck top was processed using RADAN 6.5 to measure the reflection amplitudes (dB) in each GPR data file of the individual transverse reinforcing bars within the top reinforcement mat. Signal losses in the reinforcing bar reflection amplitudes vary according to the bar size and the relative abundance of moisture and chloride in the concrete cover and concrete above the top reinforcing bar mat and have been correlated in previous studies with the location and extent of corrosion and corrosion-induced damage of the surface cover layer.

The data collected by the 1GHz air horn was accurate but lacked the resolution to pick out any individual rebar locations. In the example data, it is clearly evident that the 1GHz air horn did not resolve the individual rebar signals during this application. The analysis technique used for this project was based upon discrete rebar reflections. Therefore the air horn data was not useful in the analysis performed by Dr. Barnes since it does not have such resolution. However, a 2GHz antenna may be used to resolve these signals better. This data can then be displayed using a different processing technique and algorithms (Romero, et al. (2009). "Interstate-80 Corridor GPR Bridge Assessments: Deterioration Mapping of Asphalt and Polymer Concrete-Overlaid, Reinforced Concrete Decks – Elk County, Nevada" *Proc., TRB 88th Annual Meeting Compendium of Papers,* TRB 2009, Washington, D.C.).

The reflection amplitude data was corrected for geometric losses due to reinforcing bar depth using a statistical regression approach fit to the 90th percentile amplitude (dB) versus the two-way travel time of the GPR signal. Predictions of the location and quantities of probable delamination and probable active corrosion were evaluated using proprietary thresholds calibrated for use on exposed-surface reinforced concrete bridge decks developed in research by Mr. Christopher Barnes at Dalhousie University, Halifax, Nova Scotia, Canada, who served as our sub-consultant. This approach assumes that the 90th percentile strongest reflection amplitudes correspond to undamaged regions of the deck containing low quantities of moisture and chlorides. Areas with significantly more attenuated data below the thresholds correspond to upper reinforcement mat corrosion and/or corrosion induced-cracking of the concrete cover layer. Please note that the GPR investigation for delamination survey is most accurate for bridge deck areas with no previous repairs as discussed earlier in Section 1.

The GPR results plot is presented in Fig. 7 below. This plot shows the deck surface in plan view and indicates probable delaminations in red and probable active corrosion areas in red and yellow. The areal quantity of probable delaminations was estimated to be 1,623 ft^2, or 15.4 percent of the deck surface area. The areal quantity of probable active corrosion was estimated to be 2,100 ft^2, or 19.9 percent of the deck surface area. Depth-corrected GPR amplitudes that were outside the damage thresholds are shown in grayscale to indicate the predicted relative variation in moisture and chloride over the undamaged deck surface. Darker regions may indicate areas where moisture and chloride ingress is approaching levels sufficient to initiate corrosion.

Bridge Over North Platte River
Casper, Wyoming

Ground Penetrating Radar Evaluation

Probable Delamination Area = 1167.8 ft^2 = 10.8 % of Deck Area
Probable Active Corrosion Area = 1798.0 ft^2 = 16.7 % of Deck Area

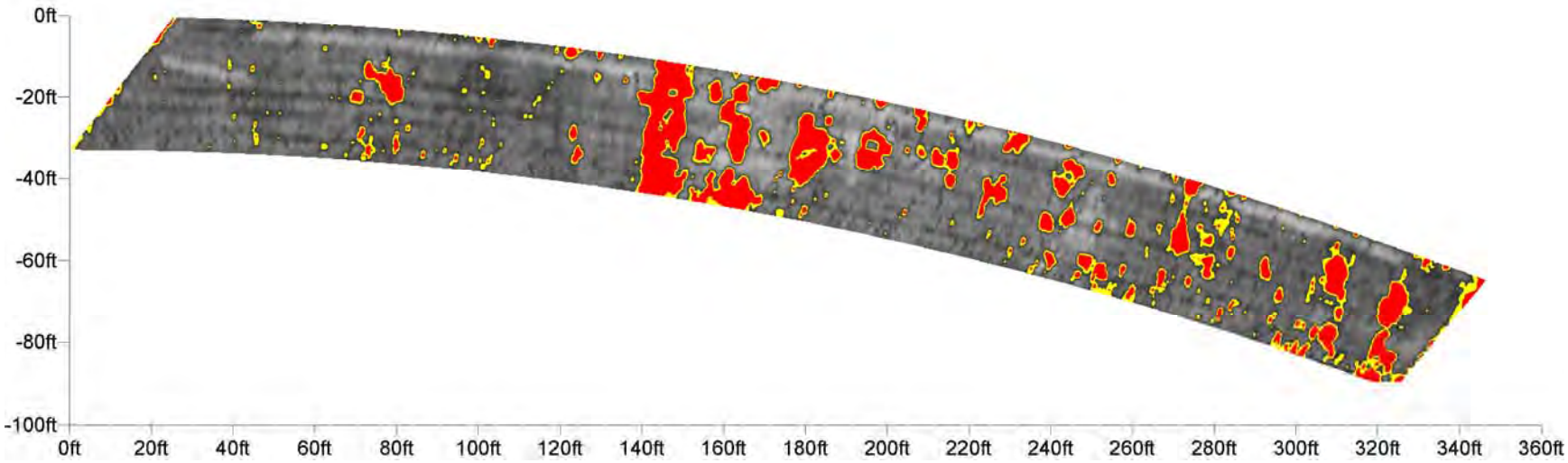

Fig. 7 – GPR Results Plot

6.0 CLOSURE

The field portion of this NDE&E investigation was performed in accordance with generally accepted testing procedures. If additional information is developed that is pertinent to the findings of this investigation or we can provide any additional information or consultation on locations for corehole drilling and potential repairs, please contact our office.

Respectfully submitted,

OLSON ENGINEERING, INC.

_____

Matthew P. Hergert
Project Engineer

_____

Larry D. Olson, P.E.
Principal Engineer

(1 copy e-mailed and 2 copies sent)

NONDESTRUCTIVE TESTING AND EVALUATION INVESTIGATION
GROUND PENETRATING RADAR FOR
BRIDGE DECK ON INTERSTATE 25
DOUGLAS, WYOMING

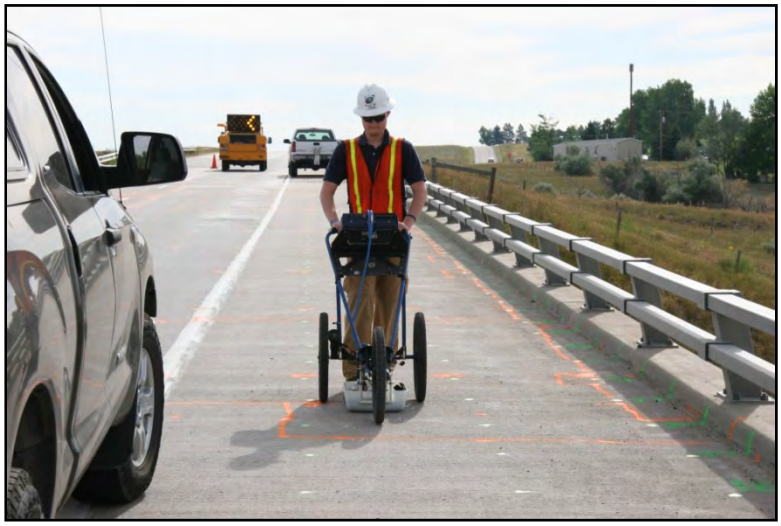

Prepared for:
University of Wyoming
Department of Civil & Architectural Engineering
Dept 3295
1000 E. University Ave
Laramie, WY 82071

Attn: Professor Jennifer Tanner
Tel: 307.766.2073
Fax: 307.766.2221
Email: TannerJ@uwyo.edu

Olson Engineering Job No. 3016B

November 13, 2009

1.0 EXECUTIVE SUMMARY

Olson Engineering was contracted by the University of Wyoming, to provide a nondestructive testing and evaluation (NDE&E) investigation of a concrete bridge deck of the eastbound side of a bridge on I-25 in Douglas, Wyoming. The Ground Penetrating Radar (GPR) test method was used in the investigation. The NDE investigation was performed by Mr. Matthew Hergert, Project Engineer, of Olson Engineering, Inc., on August 6, 2009. Summaries of the data collection procedures and investigation findings are given below.

Field NDE&E Investigation

Ground Penetrating Radar (GPR) tests were conducted using a Geophysical Survey Systems, Inc., 1500 MHz ground coupled antenna and a 2.0 GHz air horn along the length of the deck. The tests were performed from the top side of the deck. The objective of the GPR testing was to locate possible areas of delamination within the bridge deck due to corrosion of the top layer of the rebar mat. The test was scanned using a grid spacing of 1.5 feet along the N-S direction and 0.25 inch along the E-W direction (along each scan line).

The data from the 2GHz air horn investigation was not useful for analysis by Dr. Barnes, which is based upon the resolution of individual bars. Several of the scan lines contained signals that were irresolvable into individual rebar signatures. Only general magnitude changes were evident in this data. However, the testing performed with the 1500MHz ground coupled antenna was found to be very useful. This data was post-processed to allow grading of the bridge deck by area into categories of likely sound, probable delamination, and probable rebar corrosion.

The results from the GPR investigation are presented in Section 5.0. The quantity of probable delaminations was estimated to be 793.6 ft2, or 11.3 percent of the deck surface area. The quantity of probable active corrosion was estimated to be 2,394.7 ft2, or 34.2 percent of the deck surface area. Please note that the GPR investigation for delamination survey is most accurate for bridge deck areas with no previous repairs. This is because the reflections of radar electromagnetic waves from all the rebar are used for grading purposes.

2.0 GROUND PENETRATING RADAR (GPR) METHOD

The GPR method involves moving an antenna across a test surface while periodically pulsing the antenna and recording the received echoes, as shown in Figure 1. Pulses are sent out from the GPR computer driving the antenna at a frequency range centered on the design center frequency of the antenna; in this case 1500 Megahertz (MHZ) equal to 1.5 Gigahertz (GHz) and 2000 Megahertz (MHZ) equal to 2.0 Gigahertz (GHz). These electromagnetic wave pulses propagate through the material directly under the antenna, with some energy reflecting back whenever the wave encounters a change in electrical impedance, such as at a rebar or other steel embedment or air-filled void. The antenna then receives these echoes, which are amplified and filtered in the GPR computer, and then digitized and stored. A distance wheel records scan distance across the test surface and embedded features can be located as a given distance from the scan start position. For repetitive scanning, a standard survey is designed and adhered to as field conditions allow to minimize mistakes and maximize data quality.

The scans for this investigation were created from pulses sent out at lateral intervals of approximately 48 pulses per foot (4 pulses per inch). The resulting raw data is in the form of echo amplitude versus time. By inputting the dielectric constant, which defines the material velocity, and by estimating the signal zero point, the echo time data can be converted to echo depth. The following equations explain this conversion:

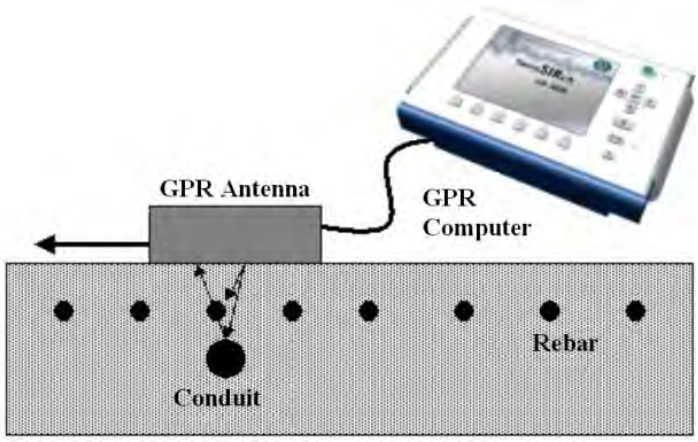

Figure 1: GPR Method Schematic

$V_{EM} = c / {}_r^{0.5}$ $D = (V_{EM} * T) / 2$

where V_{EM} is the material electromagnetic velocity, c is the speed of light (in air), $_r$ is the material relative dielectric constant, D is depth, and T is the two-way radar pulse travel time. If more accurate depth data is required, a depth calibration can be done if an embedment of a

known depth is available to scan over (or the backside reflection of the slab). The scans are then typically plotted as waterfall plots of all of the individual data traces collected, with the lightness or darkness (or color) of each point in the plot being set by the amplitude and polarity (positive or negative) of the data at a given depth in each trace. Further, if data are collected along evenly spaced gridlines, a 3-D interpolation can be performed to generate a cubic display of data. This data cube can then be sliced along certain planes (typically XY, XZ, and YZ) to enhance recognition and display of target features. Also, amplitude threshold constraints can be set to allow display of GPR reflections within the given threshold values. Regional features are often more easily recognized when viewing a slice of 3-D interpolated data.

Figure 2 - SIR-3000 GPR system with a 1500MHz ground coupled antenna mounted on a cart.

3.0 FIELD INVESTIGATION

The GPR tests were performed using a Geophysical Survey Systems, Inc., 1500 MHz ground coupled antenna as well as a 2 GHz (2000 MHz) air horn antenna along the length of the concrete bridge deck. The tests were performed on the top of the deck (Figure 3) per drawings provided by the Wyoming Department of Transportation (WYDOT). Traffic control for the testing was also provided by WYDOT. The test area was scanned using a grid spacing of 1.5 feet along the N-S direction (width of the bridge) and 0.25 inch along the W-E direction (along each scan line). GPR data files were recorded in the westbound direction (in the eastbound lanes), in one and a half foot transverse intervals from the south curb edge of the bridge to the north curb edge. The 2 GHz air horn antenna collected from 4.5 feet inside the centerline to 4.5 feet from the curb due to the width of the truck the radar was mounted on. The objective of the GPR tests is to determine areas of the bridge deck with potential corrosion or delamination (cracks) at the top layer of steel reinforcement.

Figure 3 - GPR testing with the 2GHz air horn antenna on I-25 in Douglas Wyoming.

4.0 EXAMPLE DATA

Data collected with the 1500 MHz antenna contained clear reflections from each individual rebar in the deck. The raw data even shows evidence of some variance in signal attenuation within the concrete. The areas undergoing corrosion typically show up as weaker signals than areas in good condition (Figure 4). The data from the 1500 MHz antenna was of good quality as shown in the figures below.

Data from the 2GHz air horn was accurate but, in several scans, lacked the resolution to pick out individual rebar. Figures 5 and 6 show data collected with the 1500 MHz antenna and the 2 GHz air horn. Both plots show the depth and amplitude of the signal, but only the 1500 MHz data allows precise locating of the reinforcement.

1500MHz Ground Coupled Antenna

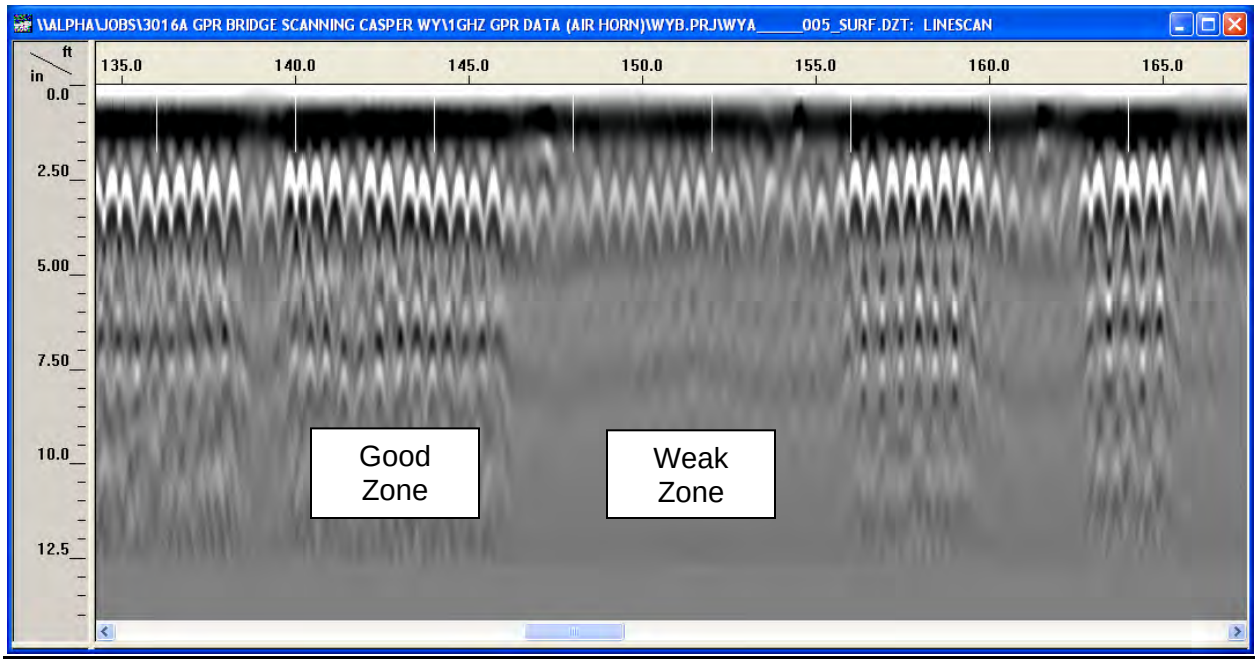

Figure 4 - GPR Scan 6 feet offset from the Bridge centerline. Note the variance of the signal strength as the radar passed areas of suspected corrosion.

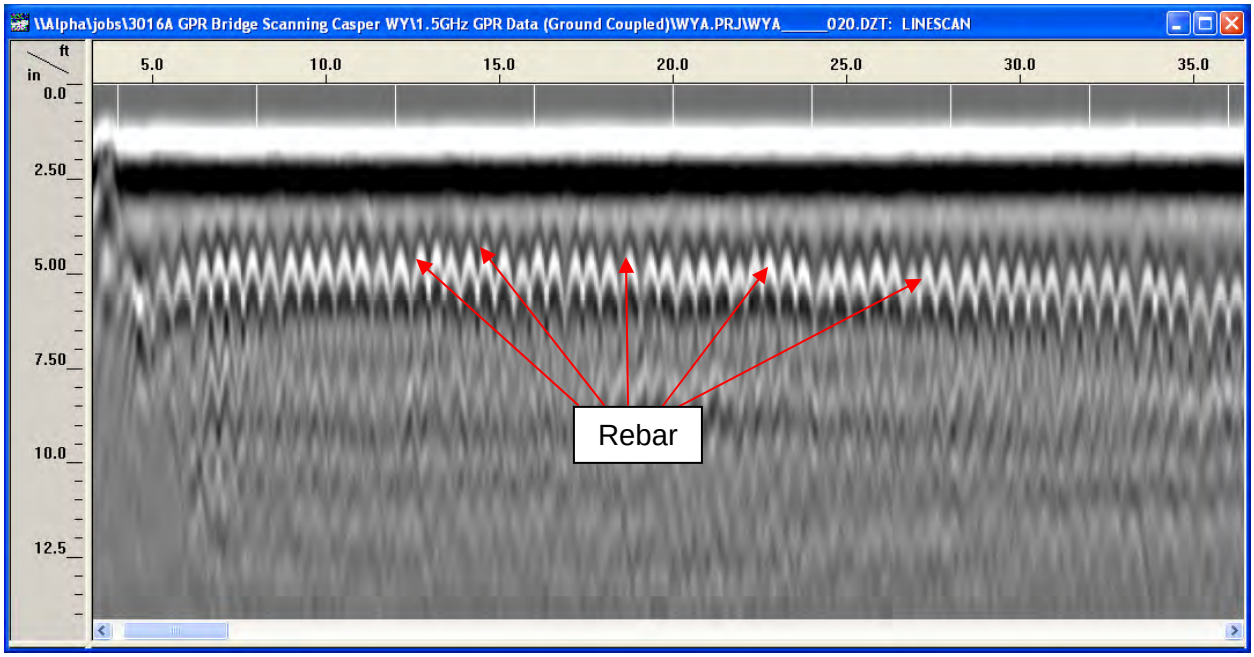

Figure 5 – 1500MHz ground coupled antenna GPR Scan 4.5 feet offset from South curb. The West joint is located at the far left of the plot.

2000MHz Air Horn Antenna

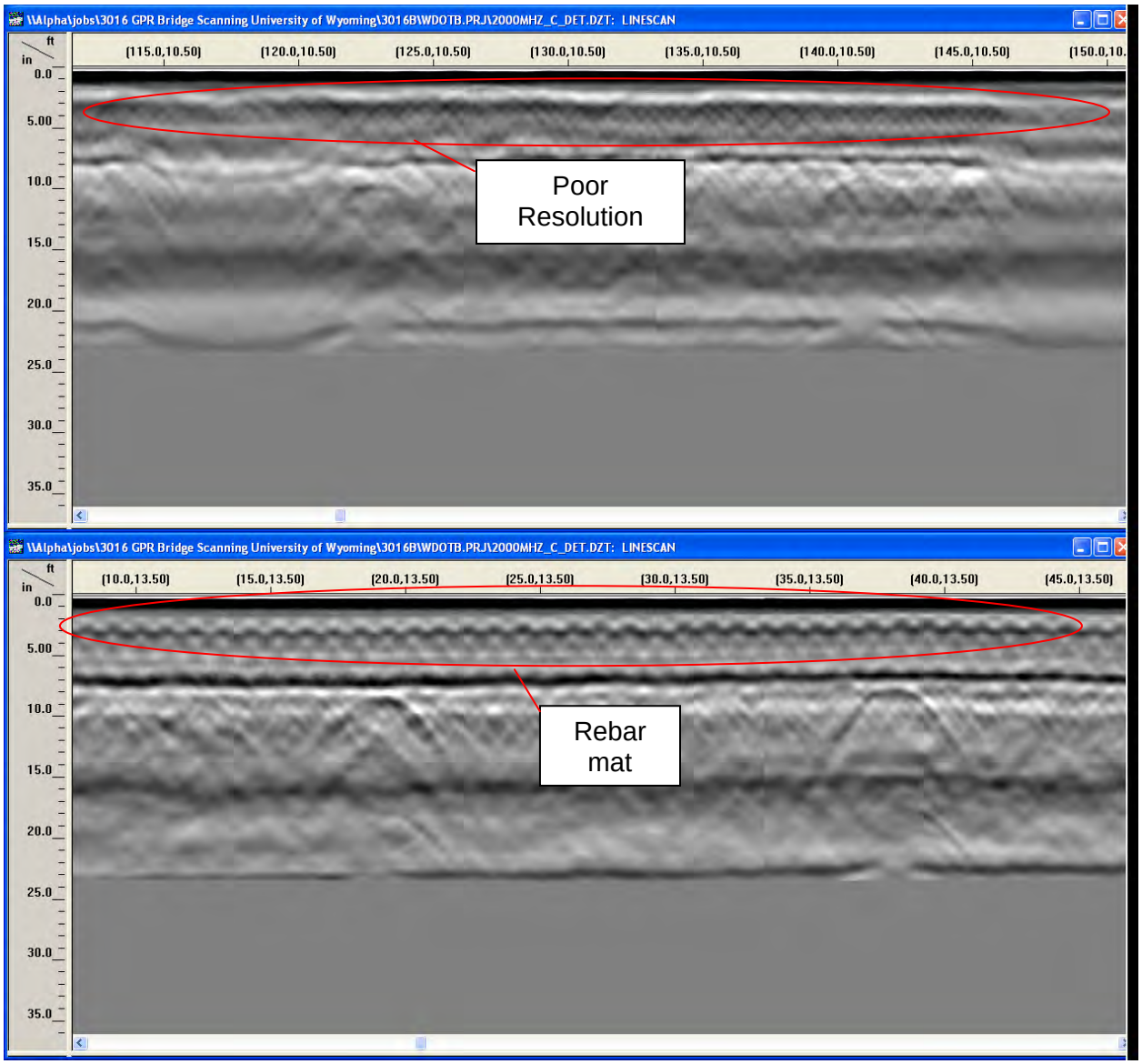

Figure 6 – 2GHz air horn antenna GPR Scans at 10.5 and 13.5 feet offset from South curb. Note that the first scan does not contain any resolvable rebar signals.

5.0 TEST RESULTS

The GPR data from the concrete deck top was processed using RADAN 6.5 to measure the reflection amplitudes (dB), in each GPR data file, of the individual transverse reinforcing bars within the top reinforcement mat. Signal losses in the reinforcing bar reflection amplitudes vary according to the bar size and the relative abundance of moisture and chloride in the concrete cover and concrete above the top reinforcing bar mat and have been correlated in previous studies with the location and extent of corrosion and corrosion-induced damage of the surface cover layer.

The data collected by the 2GHz air horn was accurate but, in several scans, lacked the resolution to pick out individual rebar locations. In the example data, it is clearly evident that the ground coupled 1500MHz antenna resolves the individual rebar signals much better than the 2GHz air horn. The analysis technique used for this project was based upon discrete rebar reflections. Therefore the air horn data was not useful in the analysis performed by Dr. Barnes since it does not have the resolution necessary for the analysis to be properly carried out. However, this data can be displayed using a different processing technique and algorithms (Romero, et al. (2009). "Interstate-80 Corridor GPR Bridge Assessments: Deterioration Mapping of Asphalt and Polymer Concrete-Overlaid, Reinforced Concrete Decks – Elk County, Nevada" *Proc., TRB 88th Annual Meeting Compendium of Papers,* TRB 2009, Washington, D.C.).

The reflection amplitude data was corrected for geometric losses due to reinforcing bar depth using a statistical regression approach fit to the 90^{th} percentile amplitude (dB) versus the two-way travel time of the GPR signal. Predictions of the location and quantities of probable delamination and probable active corrosion were evaluated using proprietary thresholds calibrated for use on exposed-surface reinforced concrete bridge decks developed in research by Mr. Christopher Barnes at Dalhousie University, Halifax, Nova Scotia, Canada who served as our sub-consultant. This approach assumes that the 90^{th} percentile strongest reflection amplitudes correspond to undamaged regions of the deck containing low quantities of moisture and chlorides. Areas with significantly more attenuated data below the thresholds correspond to upper reinforcement mat corrosion and/or corrosion induced-cracking of the concrete cover layer. Please note that the GPR investigation for delamination survey is most accurate for bridge deck areas with no previous repairs as discussed earlier in Section 1.

The GPR results plot, which shows the deck surface in plan view, indicates probable delaminations in red and probable active corrosion areas in red and yellow. The quantity of probable delaminations was estimated to be 793.6 ft^2, or 11.3 percent of the deck surface area. The quantity of probable active corrosion was estimated to be 2,394.7 ft^2, or 34.2 percent of the deck surface area. Depth-corrected GPR amplitudes that were outside the damage thresholds are shown in grayscale to indicate the predicted relative variation in moisture and chloride over the undamaged deck surface. Darker regions may indicate areas where moisture and chloride ingress is approaching levels sufficient to initiate corrosion.

Structure No. AFY
Wyoming Department of Transportation

Ground Penetrating Radar Evaluation

Probable Delamination Area = 793.6 ft^2 = 11.3 % of Deck Area
Probable Active Corrosion Area = 2394.7 ft^2 = 34.2 % of Deck Area

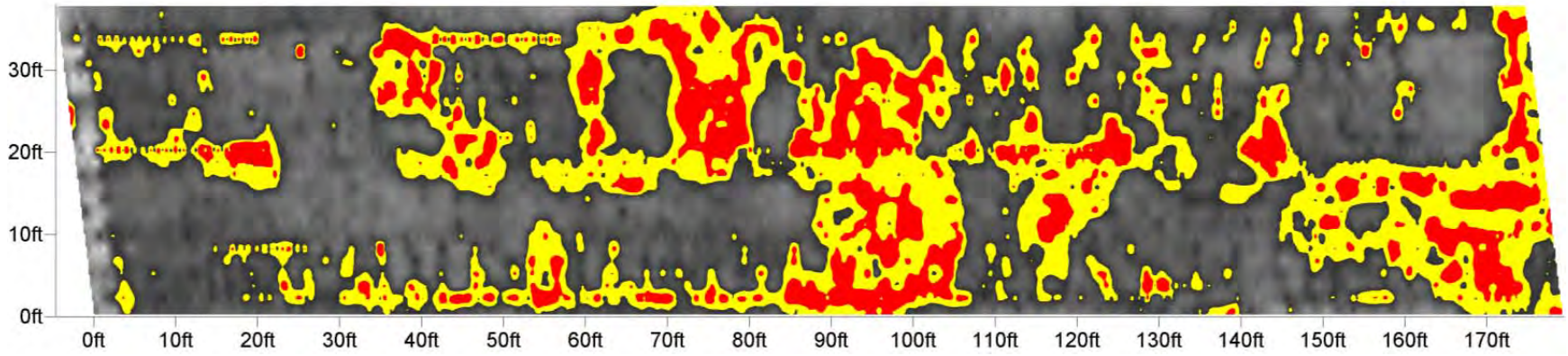

6.0 CLOSURE

The field portion of this NDE&E investigation was performed in accordance with generally accepted testing procedures. If additional information is developed that is pertinent to the findings of this investigation or we can provide any additional information or consultation on locations for corehole drilling and potential repairs, please contact our office.

Respectfully submitted,
OLSON ENGINEERING, INC.

_____

Matthew P. Hergert
Project Engineer

_____

Dennis A. Sack, P.E.
Associate Engineer

(1 copy e-mailed and 2 copies sent)

Ground Penetrating Radar (GPR)
Bridge Deck Evaluation

Overhead Crossing C. & N.W. Railroad
Station 1249 + 37.60
Douglas-Marginal
Wyo. Proj. No. I-25-3(23)144
Converse County

Inspection Report

Prepared for:

University of Wyoming
Dept of Civil and Architectural Engineering
1000 E. University Ave
Laramie, WY 82071

Prepared by:

Resource International, Inc.
6350 Presidential Gateway
Columbus, Ohio 43231

Rii # W-10-086
August 26, 2010

1. BRIDGE IDENTIFICATION AND LOCATION

Wyo. Proj. No.:	I-25-3(23) 144
Feature intersected:	Irvine Rd and C. & N.W. railroad
Surface type:	Concrete
Length:	179 feet
Width:	40 feet
Deck area:	7,160 square feet
Number of lanes:	2

2. GPR RESULT SUMMARY

Date of inspection:	06/06/2010
Weather conditions:	Dry, Sunny, 79^{0}F

Bridge deck:

Average concrete cover over the top reinforcing steel*:	3 inches
Transverse rebar spacing:	12 inches
Percentage of deteriorated concrete:	16.7%

*Including overlay.

3. GENERAL DESCRIPTION

Interstate 25 (I-25) is the main north–south expressway through Wyoming, Colorado, and New Mexico. It stretches from Interstate 10 at Las Cruces, New Mexico, to Interstate 90 in Buffalo, Wyoming. In the state of Wyoming, I-25 is a north-south state highway through Cheyenne and Casper. Through University of Wyoming, Wyoming Department of Transportation (WYDOT) elected to evaluate the conditions of a bridge deck using Ground Penetrating Radar (GPR). The bridge deck is signed as part of the I-25 Highway in the city of Douglas in Converse County. The purpose of the survey was to locate and map deterioration in the concrete deck through the overlay wearing surface on the bridge.

Photograph 1. Bridge on I-25 in Douglas, Converse County,

This report describes the bridge. It includes a scaled plan view of the deck showing the location and size of the delaminations. It also provides the total percent deterioration of the deck area.

4. GPR TESTING OF THE BRIDGE DECK

Ground Penetrating Radar (GPR) is extensively used today to assess the conditions of bridge decks, in search of concrete deterioration, moisture or even debonding of the deck overlay when applicable. It is preferred to other traditional techniques such as deck coring, chain dragging or hammer sounding that require lane closure, a task that most DOTs would like to avoid, especially in heavy traffic road. Consultants use van-mounted antennas moving at a speed such that a lane closure is not necessary. Depending on the number of antennas used and the output resolution desired, the speed varies from 25 miles per hour to 50 miles per hour. The speed can be augmented but at a risk of decreasing the data output resolution.

GPR was used to collect data related to the condition of the bridge deck. The work has been performed day time during regular working hours. The bridge was surveyed on August 6, 2010 for a total time at site of approximately 2 hours. GPR equipment used in this project and the procedure to collect deck condition data is described in Appendix A. The driving lanes of the bridge deck were scanned by the GPR at intervals of 2-inch longitudinally and 1.5-foot transversely for the entire length and width of the deck between the curbs. The GPR data was collected at a travel speed of 30 miles per hour. The work has been completed in accordance with all applicable segments of ASTM

The following setting was used during data collection for both 1000 MHz antennas:

- Samples per scan: 512
- Resolution: 16 bits
- Scans per second: 305
- Scans per foot: 6
- Transmit rate: 500 KHz

The depth of viewing window is approximately 2 feet for the 1000 MHz antenna, assuming a dielectric constant of 6.5. A vertical high pass filter of 250 MHz and a vertical low pass filter of 3170 MHz were applied to the data to decrease inappropriate interferences.

A single-polarization methodology utilizing two air-launched horn antennas (1000 MHz), mounted on booms so that the antennas scan on two different paths, were used to collect the data (see photograph 2 for the single-polarization setting). It is probably the most common method of GPR bridge deck evaluation. It has been around the longest and provides good, overall results. The antennas were deployed at an orientation where they were sensitive to the reinforcing steel placed in the transverse directions within the deck. The single-polarization method using two antennas has the advantage of covering more deck surface in a single day. For instance, the bridge was surveyed in less than 2 hours. The method provides fairly accurate deterioration quantity assessments that can be used to help decide identify locations that can best confirm that corrosion is taking place in predicted areas.

Traffic control during GPR data collection consisted of a truck with an arrow-board behind the testing vehicle, provided by WYDOT.

Photograph 2. GPR vehicle used during data collection

5. ANALYSIS OF GPR DATA

GPR data collected from the field was used to evaluate the condition of the bridge deck. The software developed by the manufacturer of the GPR equipment *Geophysical Survey Systems Incorporated* (GSSI), called RADAN (Radar Data Analyzer for Windows NT), was used to process the field data according to the procedure developed by GSSI

and in compliance with ASTM D 6087-08 specifications. Several processing functions such as data horizontal and vertical filtering, surface normalization, distance normalization, velocity correction, migration and background remo have been applied to the raw data to produce high quality data. The results of this analysis were used to determine the bridge deck deterioration conditions.

The most serious cause of accelerated deterioration of the integrity of a reinforced concrete bridge deck is corrosion of the reinforcing steel. GPR is a tool that can identify quantities and locations of impending or advanced corrosion conditions that will cause reinforcement to corrode, concrete integrity and chemistry to change, and damage (such as cracking, delamination or spalling) to concrete. One GPR analysis method is to measure the dielectric values of the concrete. If at some locations the concrete has high chloride content or high moisture as a result of corrosion and concrete breakdown, it will produce anomalously high dielectric values at these locations. Another method that is used to assess the quality of the concrete is to measure the amplitude of the reflection from the top mat rebar of the deck. A low amplitude reflected signal is interpreted to mean poor quality concrete. Conversely, relatively low signal loss is considered to mean the concrete quality is good. A third method calculates deterioration based on the reflection from the bottom of the deck relative to the surface of the deck. If the radar signal has been strongly attenuated as a result of moisture and chloride within the concrete deck, the amplitude of the reflected signal will be greatly reduced.

6. RESULTS OF BRIDGE DECK EVALUATION

Figure 1 shows a raw data of a GPR scan and a radar return waveform collected from the outside lane of the bridge. According to the bridge plans, reinforcement is not uniform throughout the deck. A higher signal reflection is shown in locations with more reinforcement (see for instance Figure 1 below). In this case, the GPR methods that measure the amplitude of the reflection from the top mat rebar or the bottom of the deck are not effective in assessing the quality of the concrete. However the measurement of the concrete dielectric values throughout the deck is the method that gives more accurate results in such situations. Delamination problems are anticipated when the reflection from the top of the deck increases significantly.

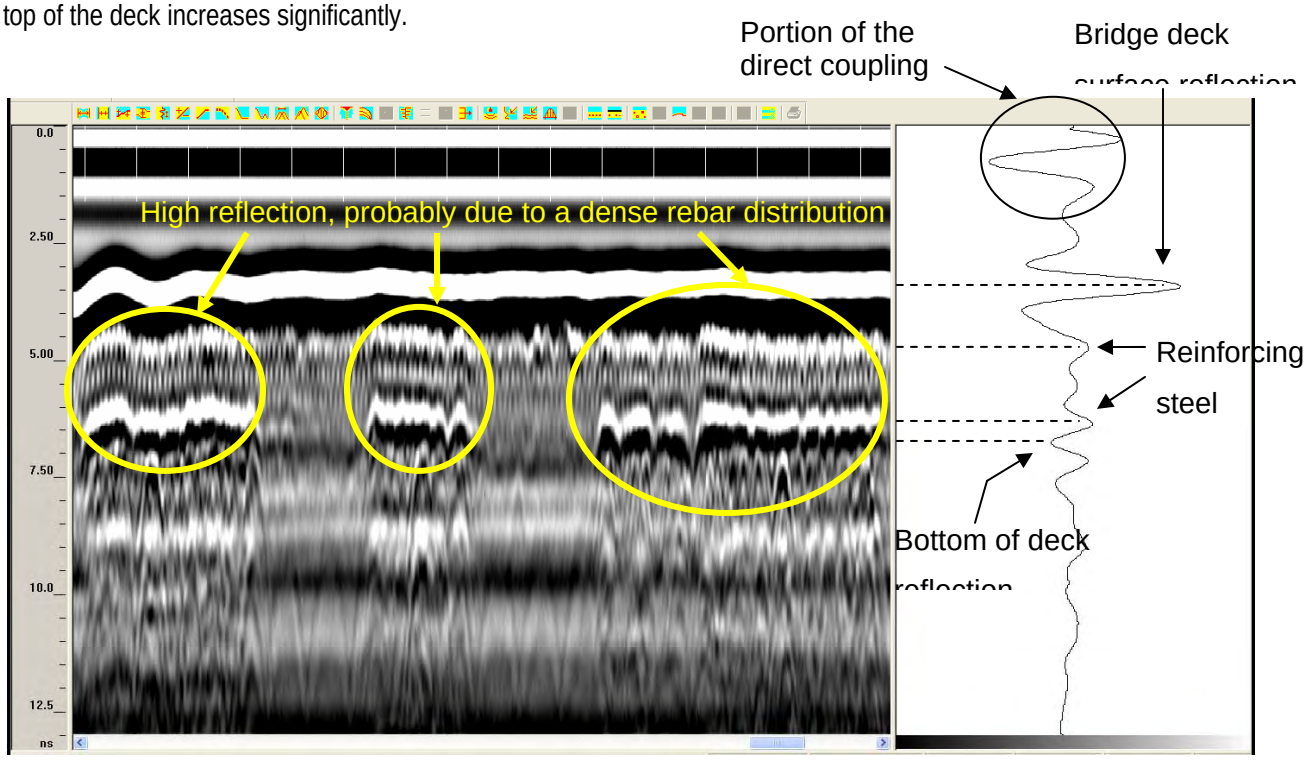

Figure 1. Raw data showing a GPR scan and a radar return waveform from Wyo. Proj.I-25-3(23) 144

The results of GPR data analysis were plotted on the plan sheet of the bridge deck, as shown in Figure 2. These results, indicating the deterioration conditions of the deck are also presented in Table 1. This table provides as well the total percent deterioration of each deck area.

Table 1. Bridge deck concrete

Region	Concrete Condition	Percent	Area (SF)
Red	Deteriorated concrete	7.4%	490.72
Orange	Less deteriorated concrete	9.3%	591.04
Green	Sound concrete	35.4%	1969.12
Blue	Sound concrete	47.9%	2629.12

Figure 2 is the deterioration map of the bridge generated from the data collected using 1 GHz Single-Polarization method. The map indicates the deterioration conditions of the deck. Blue and green regions on the map represent areas where concrete is considered sound. Sound concrete is free from or has minor indications of chloride contents, moisture, delamination, or steel corrosion. Orange indicates the areas where deterioration may have started but the process is in its early age. Red regions indicate those areas where deterioration may have reached its advanced stage. The gap with no data on the deterioration map between the driving lane and the passing lane is due to the presence of cones on the center line during data collection (see Photograph 1).

The distance measuring instrument of the GPR system was used during data collection to measure the spacing between transverse rebar of the bridge. As shown in the GPR scan of Figure 3 below, this spacing was accurately determined to be 12".

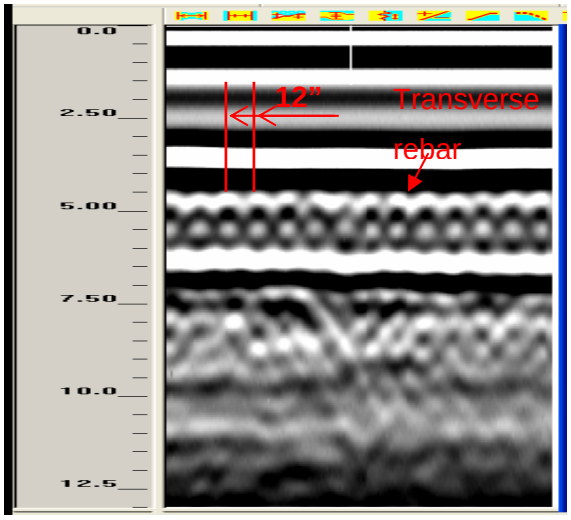

Figure 3. Spacing of transverse rebar

GPR is best used with other methods such as coring and visual surveys, not as a stand-alone tool. Therefore coring and underside visual survey together with GPR would identify areas of full-depth deck repair.

INTERSTATE ROUTE 25
STRUCTURE # I-25-3(23)144
OVER IRVINE ROAD AND C. & N.W. RAILROAD
CONVERSE COUNTY
STATE OF WYOMING

DETERIORATION MAP

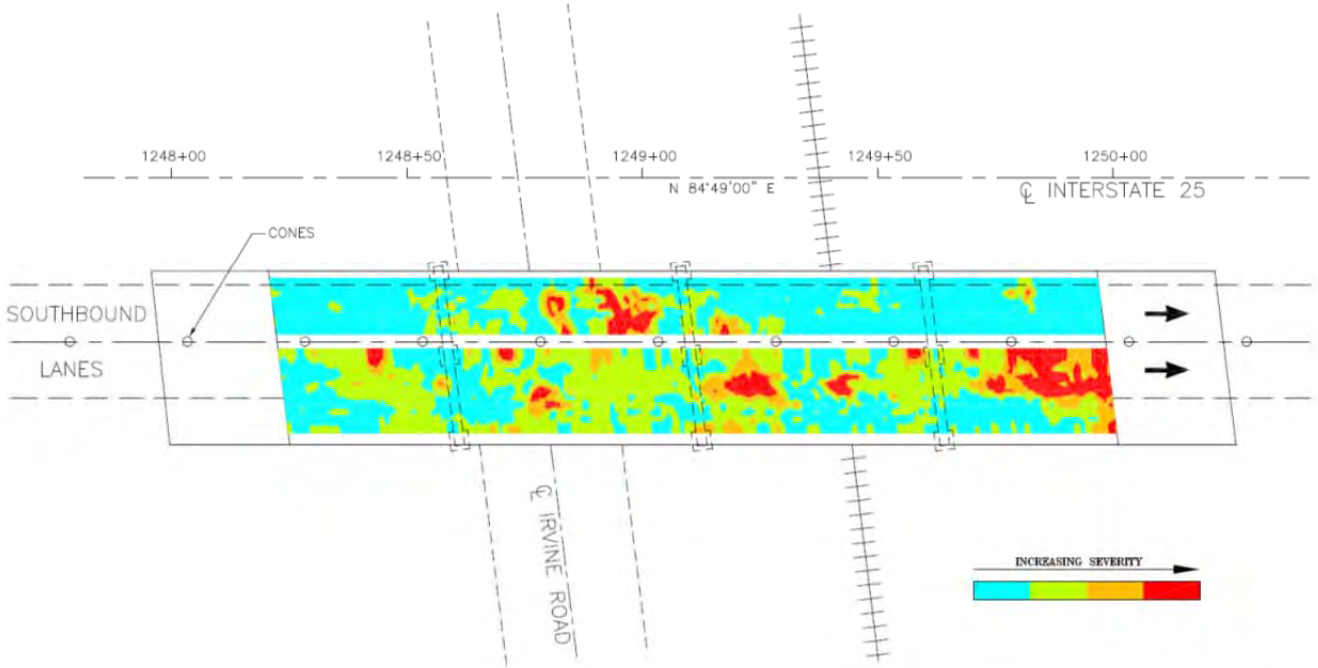

FIGURE 2
PAGE 6

GRAPHIC SCALE
0 10 20 30 40
(IN FEET)
1 INCH = 20 FT.

DETERIORATION MAP OF
INTERSTATE ROUTE 25
STRUCTURE # I-25-3(23)144
OVER IRVINE ROAD AND
C. & N.W. RAILROAD
CONVERSE COUNTY
STATE OF WYOMING

DRAWN BY:	NLC	DATE:	09-19-2010
CHECKED BY:	CAY	DRAWING NO:	03-3
JOB NO.:	98-10-086	SHEET:	1 OF 1

NONDESTRUCTIVE TESTING AND EVALUATION INVESTIGATION
GROUND PENETRATING RADAR FOR
BRIDGE DECK ON INTERSTATE 25
DOUGLAS, WYOMING

Prepared for:
University of Wyoming
Department of Civil & Architectural Engineering
Dept 3295
1000 E. University Ave
Laramie, WY 82071

Attn: Professor Jennifer Tanner
Tel: 307.766.2073
Fax: 307.766.2221
Email: TannerJ@uwyo.edu

Olson Engineering Job No. 3016B

September 21, 2010

1.0 EXECUTIVE SUMMARY

Olson Engineering was contracted by the University of Wyoming, to provide a follow-up nondestructive testing and evaluation (NDE&E) investigation of a concrete bridge deck of the eastbound side of a bridge on I-25 in Douglas, Wyoming. The primary purpose of this follow-up study to test the bridge surface with the top one inch concrete layer removed. The Ground Penetrating Radar (GPR) test method was used in the investigation. The NDE investigation was performed by Mr. Colin Leek, Project Engineer, of Olson Engineering, Inc., on August 27, 2010. Summaries of the data collection procedures and investigation findings are given below.

Field NDE&E Investigation

Follow-up Ground Penetrating Radar (GPR) tests were conducted using a Geophysical Survey Systems, Inc., 1500 MHz ground coupled antenna along the length of the deck with the surface of the deck being stripped off by one inch. The tests were performed from the top side of the deck. The objective of the GPR testing was to locate possible areas of delamination within the bridge deck due to corrosion of the top layer of the rebar mat. The test was scanned using a grid spacing of 1.5 feet along the N-S direction and 0.25 inch along the E-W direction (along each scan line).

The testing performed with the 1500MHz ground coupled antenna was found to be no longer useful along the stripped surface of the bridge. This data was post-processed to allow for testing of possible grading of the bridge deck by area into categories of likely sound, probable delamination, and probable rebar corrosion. Due to the shallow near-surface depth of the rebar from the stripped surface, direct coupling interference of the radar electromagnetic wave energy took place causing the results of the data to indicate the bridge deck was much more corroded then it actually is. This occurs due to near surface amplitude reflection being greatly reduced which in turn causes the electromagnetic wave energy to attenuate abnormally.

Due to these results, no comparisons could be made between the previous data with the entire bridge surface and the latest data with the bridge surface stripped.

2.0 GROUND PENETRATING RADAR (GPR) METHOD

The GPR method involves moving an antenna across a test surface while periodically pulsing the antenna and recording the received echoes, as shown in Figure 1. Pulses are sent out from the GPR computer driving the antenna at a frequency range centered on the design center frequency of the antenna; in this case 1500 Megahertz (MHZ) equal to 1.5 Gigahertz (GHz) and 2000 Megahertz (MHZ) equal to 2.0 Gigahertz (GHz). These electromagnetic wave pulses propagate through the material directly under the antenna, with some energy reflecting back whenever the wave encounters a change in electrical impedance, such as at a rebar or other steel embedment or air-filled void. The antenna then receives these echoes, which are amplified and filtered in the GPR computer, and then digitized and stored. A distance wheel records scan distance across the test surface and embedded features can be located as a given distance from the scan start position. For repetitive scanning, a standard survey is designed and adhered to as field conditions allow to minimize mistakes and maximize data quality.

The scans for this investigation were created from pulses sent out at lateral intervals of approximately 48 pulses per foot (4 pulses per inch). The resulting raw data is in the form of echo amplitude versus time. By inputting the dielectric constant, which defines the material velocity, and by estimating the signal zero point, the echo time data can be converted to echo depth. The following equations explain this conversion:

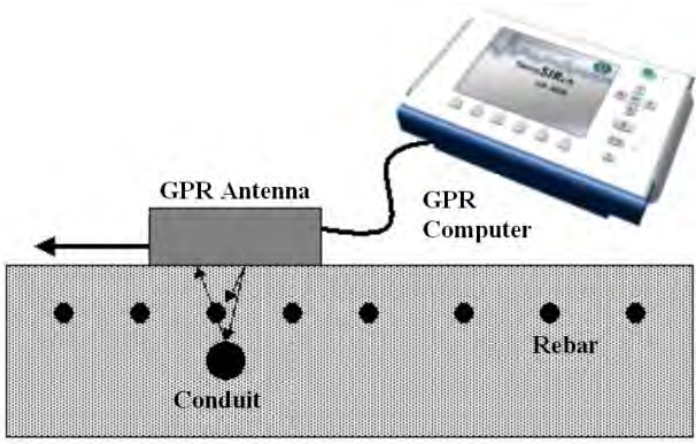

$V_{EM} = c / 0_r^{0.5}$ $D = (V_{EM} * T) / 2$ **Figure 1: GPR Method Schematic**

where V_{EM} is the material electromagnetic velocity, c is the speed of light (in air), 0_r is the material relative dielectric constant, D is depth, and T is the two-way radar pulse travel time. If more accurate depth data is required, a depth calibration can be done if an embedment of a known depth is available to scan over (or the backside reflection of the slab). The scans are then typically plotted as waterfall plots of all of the individual data traces collected, with the

lightness or darkness (or color) of each point in the plot being set by the amplitude and polarity (positive or negative) of the data at a given depth in each trace. Further, if data are collected along evenly spaced gridlines, a 3-D interpolation can be performed to generate a cubic display of data. This data cube can then be sliced along certain planes (typically XY, XZ, and YZ) to enhance recognition and display of target features. Also, amplitude threshold constraints can be set to allow display of GPR reflections within the given threshold values. Regional features are often more easily recognized when viewing a slice of 3-D interpolated data.

3.0 FIELD INVESTIGATION

The GPR tests were performed using a Geophysical Survey Systems, Inc., 1500 MHz ground coupled antenna along the length of the concrete bridge deck with the top one inch of the bridge being stripped off. The tests were performed on the top of the deck (Figure 3) per drawings provided by the Wyoming Department of Transportation (WYDOT). Traffic control for the testing was also provided by WYDOT. The test was scanned using a grid spacing of 1.5 feet along the N-S direction (width of the bridge) and 0.25 inch along the W-E direction (along each scan line). GPR data files were recorded back and forth in the westbound and eastbound directions (in the eastbound lanes), in one and a half foot transverse intervals from the south curb edge of the bridge to the north curb edge. The objective of the GPR tests is to determine areas of the bridge deck with potential corrosion or delamination (cracks) at the top layer of steel reinforcement.

Figure 3 - GPR testing along the stripped surface of the bridge in Douglas Wyoming.

4.0 EXAMPLE DATA

Data collected with the 1500 MHz antenna contained clear reflections from each individual rebar in the deck. Due to the near-surface direct coupling of the rebar and the antenna however, no corrosion determinations could be made. Example data (Figure 4) is given to show just how close the rebar grid was to the antenna. Notice the direct coupling artifacts within the data. Normal data would not have such increased amplitude at each bar location. It would rather appear more hyperbolic instead of just a dark point.

1500MHz Ground Coupled Antenna

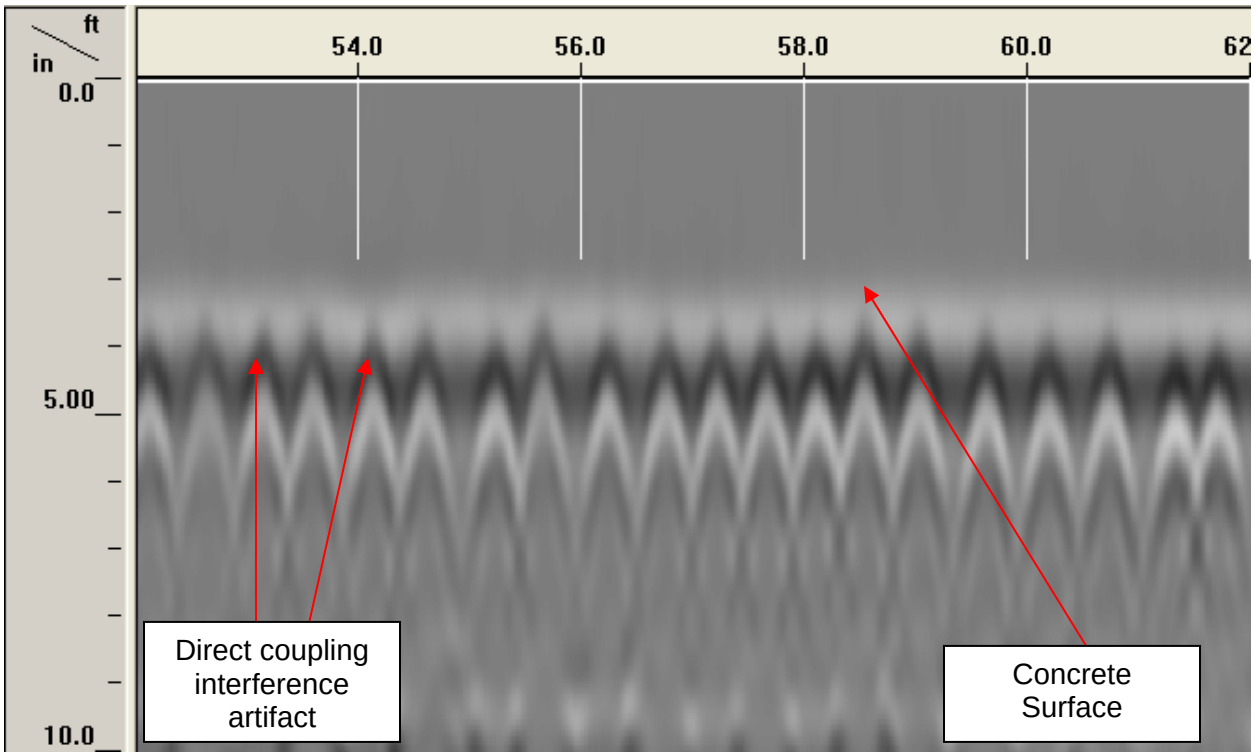

Figure 4 - GPR scan heading north 30 feet from the west end of the Douglas bridge deck. The displayed scan is indicating near surface rebar and direct coupling interference artifacts. The concrete surface is shown as nominally 3 inches down due to the chosen dielectric constant. Allowing for the surface to be visible in the data provides easier data interpretation in the field (rather then having all data start from zero in the given z-direction).

5.0 TEST RESULTS

The GPR data from the concrete deck stripped surface was processed using RADAN 6.5 to measure the reflection amplitudes (dB), in each GPR data file, of the individual transverse reinforcing bars within the top reinforcement mat. Signal losses in the reinforcing bar reflection amplitudes vary according to the bar size and the relative abundance of moisture and chloride in the concrete cover and concrete above the top reinforcing bar mat and have been correlated in previous studies with the location and extent of corrosion and corrosion-induced damage of the surface cover layer.

The reflection amplitude data was attempted to be corrected for geometric losses due to reinforcing bar depth using a statistical regression approach fit to the 90th percentile amplitude (dB) versus the two-way travel time of the GPR signal. Predictions of the location and quantities of probable delamination and probable active corrosion were evaluated using proprietary thresholds calibrated for use on exposed-surface reinforced concrete bridge decks developed in research by Dr. Christopher Barnes at Dalhousie University, Halifax, Nova Scotia, Canada who served as our sub-consultant. This approach assumes that the 90th percentile strongest reflection amplitudes correspond to undamaged regions of the deck containing low quantities of moisture and chlorides. Areas with significantly more attenuated data below the thresholds correspond to upper reinforcement mat corrosion and/or corrosion induced-cracking of the concrete cover layer.

Due to the shallow (½ to 1 inch from reinforcement to surface), near-surface depth of the rebar from the stripped surface, direct coupling interference took place causing the analysis results of the data to indicate the bridge deck as much more corroded then it actually is. This occurs due to near surface amplitude reflection attenuation. The theory of this is based on the superposition of the direct coupling radar wave (the wave which travels directly from the transmitter to the receiver in the antenna, parallel to the flat bottom of the antenna and following the interface between the antenna and the deck surface) and the rebar reflections. If the antenna and the subsurface reinforcement bar are not separated enough by the width of a reflection peak, there will be superposition of the two signals. The summation of the large negative direct coupling and the weaker positive rebar reflection will draw the rebar reflection more and more negative as the 2-way travel time of the rebar reflection decreases, eventually causing the signal to attenuate.

With the final results and attenuation of the data, no corrosion or delamination could be determined. The final results shown (Figure 5) in plan view are displayed in terms of Two-Way Travel Time, Estimated Cover Depth, and Depth Corrected Reflection Amplitude. Notice the correlation between all data sets. This correlation fortifies the argument of direct coupling interference occurring.

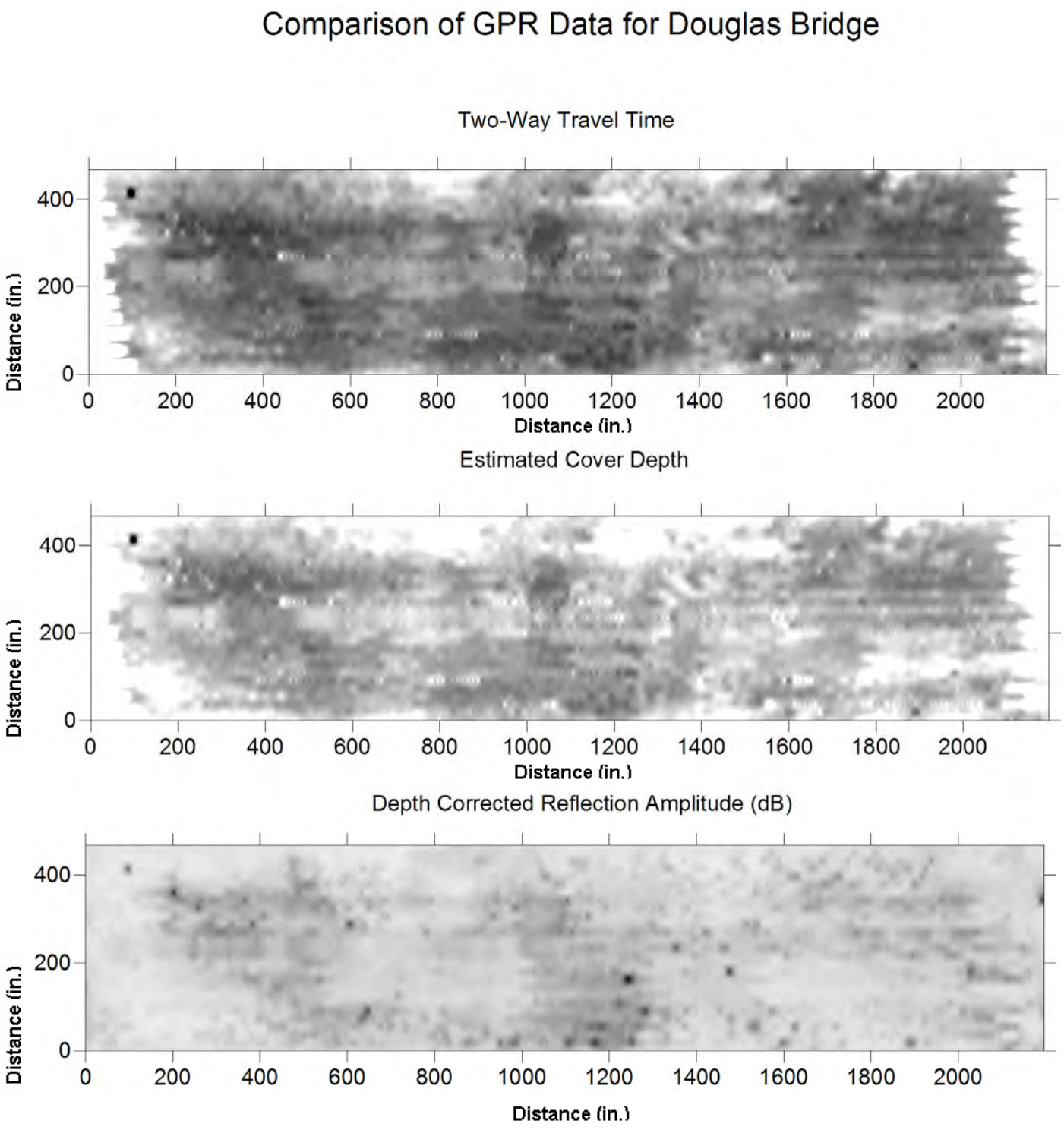

Figure 5 – Final results shown in Two-Way Travel Time, Estimated Cover Depth, and Depth Corrected Reflection Amplitude (dB). The correlation between all data is a direct effect of the direct coupling interference.

6.0 CLOSURE

The field portion of this NDE&E investigation was performed in accordance with generally accepted testing procedures. If additional information is developed that is pertinent to the findings of this investigation or we can provide any additional information or consultation, please contact our office.

Respectfully submitted,

OLSON ENGINEERING, INC.

_____

Colin O. Leek

Project Engineer

_____

Larry D. Olson, P.E.

Principal Engineer

(1 copy e-mailed and 2 copies sent)

NONDESTRUCTIVE TESTING AND EVALUATION INVESTIGATION
GROUND PENETRATING RADAR FOR
REMOUNT BRIDGE DECK WITH ASPHALT OVERLAY
INTERSTATE 80 EASTBOUND LANES AT BUFORD, WYOMING

Prepared for:
University of Wyoming
Department of Civil & Architectural Engineering
Dept 3295
1000 E. University Ave
Laramie, WY 82071

Attn: Professor Jennifer Tanner
Tel: 307.766.2073
Fax: 307.766.2221
Email: tannerj@uwyo.edu

Olson Engineering Job No. 3016C

November 30, 2010

1.0 EXECUTIVE SUMMARY

Olson Engineering was contracted by the University of Wyoming (UW), to provide a nondestructive testing and evaluation (NDE&E) investigation of an asphalt overlaid concrete bridge deck on the eastbound side of a bridge on I-80 east of Buford, Wyoming Exit 339 over Remount Road. Ground Penetrating Radar (GPR) and Bridge Deck Scanner (BDS) test method was used in the investigation. The NDE investigation was performed by Mr. Colin Leek, Project Engineer of Olson Engineering, Inc. with the assistance of Mr. Tyler Robison, UW graduate student, on July 7, 8, and 9, 2010 for initial testing. Summaries of the data collection procedures and investigation findings are given below.

This bridge was the third bridge tested and the only one to be covered with asphalt. The asphalt overlay complicates both the application of GPR and the Impact Echo Based Bridge Deck Scanner to detect delamination conditions as follows:

1. de-icing salts can be trapped between the asphalt and concrete which attenuates the GPR energy thereby masking the presence of corroded rebar (similar to attenuation due to corrosion by-products around rebar); and,

2. the BDS-IE results will not penetrate into the deck concrete if the asphalt is debonded from the concrete (air-gap blocks the compressional sound wave energy).

Tests with the BDS-IE system did find that the asphalt was debonded from the concrete, so none of this data is reported herein as the impact echo wave energy could not penetrate the debonded asphalt air gap in order to evaluate the concrete deck below the asphalt. The GPR results were also adversely affected by the debonded asphalt conditions and the apparent collection of de-icing salts at the asphalt-concrete boundary as discussed below.

Field NDE&E Investigation and Results

Field GPR Test Program. Ground Penetrating Radar (GPR) tests were conducted using an Ingegneria Dei Sistemi (IDS) Aladdin acquisition system with a full-polar (bi-polar) 2000 MHz antenna and a Geophysical Survey Systems, Inc., mono-polar1600 MHz antenna. The tests were performed from the top side of the deck. The objective of the GPR testing was to locate possible areas of delamination within the bridge deck due to possible corrosion of the top layer of the rebar mat. The tests with the 1600 MHz antenna were conducted using a grid spacing of 1 foot along the E-W direction and 0.25 inches along the N-S direction (along each scan line). The tests with the Ingegneria Dei Sistemi (IDS) Aladdin acquisition system were conducted using a grid spacing of 4 inches along the E-W direction and 0.20 inches along the N-S direction.

GPR Processing by Dr. Barnes. This data was post-processed with the procedures used for bare concrete decks to allow grading of the bridge deck by area into categories of likely sound and probable delamination or corrosion. Representative data from the GPR investigation of the asphalt overlaid concrete deck are presented in Section 5.0. The quantity of probable delamination from the 1600 MHz antenna was estimated to be 21.96 ft^2, or 6.7 percent of the deck surface area. The quantity of probable active corrosion was estimated to be 79.82 ft^2, or 24.5 percent of the deck surface area. The quantity of probable delamination and corrosion from IDS's full-polar 2000 MHz antenna was more than double that of the GSSI 1600 MHz antenna. Due to time constraints and the direct interest of a comparison study between IDS's 2000 MHz Aladdin antenna and the 1600 MHz antenna, only a section of the Aladdin data was analyzed within IDS's *GRED* processing software and directly compared with a section of the full survey from the 1600 MHz antenna by Dr. Christopher Barnes of Dalhousie University, Halifax, Nova Scotia. As reported in Section 5, the 2000 MHz full-polar antenna did appear to correlate in some areas with the 1600 MHz antenna. Overall however, the data from the Aladdin system appeared much more sensitive to apparent areas of signal attenuation (possible delamination/corrosion) than the GSSI system. This may be due to the higher frequency antenna having shorter wavelengths which can be attenuated more severely.

GPR Processing of Aladdin Data by IDS. The Aladdin data were sent to IDS's Georadar group in Pisa, Italy for further processing. Amplitude and frequency data were processed and analyzed, though no direct comparison can yet be made from this information to Dr. Christopher

Barnes results. It can be inferred that the difference in signal frequency between the two systems is the primary cause for such a contrast in results as discussed in the preceding paragraph.

Comments on Core Results versus GPR Results. In any NDE investigation, ground-truthing of NDE results with cores is a highly recommended practice, particularly in this case where GPR and BDS-IE have had limited use on asphalt overlaid bridge decks. Cores were drilled and examined as part of the UW project for WYDOT. It is our understanding that the cores did not reveal significant corrosion of the top deck steel rebar which is consistent with the GPR results not showing significant attenuation in spite of the direct coupling problem with the shallow rebar. Delamination results between the concrete and asphalt overlay could not be determined as the cores were taken after the asphalt overlay had been removed. The cause for the misleading GPR results is most likely due to misleading attenuation of the radar signals by the likely presence of de-icing salts between the debonded asphalt overlay and top of the concrete deck. Olson Engineering has previously tested an asphalt overlaid deck in Colorado Springs with the GSSI GPR system from the top surface. That study found similar complications in terms of misleading GPR determinations of delamination and corrosion. This was confirmed by the much more accurate Impact Echo tests from the bare concrete on the bottomside of this other deck and core results.

Bridge Deck Scanner – Impact Echo Results. As discussed above, the Bridge Deck Scanner – Impact Echo (BDS-IE) system was used for this deck survey as well. However, due to the debonding between the asphalt overlay and the concrete bridge deck, the sound waves were trapped in the asphalt layer by total reflection at the debonded air gap. Consequently, the sound waves were unable to penetrate into the underlying concrete deck to check the deck integrity in terms of top or bottom steel delaminations or full thickness echoes indicative of sound concrete.

Current and Future NDE Research Activities. Olson Engineering and IDS jointly conducted NDE fieldwork for condition evaluation of a bare concrete bridge deck and submitted the results to Dr. Nenad Gucunski of Rutgers University as part of their SHRP 2 R06(A) Bridge Deck Validation study. We conducted BDS-IE and GPR delamination and corrosion surveys with the GSSI and IDS systems on the James Madison Highway - US 15 Bridge over Route 66 in Haymarket, Virginia. The results of this study indicate that the most accurate methods were the BDS-IE and Aladdin

radar systems (these results will ultimately become generally available). There is also interest in researching the application of NDE to asphalt overlaid decks as it is worth researching the possibility that one can mitigate the effects of de-icing salts on GPR data for bridge deck corrosion/delamination surveys.

2.0 GROUND PENETRATING RADAR (GPR) METHOD – IDS ALADDIN

The GPR method involves moving an antenna across a test surface while periodically pulsing both antenna and recording the received echoes in both the longitudinal and transversal directions, as diagramed in Figure 1. Pulses are sent out from the GPR computer driving the antenna at a frequency range centered on the design center frequency of the antenna, in this case 2000 MegaHertz (MHz) equal to 2.0 GigaHertz (GHz) for the IDS Aladdin system. These electromagnetic wave pulses propagate through the material directly under the antenna, with some energy reflecting back whenever the wave encounters a change in electrical impedance, such as at a rebar or other steel embedment or air-filled void. The antenna then receives these echoes, which are amplified and filtered in the GPR computer, and then digitized and stored. A distance wheel records scan distance across the test surface and embedded features can be located as a given distance from the scan start position. For repetitive scanning, a standard survey is designed and adhered to as field conditions allow in order to minimize mistakes and maximize data quality.

The scans for this investigation were created from pulses sent out at lateral intervals of approximately 200,000 samples per second and the system is shown in Figure 2. The resulting raw data is in the form of echo amplitude versus time. By inputting the dielectric constant, which defines the material velocity, and by estimating the signal zero point, the echo time data can be converted to echo depth. This is expressed in the following equations:

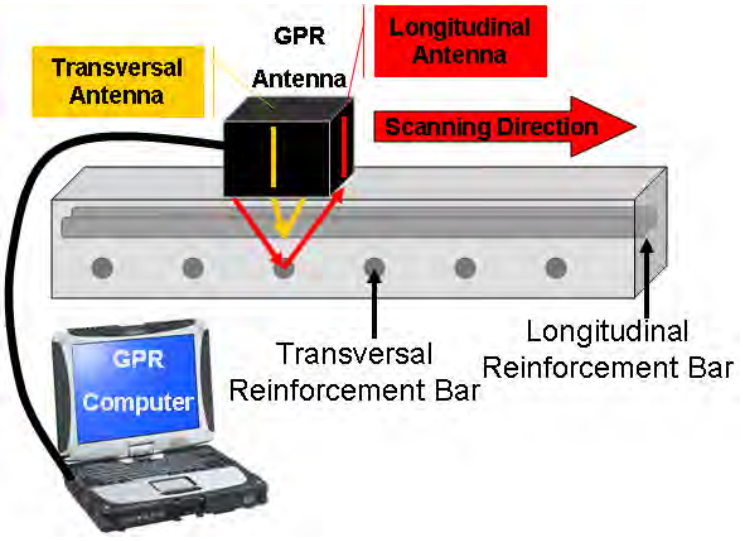

Figure 1 -Typical Full-polar GPR field setup

$$V_{EM} = c / \varepsilon_r^{0.5} \qquad D = (V_{EM} * T) / 2$$

where V_{EM} is the material electromagnetic velocity, c is the speed of light (in air), ε_r is the material relative dielectric constant (relative to air), D is depth, and T is the two-way radar pulse travel time. If more accurate depth data is required, a depth calibration can be done if an embedment of a known depth is available to scan over (or the backside reflection of the wall). The scans are then typically plotted as two-dimensional (2D) waterfall plots of all of the individual data traces collected, with the lightness or darkness (or color) of each point in the plot being set by the amplitude and polarity (positive or negative) of the data at a given depth in each trace. Further 3-D interpolation can be performed to generate a cubic display of data by combining both the longitudinal and transversal data that are collected along a single longitudinal scan (due to the full-polar mechanics of the antenna). This data cube can then be sliced along certain planes (typically XY, XZ, and YZ) to enhance recognition and display of target features. Also, amplitude threshold constraints can be set to allow display of GPR reflections within the given threshold values. Regional features are often more easily recognized when viewing a slice of 3-D interpolated data. With tight scan spacing and the ability to measure both the longitudinal and transversal directions at the same time however, it is very possible to develop high resolution three-dimensional (3D) imaging for locating specific features that are not regional to a specific survey.

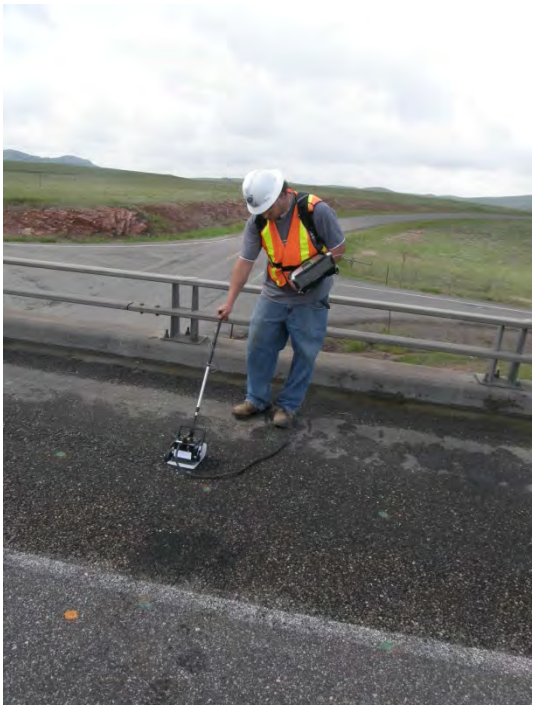

Figure 2 - Ingegneria Dei Sistemi (IDS) Aladdin acquisition system with a full-polar 2000 MHz antenna and Panasonic Toughbook CF-19.

3.0 GROUND PENETRATING RADAR (GPR) METHOD – GSSI SIR 3000

The GPR method involves moving an antenna across a test surface while periodically pulsing the antenna and recording the received echoes, as shown in Figure 3. Pulses are sent out from the GPR computer driving the antenna at a frequency range centered on the design center frequency of the antenna; in this case 1600 Megahertz (MHz) equal to 1.6 Gigahertz (GHz). These electromagnetic wave pulses propagate through the material directly under the antenna, with some energy reflecting back whenever the wave encounters a change in electrical impedance, such as at a rebar or other steel embedment or air-filled void. The antenna then receives these echoes, which are amplified and filtered in the GPR computer, and then digitized and stored. A distance wheel records scan distance across the test surface and embedded features can be located as a given distance from the scan start position. For repetitive scanning, a standard survey is designed and adhered to as field conditions allow to minimize mistakes and maximize data quality.

The scans for this investigation were created from pulses sent out at lateral intervals of approximately 75,000 samples per second. The resulting raw data is in the form of echo amplitude versus time. The analysis of the data was described in the previous section.

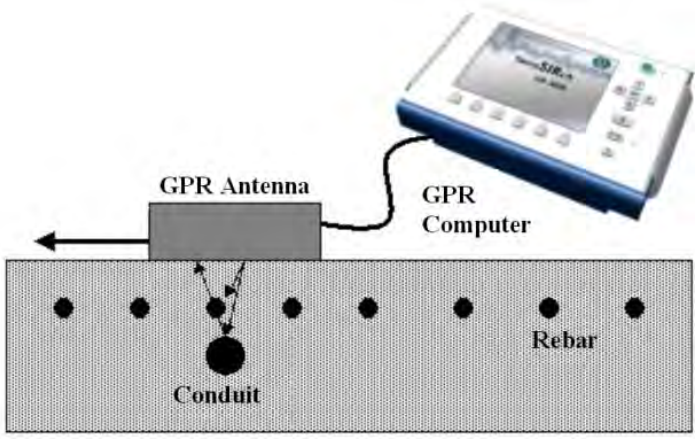

Figure 3 - GSSI SIR 3000 GPR System

4.0 FIELD INVESTIGATION

The GPR tests were conducted using an Ingegneria Dei Sistemi (IDS of Pisa, Italy) Aladdin acquisition system with a full-polar 2000 MHz antenna and a Geophysical Survey Systems, Inc., SIR 3000 System (GSSI of Salem, New Hampshire) with a 1600 MHz ground coupled antenna along the length of the asphalt overlaid concrete bridge deck. The tests were performed on the top of the deck (Figure 2) per drawings provided by the Wyoming Department of Transportation (WYDOT). Traffic control for the testing was also provided by WYDOT.

The deck was scanned using a grid spacing of 4 inches for the 2000 MHz antenna and 1 foot for the 1600 MHz antenna along the E-W direction (width of the bridge). Scan spacing of 0.20 inches for the IDS full-polar 2000 MHz Aladdin antenna and 0.25 inches for the GSSI 1600 MHz antenna were used along the N-S direction (along each scan line). GPR data files were recorded in the eastbound direction (in the eastbound lanes), in four inch transverse intervals for the 2000 MHz Aladdin antenna and in one foot transverse intervals for the 1600 MHz antenna from the centerline and outward towards the north and south ends heading east along the eastbound bridge.

The objective of the GPR tests is to determine areas of the bridge deck with potential corrosion or delamination at the top layer of steel reinforcement. The results of this study are then compared between IDS's Aladdin full-polar 2000 MHz antenna and the GSSI single-polar 1600 MHz antenna.

5.0 EXAMPLE GPR SCAN DATA

Figures 4 and 5 present 2-D scan data collected with the IDS 2000 MHz full-polar Aladdin antenna and the GSSI 1600 MHz single antenna, respectively, with the nominally 1.5 inch thick asphalt overlay in-place over the concrete deck. Review of the data indicates similar rebar spacing for the two scans. The rebar reflections are more rounded in appearance for the IDS system than the GSSI system.

2000 MHz Full-polar Antenna

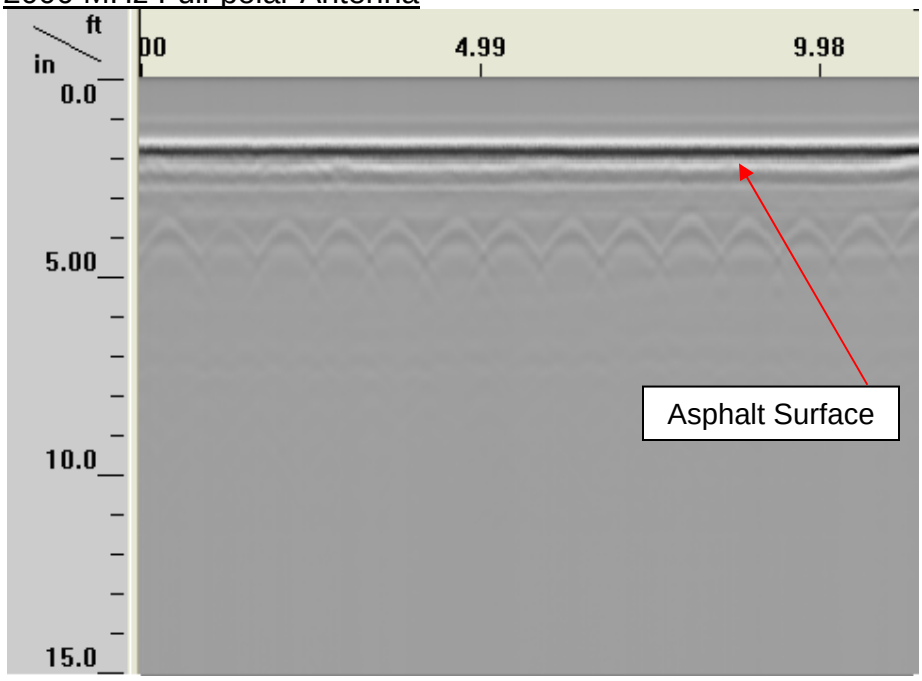

Figure 4 – IDS Aladdin 2000 MHz GPR Data from initial testing with asphalt overlay in place. Notice the round hyperbolic signals for each steel reinforcement bar radar reflection.

1600MHz Single Antenna

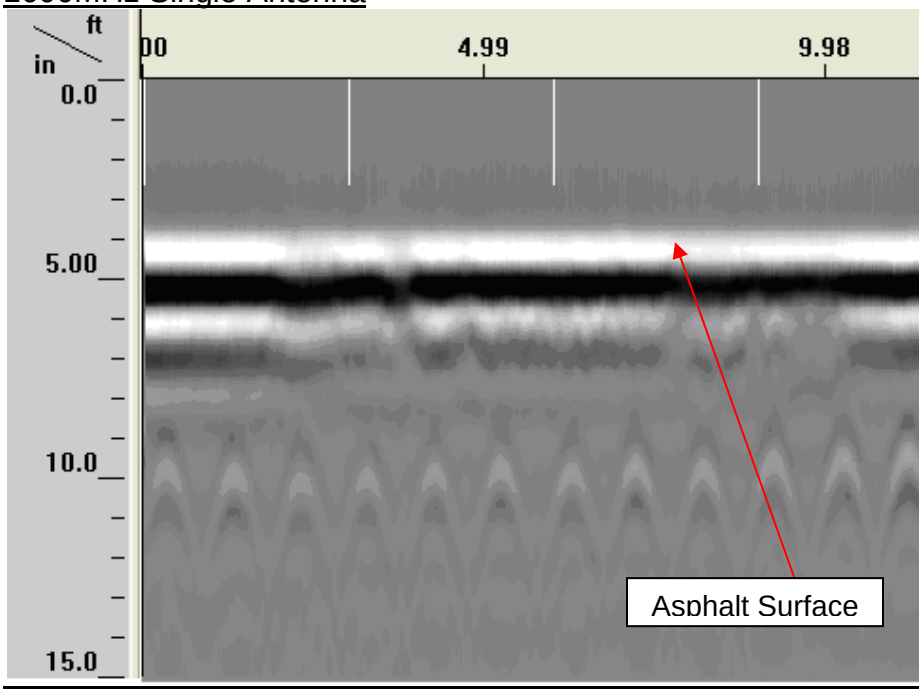

Figure 5 – GSSI 1600 MHz GPR Data from initial testing of the asphalt overlaid deck before surface stripping. Notice the fading within the signal. This is most likely due to potential corrosion or delamination. This information in the data is most likely visible due to the lower frequency of the antenna in comparison to the 2000 MHz antenna.

6.0 ANALYSIS OF GPR TEST RESULTS

The GPR data from the concrete deck top was processed using GRED 02.01.015 for the IDS full-polar 2000 MHz antenna data and GSSI RADAN 6.5 for the 1600 MHz antenna to measure the scanned reflection normalized amplitudes (dB) of the individual transverse reinforcing bars within the top reinforcement steel. The primary concern in processing delamination and corrosion involves focusing on signal losses in the reinforcing bar reflection amplitudes which vary according to the bar size and the relative abundance of moisture and chloride in the concrete cover along with corrosion byproducts. This is also a direct relationship with the concrete above the top reinforcing bar mat which has been correlated in previous studies with the location and extent of delamination, corrosion, and corrosion-induced damage of the surface cover layer.

The reflection amplitude data are corrected for geometric losses due to reinforcing bar depth using a statistical regression approach fit to the 90^{th} percentile normalized amplitude (dB) versus the two-way travel time of the GPR signal. Predictions of the location and quantities of probable delamination and probable active corrosion are then evaluated using proprietary thresholds calibrated for use on exposed-surface reinforced concrete bridge decks developed in research by our sub-consultant; Dr. Christopher Barnes at Dalhousie University, Halifax, Nova Scotia, Canada. This approach assumes that the 90^{th} percentile strongest reflection amplitudes correspond to undamaged regions of the deck containing low quantities of moisture and chlorides. Areas with significantly more attenuated data below the thresholds correspond to upper reinforcement mat corrosion and/or corrosion induced-cracking of the concrete cover layer. Please note that the GPR investigation for delamination survey is most accurate for bridge deck areas with no previous repairs and bare concrete. The use of GPR on asphalt overlaid decks is also a comparatively new research area as discussed in Section 1.

For the 1600 MHz results, all bridge deck data displayed in plan view indicates probable delaminations in red and probable active corrosion areas in yellow in Figures 6 and 7. The delamination and corrosion results for the 1600 MHz antenna show depth-corrected GPR amplitudes that were outside the damage thresholds in grayscale to indicate the predicted relative variation in moisture and chloride over the undamaged deck surface. Darker regions may indicate areas where moisture and chloride ingress is approaching levels sufficient to initiate corrosion. The quantity of probable delaminations from the 1600 MHz antenna was estimated to be 21.96 ft^2, or 6.7 percent of the deck surface area. The quantity of probable active corrosion was estimated to be 79.82 ft^2, or 24.5 percent of the deck surface area.

When reviewing the 1600 MHz antenna directly, there is a difference in displayed levels of delamination and corrosion from the North and South sides of the bridge for the 1600 MHz data. This is due to a difference in output power from the 1600 MHz single antenna during different testing periods. Though it is ideal to have a single level of output power for both sides of the bridge, interpretations and corrections can be made, so the power-variation in the field is not considered significant.

The difference in antenna frequency causes a contrast in corrosion and delamination results along the bridge deck due to the difference in signal attenuation that occurs at different levels of frequency within each radar antenna. This difference in frequency is critical as corrosion problems are predicted from the GPR signal losses that result as the signal travels from the deck surface to the bar and back to the surface again. The inference is that if there are enough losses distributed throughout the total cover thickness, then corrosion is probable - based on empirical data developed by Dr. Christopher Barnes. This post processing technique used estimates the geometric losses (due to varying cover thickness) and statistically normalizes all of the data to a common geometric loss value. Since higher frequencies tend to attenuate quicker due to lower wavelengths and increased chance of signal loss, geometric loss values used to detect bridge deck delamination and corrosion are greatly affected.

The possibility of signal loss with a higher frequency antenna was analyzed through comparing a section of the 1600 MHz antenna data with a section of IDS's full-polar 2000 MHz Aladdin antenna data. The Aladdin data was processed in GRED and the 1600 MHz antenna was processed in RADAN in order to achieve similar output information for further analysis. After full processing for corrosion and delamination, some correlation between the two data sets could be seen. It is clear however that the 2000 MHz antenna (compared to the 1600 MHz antenna) is experiencing much more evidence of corrosion which in this case is likely artificial due to the high frequency content of the antenna (Figures 8). Threshold adjustments were carried out in an attempt to correct for this signal attenuation experienced by the 2000 MHz antenna (Figure 9). Though subtle changes are visible, the results were still deemed relatively unfeasible. Other probable factors regarding the differences in the two data sets have also been considered. These factors may involve field intensity and spatial resolution regarding the difference in survey grids of the two different antenna. As no absolute conclusion can yet be made, this comparison study of delamination and corrosion for each antenna are still under further research.

Efforts to understand this phenomenon are being researched and corrected for by both our firm as well as the Aladdin manufacturer (IDS of Pisa, Italy). IDS's Georadar Group has processed these data through analyzing the amplitude and frequency response correlated directly with the locations of reflected reinforcement bar signals throughout the survey (Figures 10, 11 and 12). Though it is unknown how this information directly correlates with Dr. Christopher Barnes' empirical software, some similarities clearly exist within the 2000 MHz Aladdin data and the 1600 MHz data.

This study of bridge deck analysis has continued even further and has thus far the 2000 MHz IDS Aladdin system has concluded to be more accurate in determining delamination and corrosion of concrete bridge decks with no asphalt surface overlay; per a recent GPR delamination and corrosion survey conducted on the James Madison

Highway - US 15 Bridge over Route 66 in Haymarket, Virginia as part of Dr. Nenad Gucunski's SHRP 2 R06(A) Bridge Deck Validation study.

With these successful results, IDS is expanding on the idea of bridge deck analysis using ground penetrating radar is also currently researching and developing an 8 pair, full-polar antenna system (known as RIS Hi-Bright) for bridge deck scanning over 80 cm in width and 10 cm antenna spacing. This system is currently being tested in Europe and may result in accurate analysis and testing of corrosion and delamination with an IDS system in the future.

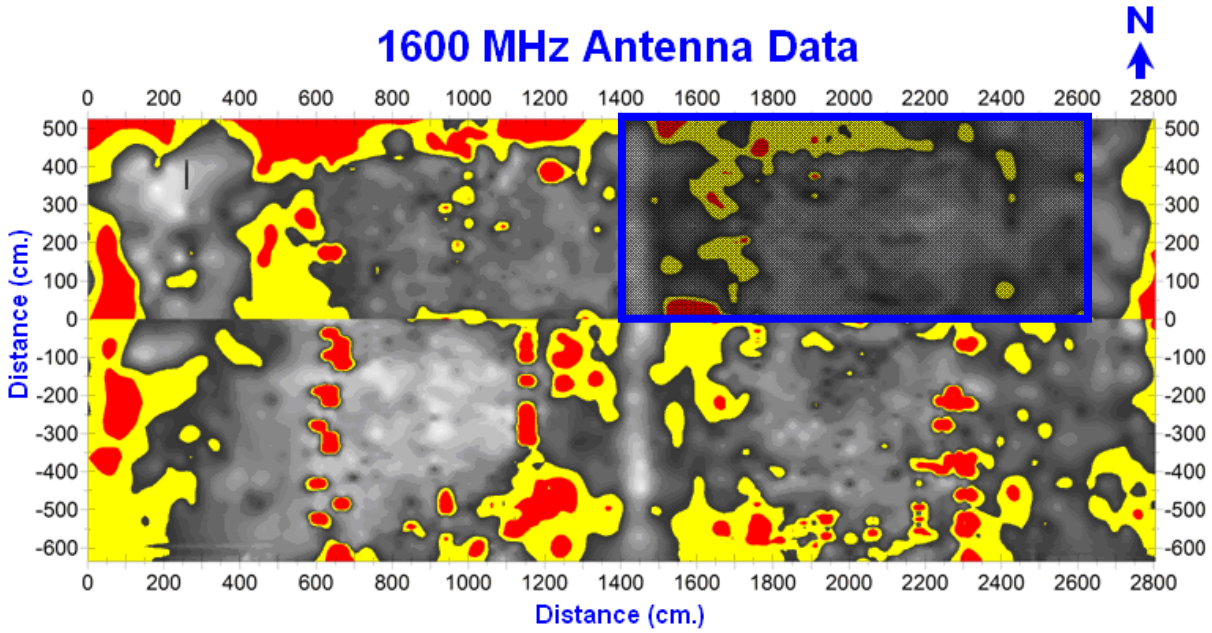

Figure 6 – 1600 MHz antenna data for delamination (red) and corrosion (yellow) results. Notice the darkened region highlighted in blue. This is where IDS's full-polar 2000 MHz Aladdin antenna and the 1600 MHz antenna are directly compared.

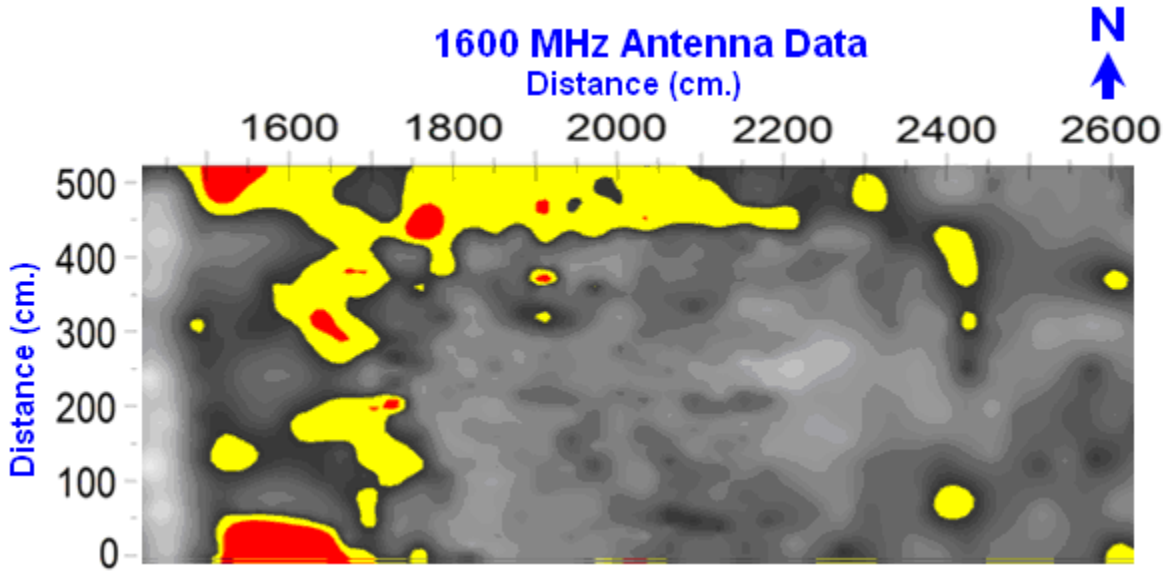

Figure 7 – 1600 MHz Data at the location in which it is to be directly compared with IDS's full-polar 2000 MHz Aladdin Data.

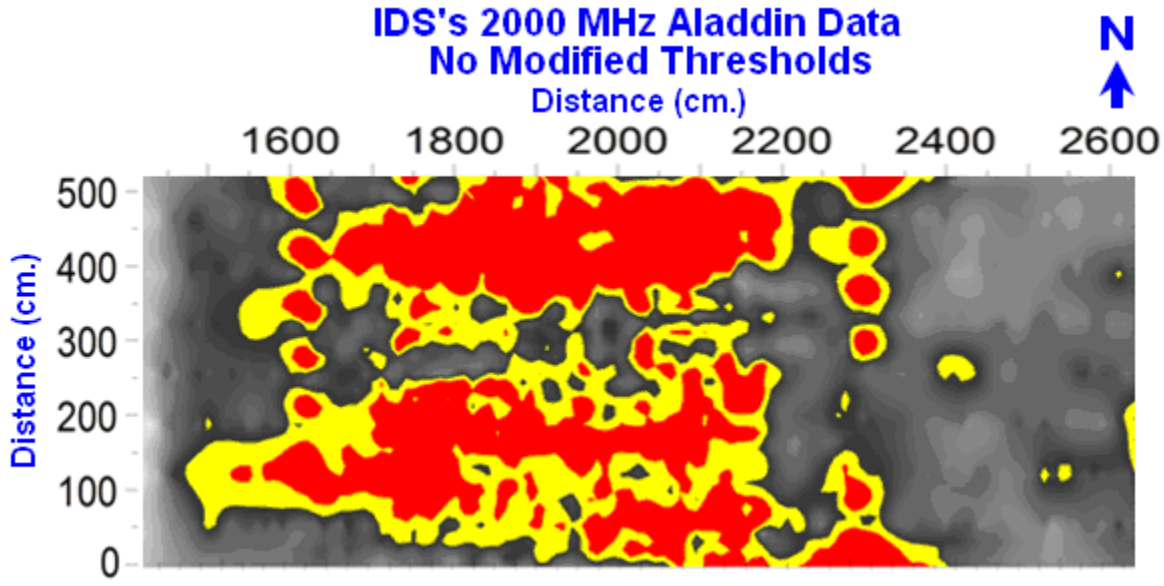

Figure 8 – IDS's full-polar 2000 MHz Aladdin Data for delamination (red) and corrosion (yellow). Notice the extensive area of potential corrosion and delamination compared to the 1600 MHz antenna. These results are likely due to the higher frequency attenuation occurring from the Aladdin antenna

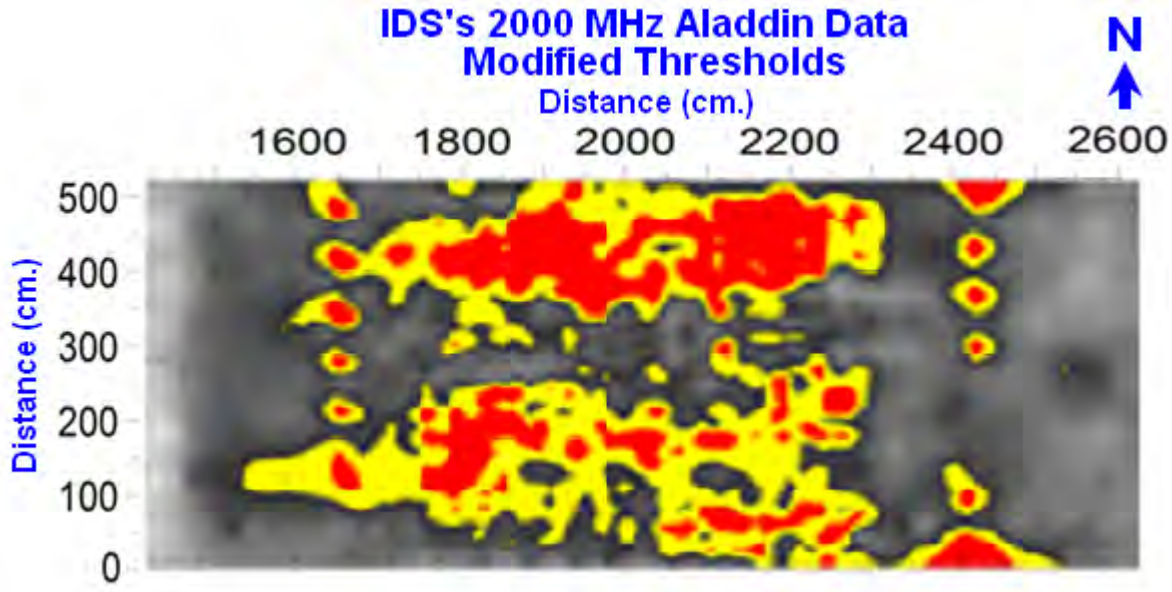

9

Figure 9 – IDS's full-polar 2000 MHz Aladdin Data for delamination (red) and corrosion (yellow) with modified defect value thresholds. Notice the extensive area of potential corrosion and delamination is slightly less compared to the previous data set from the Aladdin antenna (Figure 6.4). This is due to a threshold correction in an attempt to correct for the signal attenuation occurring with the higher frequency antenna.

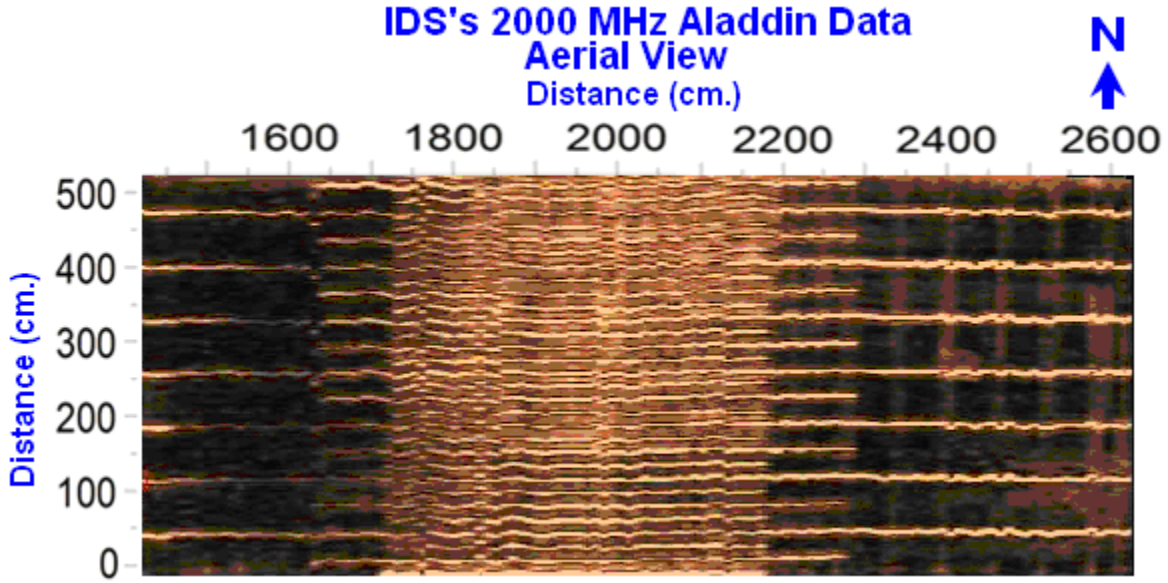

Figure 10 – Aerial view of Aladdin Data processed through IDS's Georadar group. The light linear reflectors are the steel reinforcement within the slab. Some rebar appear squiggly due to the slight variations in scanned distances throughout the survey. There is also no clear attenuation existing within the middle of the survey where the bars appear to thin or disappear entirely within the tight rebar grid. Also notice the linear transversal bars on the east side of the survey. The ability to even detect this information with data collected in only one direction is a strong advantage for IDS's full-polar 200MHz Aladdin antenna.

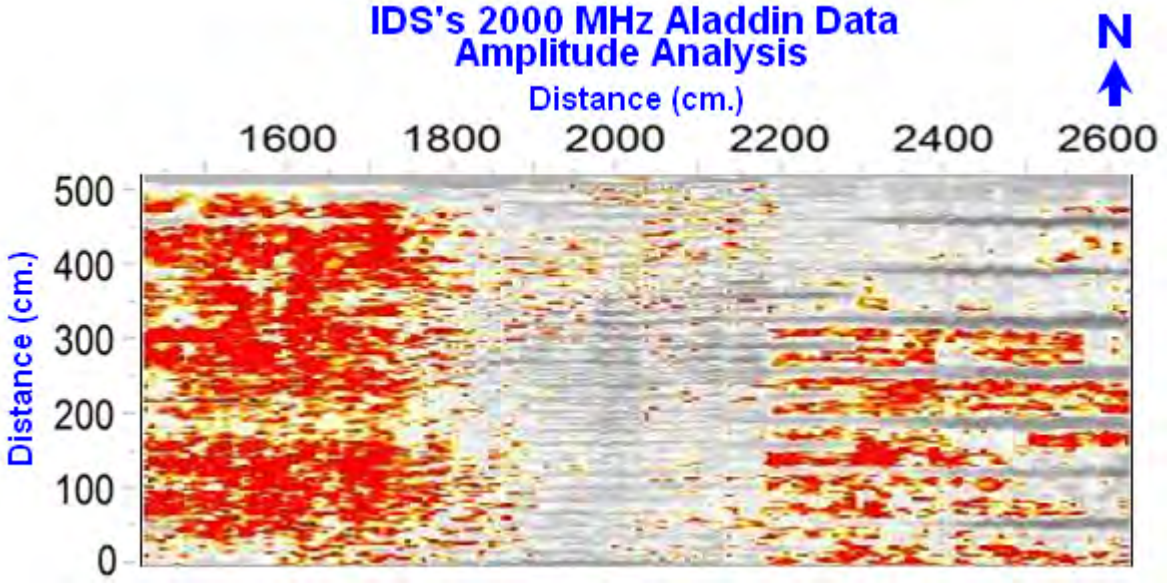

Figure 11 – IDS's Georadar Group Amplitude Analysis. The red areas are indications of high amplitude reflections within the survey and the center lighter area indicates higher attenuation.

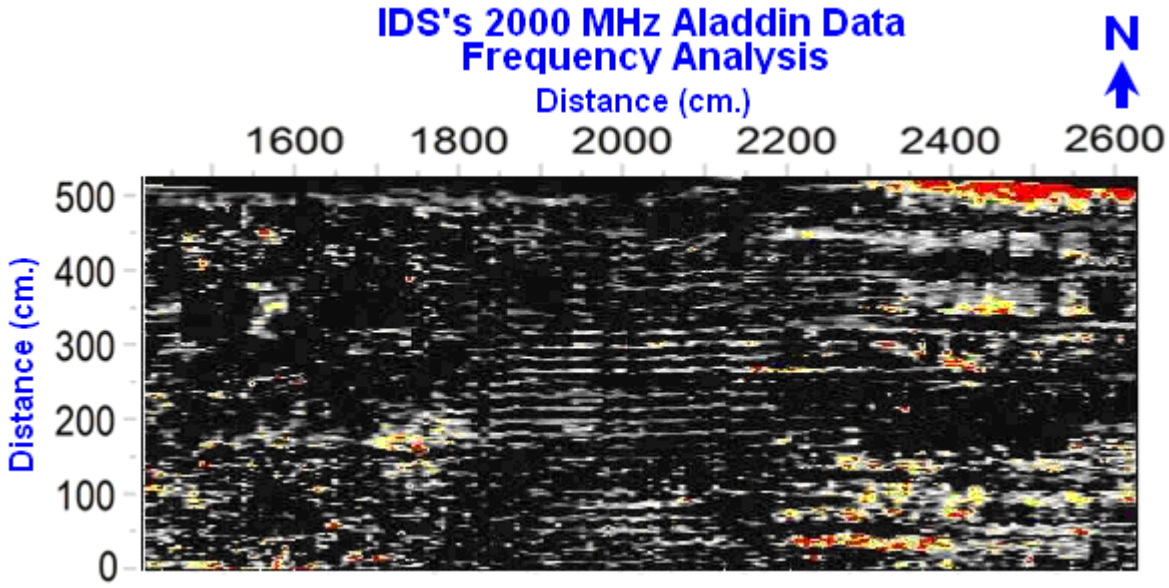

Figure 12 – IDS's Georadar Group Frequency Analysis. The red areas are indications of high frequency reflections within the survey.

Comments on Core Results versus GPR Results. As discussed in Section 1.0, cores were drilled and examined as part of the UW project for WYDOT. It is our understanding that the cores did not reveal significant corrosion of the top deck steel rebar which is consistent with the GPR results not showing significant attenuation in spite of the direct coupling problem with the shallow rebar. Delamination results between the concrete and asphalt overlay could not be determined as the cores were taken after the asphalt overlay had been removed. The cause for the misleading GPR results is most likely due to misleading attenuation of the radar signals by the likely presence of de-icing salts between the debonded asphalt overlay and top of the concrete deck. De-icing salts will also severely attenuate signals, even if corrosion is not present. Olson Engineering has previously tested an asphalt overlaid deck in Colorado Springs with the GSSI GPR system from the top surface. That study found similar complications in terms of misleading GPR determinations of delamination and corrosion. This was confirmed by the much more accurate Impact Echo tests from the bare concrete on the bottomside of this other deck and core results.

7.0 CLOSURE

The field portion of this NDE investigation was performed in accordance with generally accepted testing procedures. If additional information is developed that is pertinent to the findings of this investigation or we can provide any additional information or consultation, please contact our office.

Respectfully submitted,

OLSON ENGINEERING, INC.

_____
Colin O. Leek
Project Engineer

_____
Larry D. Olson, P.E.
Principal Engineer

(1 copy e-mailed and 2 copies sent)

NONDESTRUCTIVE TESTING AND EVALUATION INVESTIGATION GROUND PENETRATING RADAR FOR REMOUNT BRIDGE DECK - BARE CONCRETE AFTER SRIPPING ASPHALT OVERLAY INTERSTATE 80 EASTBOUND LANES AT BUFORD, WYOMING

Prepared for:
University of Wyoming
Department of Civil & Architectural Engineering
Dept 3295
1000 E. University Ave
Laramie, WY 82071

Attn: Professor Jennifer Tanner
Tel: 307.766.2073
Fax: 307.766.2221
Email: tannerj@uwyo.edu

Olson Engineering Job No. 3016C

November 30, 2010

1.0 EXECUTIVE SUMMARY

Olson Engineering was contracted by the University of Wyoming, to provide a nondestructive testing and evaluation (NDE&E) investigation of a bare concrete bridge deck (asphalt overlay had been stripped) on the eastbound lanes of the Interstate 80 (I-80) bridge over Remount Road east of Exit 339 at Buford, Wyoming. The Ground Penetrating Radar (GPR) and Bridge Deck Scanner (BDS) test methods were used in the investigation. The NDE investigation was performed by Mr. Colin Leek, Project Engineer of Olson Engineering, Inc., with the assistance of Mr. Tyler Robison, graduate student of the University of Wyoming. The NDE was conducted on August 8th and August 30th, 2010 after the removal of the 1.5 inch asphalt overlay and 1 inch of the deck concrete. The IDS and GSSI systems were described in the report on testing of the asphalt overlaid Remount Bridge Deck. Summaries of the data collection procedures and investigation findings are given below.

Field NDE&E Investigation

Field GPR Test Investigation. Ground Penetrating Radar (GPR) tests were conducted using an Ingegneria Dei Sistemi (IDS) Aladdin acquisition system with a full-polar 2000 MHz antenna and a Geophysical Survey Systems, Inc., 1600 MHz antenna. The tests were performed from the top side of the deck. The objective of the GPR testing was to locate possible areas of delamination within the bridge deck due to corrosion of the top layer of the rebar mat. The test for the Ingegneria Dei Sistemi (IDS) Aladdin acquisition system was scanned using a grid spacing of 4 inches along the E-W direction and 0.20 inches along the N-S direction. The test for the 1600 MHz antenna was scanned using a grid spacing of 1 foot along the E-W direction and 0.25 inches along the N-S direction (along each scan line).

GPR Processing by Dr. Barnes. The results from this final GPR investigation covering the bridge deck after the top asphalt overlay and approximately one inch of concrete had been removed showed drastically different results from the initial survey. The shallow, near-surface depth of rebar from the now stripped concrete surface, resulted in direct coupling interference that caused the data to indicate the bridge deck was much more corroded then it actually is. This occurs due to near surface amplitude reflections being greatly reduced after surface stripping, causing the data to attenuate abnormally for shallow rebar. Considering these results, amplitude data were extrapolated with attempts of interpretation.

No corrosion or delamination comparisons however were possible between the initial survey data with the original bridge surface and the final survey data with the bridge surface stripped. This was the case for both IDS's full-polar 2000 MHz Aladdin antenna and the GSSI 1600 MHz antenna. However, it should be noted that neither antenna system showed significant attenuation which may reflect a lack of corrosion of the top reinforcing deck steel. In this event, the initially predicted apparent corrosion by the GPR results is likely due to deicing salts in the debonded asphalt-concrete interface as discussed in the Remount Bridge Deck report with the asphalt overlay in-place.

Comments on Core Results versus GPR Results. Cores were drilled and examined as part of the UW project for WYDOT. Delamination results between the concrete and asphalt overlay could not be determined as the cores were taken after the asphalt overlay had been removed. It is our understanding that the cores did not reveal significant corrosion of the top deck steel rebar which is consistent with the GPR results not showing significant attenuation in spite of the direct coupling problem with the shallow rebar.

Bridge Deck Scanner – Impact Echo Results. As discussed above, the Bridge Deck Scanner – Impact Echo (BDS-IE) system was used for this deck survey as well. However, due to the extremely rough concrete surface, good quality impact echo could not be obtained from the stripped deck as the surface was extremely rough after removal of 1 inch of concrete.

2.0 FIELD INVESTIGATION

The GPR tests were conducted using a Ingegneria Dei Sistemi (IDS) Aladdin acquisition system with a full-polar 2000 MHz antenna and a Geophysical Survey Systems, Inc., 1600 MHz ground coupled antenna along the length of the asphalt overlaid concrete bridge deck. The tests were performed on the top of the deck per drawings provided by the Wyoming Department of Transportation (WYDOT). Traffic control for the testing was also provided by WYDOT.

The test was scanned using a grid spacing of 4 inches for the 2000 MHz antenna and 1 foot for the 1600 MHz antenna along the E-W direction (width of the bridge). A scan spacing of 0.20 inches for IDS's full-polar 2000 MHz Aladdin antenna and 0.25 inches for the 1600 MHz antenna were used along the N-S direction (along each scan line). GPR data files were recorded in the eastbound direction (in the eastbound lanes), in four inch transverse intervals for the 2000 MHz Aladdin antenna and in one foot transverse intervals for the 1600 MHz antenna with each scan line alternated from the center of the eastbound bridge out to the north edge, then from the north edge of the deck and inward to the centerline for faster data acquisition. This alternation on survey setup though different from the initial survey has no effect on the results (or comparisons) as long as the distances for each survey line are corrected for during data processing and analysis.

The objective of the GPR tests is to determine areas of the bridge deck with potential corrosion or delamination at the top layer of steel reinforcement with the top asphalt overlay and one inch of concrete removed. The results of this study are then compared between IDS's Aladdin full-polar 2000 MHz antenna and the GSSI single-polar 1600 MHz antenna.

3.0 EXAMPLE GPR SCAN DATA

Data collected with the Aladdin full-polar 2000 MHz and the 1600 MHz antenna contained clear reflections from each individual rebar in the deck. The results from the final GPR investigation covering the bridge deck after the top one inch surface had been removed however showed drastically different results from the initial survey. Due to the shallow (½ to 1 inch between the reinforcement and the concrete surface), near-surface depth of rebar from the stripped surface, direct coupling interference had taken place causing the data to indicate the bridge was much more corroded than it actually is. This is compared in the before and after deck stripping operations for the Aladdin 2000 MHz antenna in Figures 1 and 2, respectively, and for the GSSI 1600 MHz antenna in Figures 3 and 4, respectively.

This direct coupling effect occurs due to near surface amplitude reflection attenuation. This theory is based on the superposition of the direct coupling radar wave (the wave which travels directly from the transmitter to the receiver in the antenna, parallel to the flat bottom of the antenna and following the interface between the antenna and the deck surface) and the rebar reflections. If the antenna and the subsurface reinforcement bar are not separated enough by the width of a reflection peak, there will be superposition of the two signals. The summation of the large negative direct coupling and the weaker positive rebar reflection will draw the rebar reflection more and more negative as the 2-way travel time of the rebar reflection decreases, eventually causing the signal to attenuate entirely.

Though similarities were determined between both data regarding reinforcement steel reflection (hyperbolic) artifacts, it is difficult to determine if these data are useful for analyzing corrosion and delamination of the bridge deck. This is the case for both IDS's full-polar 2000 MHz Aladdin antenna and the 1600 MHz antenna (Figures 2 and 4).

2000MHz Full-polar Antenna

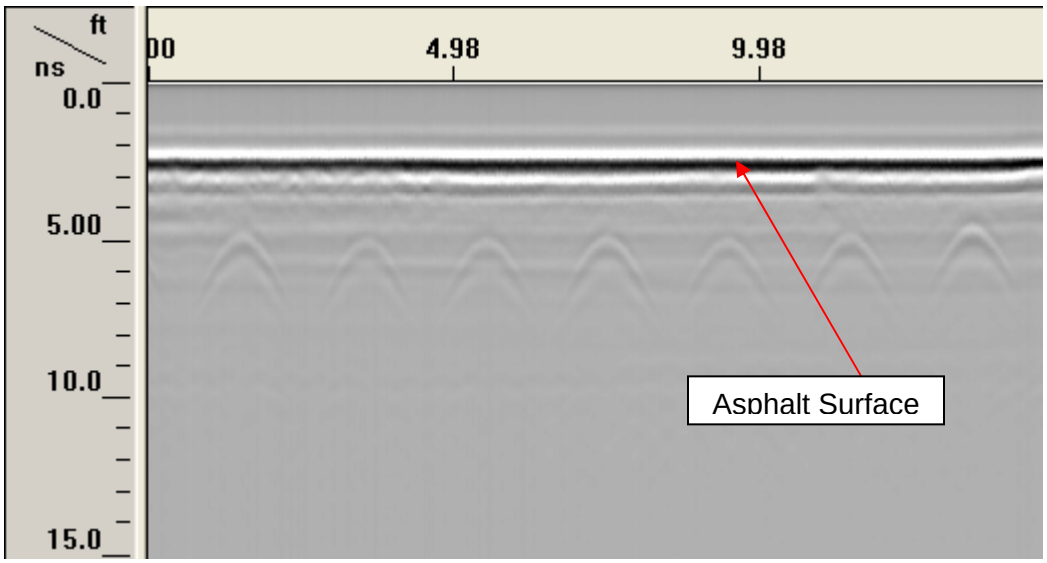

Figure 1 – IDS's Aladdin GPR Data from initial testing before surface stripping. Notice the round hyperbolic signals for each steel reinforcement bar radar reflection.

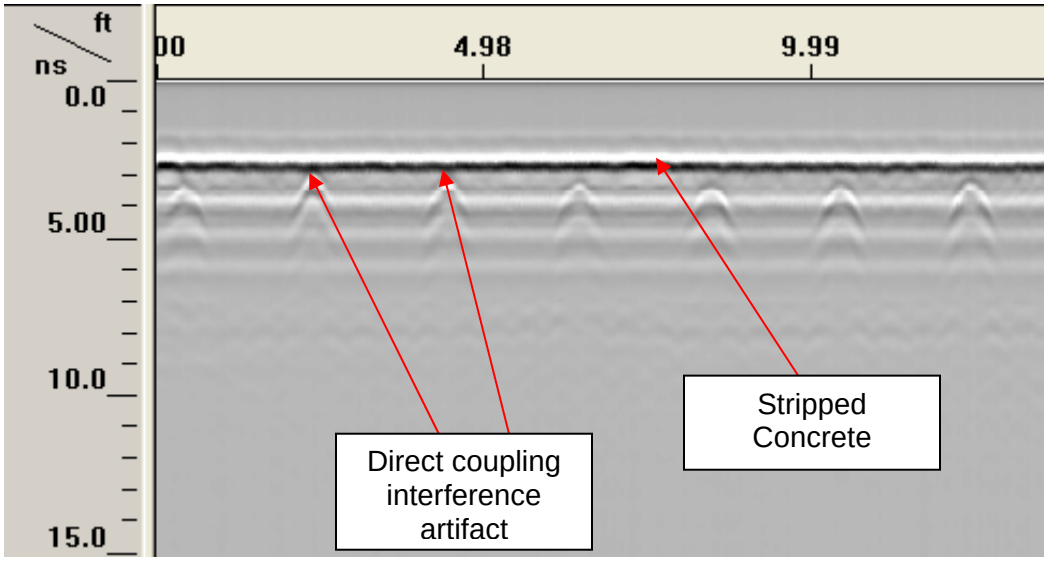

Figure 2 – IDS's Aladdin GPR Data from final testing after surface stripping. Notice the direct coupling causes the steel reinforcement bar radar reflection signal to appear much sharper compared to Figure 1 and at a much shallower depth.

1600MHz Single Antenna

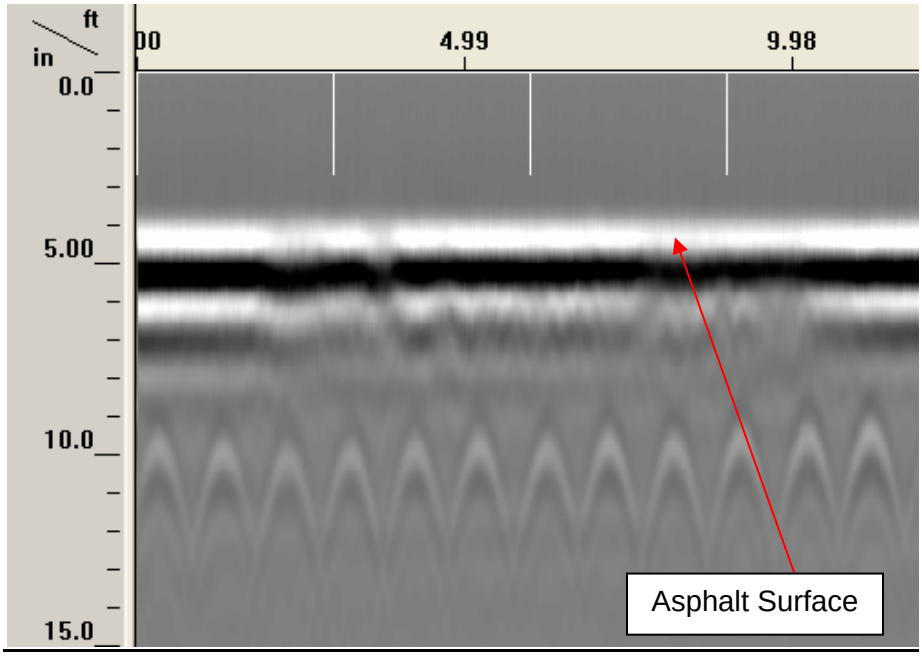

Figure 3 – 1600 MHz GPR Data from initial investigation of the asphalt overlaid deck before surface stripping. Notice the fading within the signal. This is most likely due to potential corrosion or delamination. This information in the data is most likely visible due to the lower frequency of the antenna in comparison to the 2000 MHz antenna.

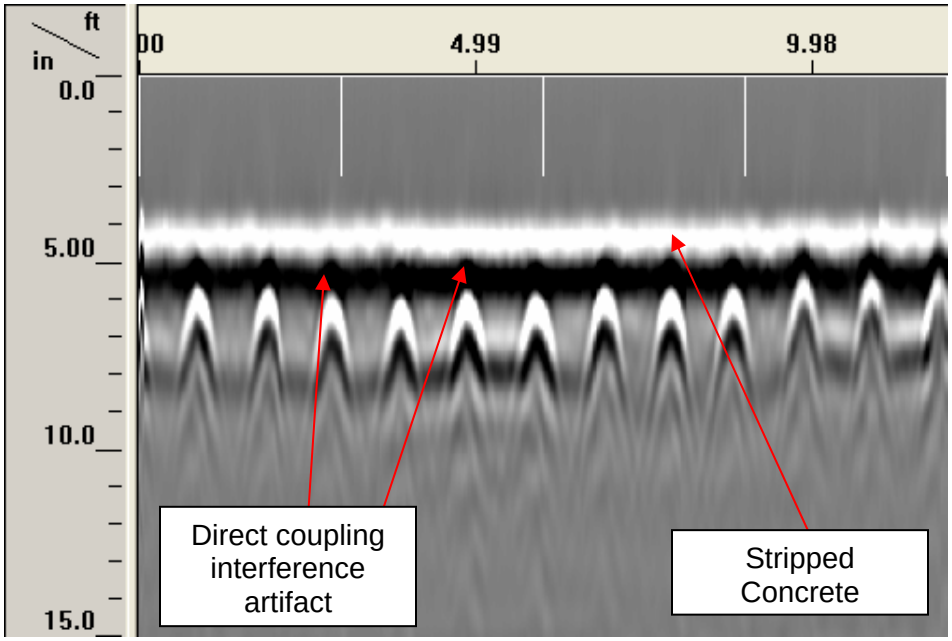

Figure 4 – 1600 MHz Data from final testing after removal of asphalt. The displayed scan is indicating near surface rebar and direct coupling interference artifacts. Notice the sharper hyperbolic reflectors and overall signal difference compared to Figure 3.

4.0 ANALYSIS OF GPR TEST RESULTS

The GPR data from the concrete deck top was processed using GRED 02.01.015 for IDS's full-polar 2000 MHz antenna and RADAN 6.5 for the 1600 MHz antenna to measure the scanned reflection normalized amplitudes (dB) of the individual transverse reinforcing bars within the top reinforcement steel. The primary concern in processing delamination and corrosion involves focusing on signal losses in the reinforcing bar reflection amplitudes which vary according to the bar size and the relative abundance of moisture and chloride in the concrete cover. This is also a direct relationship with the concrete above the top reinforcing bar mat which has been correlated in previous studies with the location and extent of delamination, corrosion, and corrosion-induced damage of the surface cover layer.

The reflection amplitude data are corrected for geometric losses due to reinforcing bar depth using a statistical regression approach fit to the 90^{th} percentile normalized amplitude (dB) versus the two-way travel time of the GPR signal. Predictions of the location and quantities of probable delamination and probable active corrosion are then evaluated using proprietary thresholds calibrated for use on exposed-surface reinforced concrete bridge decks developed in research by our sub-consultant; Dr. Christopher Barnes at Dalhousie University, Halifax, Nova Scotia, Canada. This approach assumes that the 90^{th} percentile strongest reflection amplitudes correspond to undamaged regions of the deck containing low quantities of moisture and chlorides. Areas with significantly more attenuated data below the thresholds correspond to upper reinforcement mat corrosion and/or corrosion induced-cracking of the concrete cover layer.

The quantity of probable delamination and corrosion from both antenna for the final investigation of the bridge after the top surface had been removed is undetermined due to direct coupling interference. Further analysis was attempted to correct for this direct coupling interference through analyzing all data sets within the amplitude spectrum at different values of reflection threshold for both the Aladdin (inside passing

lane) and GSSI (inside and outside lanes) as presented in Figures 8 and 9. Though similarities were determined between both data sets for potential delamination and corrosion, no direct conclusion can be made at this time. This was the case for both IDS's full-polar 2000 MHz Aladdin antenna and the 1600 MHz antenna (Figures 8 and 9). However, given that there is comparatively little attenuation in either antenna's results, this may reflect the lack of corrosion found in cores and/or the direct coupling effect.

After the Top 1 inch Layer is Removed

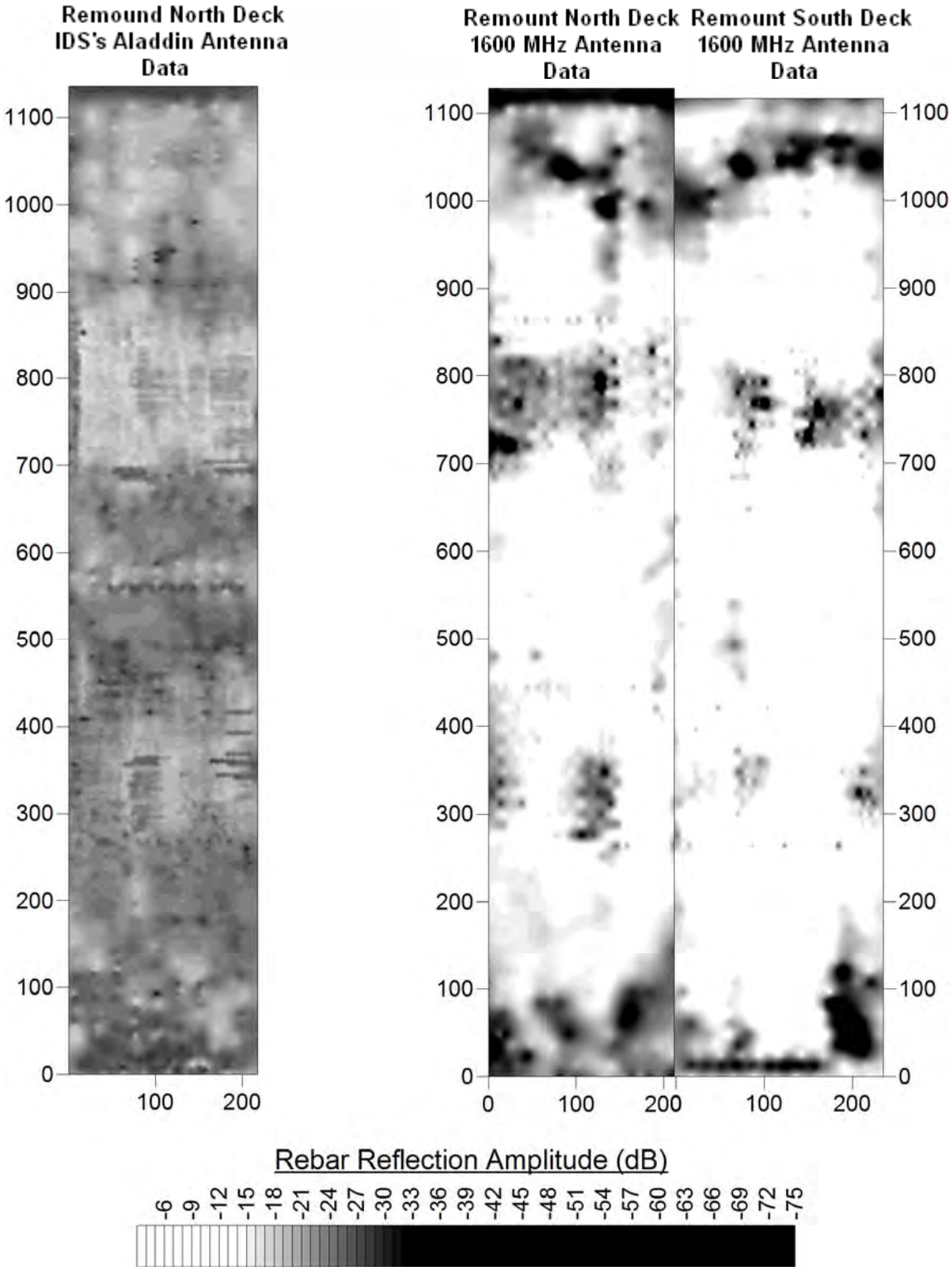

Figure 8 – Rebar reflection amplitude results for the return survey with the top asphalt overlay and 1 inch of the bridge deck removed using only the range of IDS's Aladdin antenna results (15-33 dB). Note the Aladdin North Deck data is used only for potential comparison with the originally collected data set (due to the direct coupling interference however, comparisons are difficult if not impossible to determine). All results are shown in Rebar Reflection Amplitude due to the inability (from direct coupling interference) to determine corrosion/delamination.

After the Top 1 inch Layer is Removed

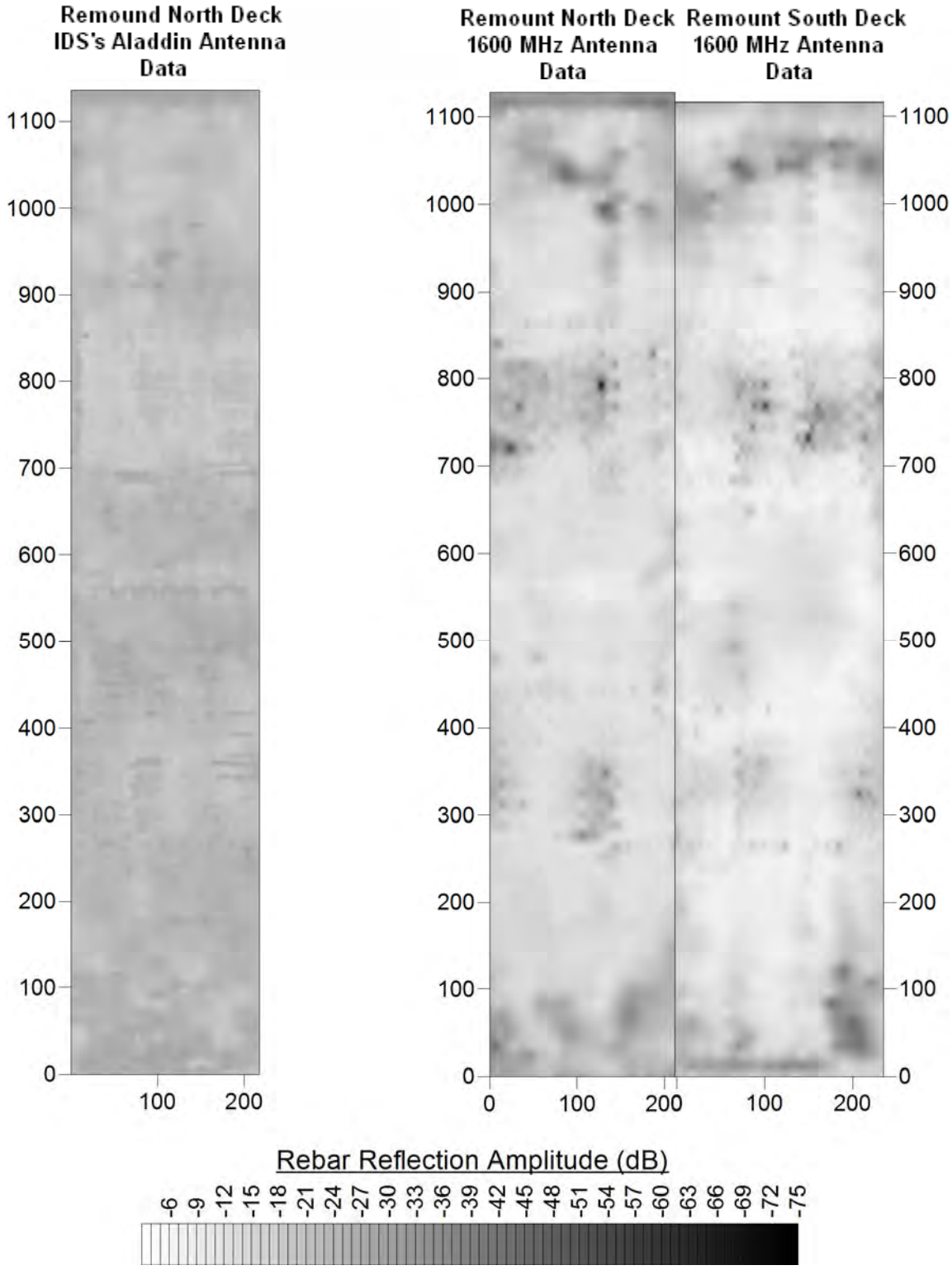

Figure 9 – Final rebar reflection amplitude results for the return survey with the top asphalt overlay and 1 inch of the bridge deck removed using the full range of the 1600 MHz results (4-75 dB). Note the IDS North Deck data is used only for potential comparison with the originally collected data set (due to the direct coupling interference however, comparisons are difficult if not impossible to determine). All results are shown in Rebar Reflection Amplitude due to the inability (from direct coupling interference) to determine corrosion/delamination.

5.0 CLOSURE

The field portion of this NDE&E investigation was performed in accordance with generally accepted testing procedures. If additional information is developed that is pertinent to the findings of this investigation or we can provide any additional information or consultation, please contact our office.

Respectfully submitted,
OLSON ENGINEERING, INC.

_____

Colin O. LeekProject Engineer

_____

Larry D. Olson, P.E.
Principal Engineer

(1 copy e-mailed and 2 copies sent)